Universidad Autónoma de Madrid
Facultad de Ciencias
Departamento de Biología Molecular

Telomere dysfunction drives pulmonary fibrosis and offers new therapeutic strategies

DOCTORAL THESIS
Juan Manuel Povedano Selfa
BSc, MSc

The entirety of the work presented in this Thesis has been carried out at the Telomeres and Telomerase Group in the Spanish National Cancer Research Centre (CNIO, Madrid), under the direction and supervision of Dr. María A. Blasco Marhuenda

Madrid, 2016

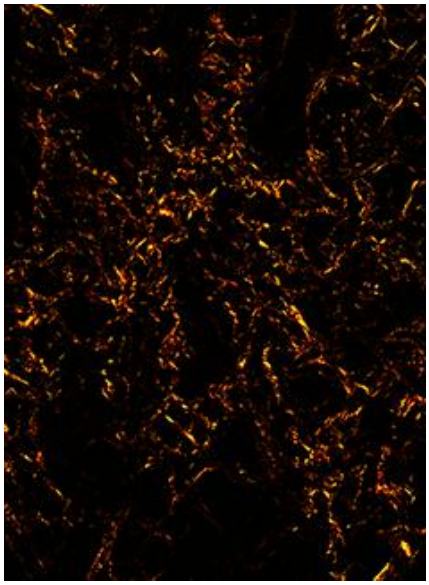

Acknowledgements

Muchas gracias Maria por darme la oportunidad de realizar la tesis en tu laboratorio, en un centro como el CNIO, ya que es una gran experiencia y te agradezco la posibilidad de estar en primera línea de la ciencia. Todo este tiempo aquí ha sido un largo, y en ocasiones duro, camino de investigación. Aunque a veces haya llegado a límites, previamente insospechados, gracias por exigirme cada día más y hacerme crecer como científico y persona.

Paula, sinceramente, no tengo páginas en esta Tesis para describir todo lo que te debo y lo agradecido que estoy por ello. Aunque pases desapercibida formalmente en esta tesis, sabes que eres parte de todo este trabajo y sin ti no podría haber sido posible. Solo decirte GRACIAS. Gracias por tu perseverancia, por tus ideas, por tus enseñanzas que tanto sirven para dentro como para fuera del labo, por tu apoyo y por estar en primera línea. No puedo desearte mas que lo mejor, por lo que te deseo que como siempre dices… “te toque la lotería y montes un club de Padel!” jajajaja.

Muchas gracias Manolo por tus consejos, tu tiempo y las ideas aportadas al proyecto. Sinceramente, estoy muy agradecido de haber podido compartir laboratorio y aprender tanto de ti y tu laboratorio. Eres un ejemplo.

Christian and Tim, thanks a lot for all the moments shared and your support during all these years! You have been an example and I learned many things from both of you. Really, you made the Thesis time better and more enjoyable.

Amigos y compañeros de los laboratorios de Telómeros y Supresión (tanto del pasado, como del presente) habéis sido grandes y buenos compañeros. Han sido 4 años intensos con sus más y sus menos, pero aún así hemos sido una pequeña familia, gracias a la cual la tesis deja un mejor sabor de boca.

Miguel Ángel y Noelia, estos últimos dos años de tesis han sido geniales y vosotros habéis aportado más de uno o dos granitos de arena a esta causa. Ya sabéis donde tenéis un amigo y en vuestro caso estoy más que seguro que esto no es más que un “nos vemos en un tiempo”. Vosotros seguid empujando, *Lok'tar ogar!!!*, porque lo conseguiréis.

Papá, mamá y hermano, al igual que al resto de la familia, gracias por estar ahí, por ayudarme y apoyarme en cualquier cosa que haga. Aunque suene a topicazo, habéis sido, sois y seréis un pilar básico en mi vida. Sois una inspiración y un ejemplo a seguir, y os debo todo, incluso ser lo que soy ahora mismo… Un “casi treintañero”

yéndose a las Américas sin saber si volverá. Pero como siempre me habéis enseñado, hay que darlo todo e intentar llegar a las metas que te propongas.

Moppie thanks! Thank you for being you, for finding me, for meeting me, for loving me, for supporting me, for standing me, for every single second next to me… It has not been easy, and probably it will not be easy in the future either, but we have each other and that will make it incredibly amazing. This is the beginning of something bigger and we know it, thank God because otherwise I wouldn't have time enough to thank you all this time. DANK JE MIJN SCHATTIE!

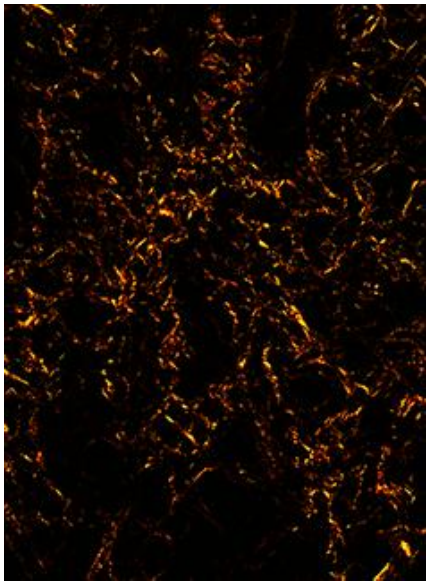

Resumen/Abstract

La fibrosis pulmonar idiopática (FPI) es una enfermedad degenerativa de los pulmones. Los pacientes presentan una supervivencia media tras el diagnóstico de 2 a 3 años. La pérdida de células alveolares tipo 2 (ATII) y la pérdida de la capacidad regenerativa de los pulmones son características de la enfermedad. Mutaciones en los componentes de la enzima telomerasa o en proteínas relacionadas con la protección de los telómeros se han encontrado tanto en casos esporádicos como familiares. Telómeros críticamente cortos o disfuncionales pueden comprometer la regeneración tisular y son un factor de riesgo para el desarrollo de FPI. Nuevas estrategias y tratamientos son necesarios, sin embargo, la falta de modelos murinos que recapitulen la enfermedad humana han obstaculizado nuevos avances al respecto.

Durante esta Tesis Doctoral hemos generado dos modelos murinos independientes de FPI producida por disfunción telomérica. En un modelo, se llevó a cabo la deleción de *Trf1* en células ATII para producir una disfunción telomérica severa. En un segundo modelo, ratones con telómeros críticamente cortos, deficientes en telomerasa, fueron sometidos a un agente inductor de daño pulmonar, la bleomicina. En ambos modelos se desarrolló fibrosis pulmonar debido a daño telomérico. En ambos modelos también se observó la pérdida de función pulmonar debido al reemplazamiento de diferentes tipos celulares por tejido fibrótico e infiltrado inflamatorio. En conclusión, ambos modelos proporcionan una prueba del papel causal del daño en el ADN telomérico en el desarrollo de la FPI e identifican a los telómeros como nuevas dianas terapéuticas.

El modelo de FPI inducido por telómeros cortos (ratones deficientes para *Tert* tratados con bleomicina) se utilizó posteriormente para comprobar la eficacia terapéutica de la re-expresión de telomerasa. Para ello usamos una estrategia de terapia génica con el vector AAV9 portando el gen *Tert* de la subunidad catalítica de la telomerasa. Encontramos que AAV9-*Tert* transduce preferentemente las células ATII. Se realizaró un seguimiento radiológico tras el tratamiento con AAV9-*Tert* y reveló una reversión de la fibrosis y remisión total en el 50% de los casos a las 7 semanas tras el diagnóstico, mientras que los animales tratados con el vector vacío seguían mostrando focos de fibrosis severa. Esta regresión fue asociada con un incremento de la longitud telomérica en células ATII, una disminución del daño en el ADN y disminución de la apoptosis y de la senescencia. El tratamiento con AAV9-*Tert* incrementó la proliferación de las células ATII y resultó en cambios en la expresión génica indicativos de la disminución de fibrosis e inducción de regeneración. Los resultados obtenidos en esta Tesis indican que la terapia génica con telomerasa constituye un tratamiento efectivo para la FPI asociada a telómeros cortos.

Idiopathic pulmonary fibrosis (IPF) is a degenerative disease of the lungs with an average survival post-diagnosis of 2-3 years. Loss of alveolar type II (ATII) cells and impairment of the regenerative capacity of the lung are also characteristic of the disease. Mutations in components of the telomere-maintenance enzyme telomerase or in proteins important for telomere protection are found both in familiar and sporadic IPF cases. Critically short or dysfunctional telomeres can impair tissue regeneration and have been established as a risk factor to develop IPF. New therapeutic targets and treatments are necessary; however, the lack of mouse models that faithfully recapitulate the human disease has hampered new advances.

Here, we generated two independent mouse models, which develop IPF owing to telomere dysfunction. Severe telomere dysfunction in the absence of telomere shortening was induced by *Trf1* deletion in ATII cells leading to pulmonary fibrosis. Mice deficient for telomerase presenting critically short telomeres were treated with low dosage of bleomycin to induce IPF. Bleomycin inoculation synergized with short telomeres provoking fibrosis in the lungs. We show that both mouse models develop pulmonary fibrosis through induction of telomere damage. Loss of lung function owing to replacement of lung cell types by fibrotic and inflammatory infiltrates was observed in both mouse models. In conclusion, those mouse models provide proof of principle of the causal role of DNA damage stemming from dysfunctional telomeres in IPF development and identifying telomeres as promising targets for new treatments.

The mouse model of pulmonary fibrosis owing to short telomeres generated (*Tert*-deficient mice subjected to a low bleomycin dose) was used to test the therapeutic efficacy of telomerase activation using AAV9 virus carrying the telomerase *Tert* gene. We find that AAV9-*Tert* preferentially targets ATII cells. AAV9-*Tert* treatment following radiological diagnosis of pulmonary fibrosis resulted in significant reversal of fibrosis and full remission in 50% of the mice 7 weeks after diagnosis, while all the mice treated with the empty vector still showed severe fibrosis. Reversal of fibrosis in AAV9-*Tert* treated mice was associated with an increase in telomere length in ATII cells, decreased DNA damage, and decreased apoptosis and senescence. AAV9-*Tert* treatment increased the percentage of proliferating ATII cells and lead to gene expression changes indicative of decreased fibrosis and increased regeneration. These results obtained during this Thesis indicate that telomerase gene therapy is effective in the treatment of pulmonary fibrosis provoked or associated with short telomeres.

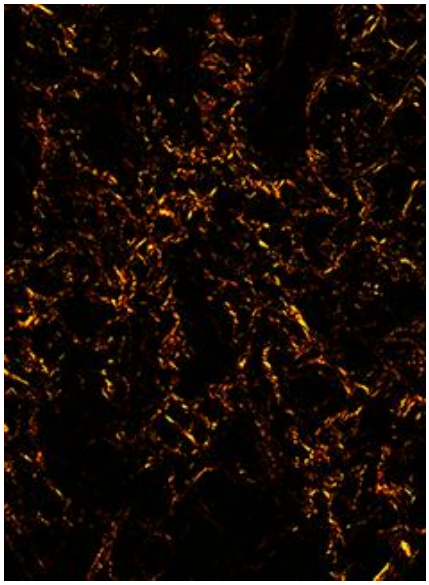

Index

Results

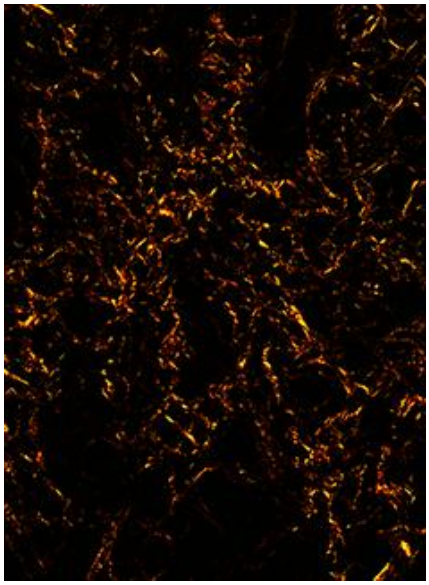

Abbreviations

γH2AX	Gamma-phosphorylated Histone 2 variant A.X
AC3	Active Caspase 3
ATI	Alveolar Type I cell
ATII	Alveolar Type II cell
a.u.f./a.u.	arbitrary units of fluorescence/arbitrary units
cDNA	complementary DNA
Cre^{ERT2}	Cre recombinase fused to an estrogen receptor domain version 2
CT	Computerized Tomography
DAPI	4,6-Diamino-2-phenylindole dihydrochloride
DDR	DNA-Damage Response
DEG	Differential Expressed Gene
DNA	Deoxyribonucleic Acid
DSB	Double Strand Breaks
eGFP	enhanced Green Fluorescence Protein
G1-G4 *Tert* $^{-/-}$	Generation 1 to Generation 4 of Tert deficient mice
GSEA	Gene Set Enrichment Analysis
hTERT	human Telomerase Reverse Transcriptase
hTERC	human Telomerase RNA Component
IF	ImmunoFluorescence
IPF	Idiopathic Pulmonary Fibrosis

kb	kilo bases
KO	Knock-Out
POT1	Protection Of Telomeres 1
(q)PCR	(quantitative) Polymerase Chain Reaction
(Q-)FISH	(Quantitative-) Fluorescence *in situ* Hybridization
SNPs	Single-Nucleotide Polymorphisms
TERT	Telomerase Reverse Transcriptase
TIN2	TERF1-Interaction Nuclear factor 2
TRF1/2	Telomere Repeat Factor 1 and 2

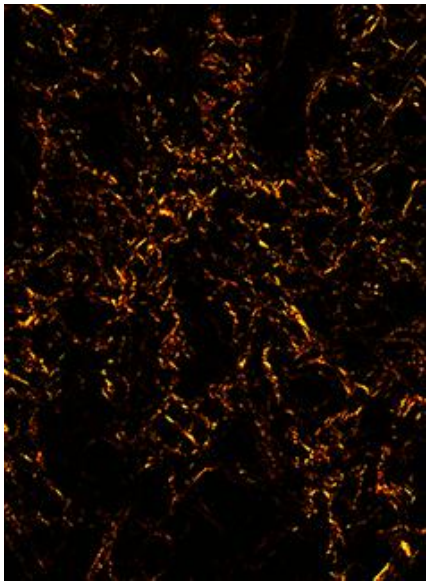

Introduction

I. Idiopathic pulmonary fibrosis

Idiopathic pulmonary fibrosis (IPF) is a life-threatening lung degenerative disease, which lacks current effective treatments and affects only in the US around 100.000 people (Armanios, 2012; King et al., 2011). The mean survival time upon diagnosis is of only 2 to 3 years (King et al., 2011). The clinical course of the disease is characterized by a progressive decline in exercise capacity, difficulty to breathe, recurrent infections, and severe impairment in lung function, which makes the patients dependent on long-term oxygen treatment. IPF is characterized by presence of lung scarring, immune infiltrates and inflammation, which in the past two decades has led to the exploration of inflammation as a therapeutic target for treatment of the disease (Selman et al., 2001). Unfortunately, recent clinical trials for IPF patients based on immune suppression had to be interrupted owing to the toxicity of the treatment (Idiopathic Pulmonary Fibrosis Clinical Research et al., 2014). More recently, IPF has been proposed to be the result of repetitive epithelial cell injury and defective regeneration, although the precise molecular cause of the damage and of the defective regeneration remains unclear (Cao et al., 2016; Hinz et al., 2007; Ryu et al., 2014). To date, lung transplantation is the only therapeutic option for less than 5% of IPF patients with very severe disease (Lama, 2009).

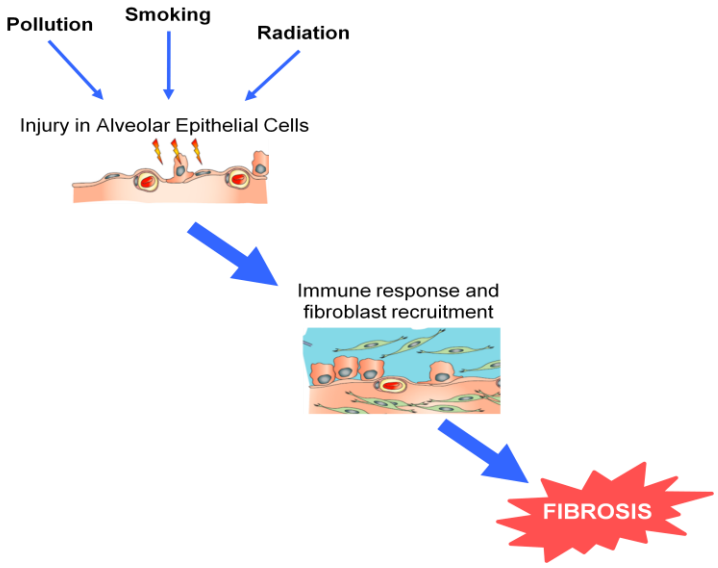

Figure 1. Schematic representation of the fibrotic process. Several factors have been proposed to induce alveolar epithelium damage such as smoke, pollution, and radiation (adapted from King *et al.*, 2011).

IPF is an age-associated disease, with a mean age at onset between 50-70 years (Armanios, 2013; King et al., 2011), affecting men more frequently than women with a 2:1 ratio (King et al., 2011). Environmental factors such as smoking, radiation or pollution, inflict damage to lung epithelial cells inducing recruitment of immune cells and fibroblast generating fibrosis (**Fig. 1**). Those environmental factors are known to increase the risk of developing IPF (Armanios, 2013; King et al., 2011).

II. Idiopathic pulmonary fibrosis: one of the telomere syndromes

In humans, a number of conditions have been associated with mutations in telomerase and other telomere related genes. Therefore, mutations in telomere maintenance genes show a variety of pathologies and disease states which have been collectively named as "telomere syndromes" (Armanios and Blackburn, 2012), and which affect both highly proliferative (bone marrow, gut, skin) and slow proliferative (liver, lung, pancreas) tissues. Genes mutated in telomere syndromes are listed as following:

Table 1. Telomere syndromes.

Gene	Syndromes
TIN2	Dyskeratosis congenita Hoyeraal-Hreidersson syndrome Revesz syndrome
RTEL1	Dyskeratosis congenita, Hoyeraal-Hreidersson syndrome
CTC1	Coats plus
Apollo	Hoyeraal-Hreidersson syndrome
TERT, TERC, NHP2, NOP10, DKC1	Idopathic Pulmonary Fibrosis Dyskeratosis congenita Aplastic Anemia
TCAB1	Dyskeratosis congenita

The most frequent condition of the telomere syndromes is IPF (Armanios, 2013; Armanios and Blackburn, 2012). Genome-wide sequencing studies have identified SNPs in *Tert* and *Terc* loci affecting telomere length associated to IPF development (Codd et al., 2013). In particular, mutations in *Tert* and *Terc* account for 8-15% of familial and 1-3% of sporadic cases (Alder et al., 2008; Armanios, 2013; Armanios et al., 2007). Both familial and sporadic IPF cases, indistinctly of telomerase mutations, present a telomere length below the 10th percentile of the average normal population (Snetselaar et al., 2015). Lately, telomerase mutations have also been found in up to

1% of smokers showing chronic obstructive pulmonary disease (COPD), also leading to abnormally short telomeres (Stanley et al., 2015).

Compelling evidence that telomere shortening contributes to aging and age related disease comes from the study of humans and also mice with defective telomerase activity (Armanios and Blackburn, 2012; Blasco, 2005, 2007). Thus, one of the hallmarks of aging in mice and humans is the progressive shortening of telomeres with increasing age (Lopez-Otin et al., 2013). Many studies have already shown that short telomeres are sufficient to cause age-related pathologies and decreased longevity in telomerase deficient mice, which show premature aging phenotypes in high-proliferating compartments (bone marrow, gut, skin, testis) (Blasco et al., 1997; Ferron et al., 2004; Herrera et al., 1999; Lee et al., 1998; Leri et al., 2003). Importantly, telomerase deficient mice show worsening of phenotypes with increasing mouse generations owing to inherited progressively shorter telomeres, with the later generations showing severe phenotypes and premature death at pre-reproductive ages (Garcia-Cao et al., 2002; Herrera et al., 1999; Lee et al., 1998). This phenomenon is also observed in humans and indicates genetic anticipation associated with telomerase deficiency (Armanios, 2012) (**Fig. 2**).

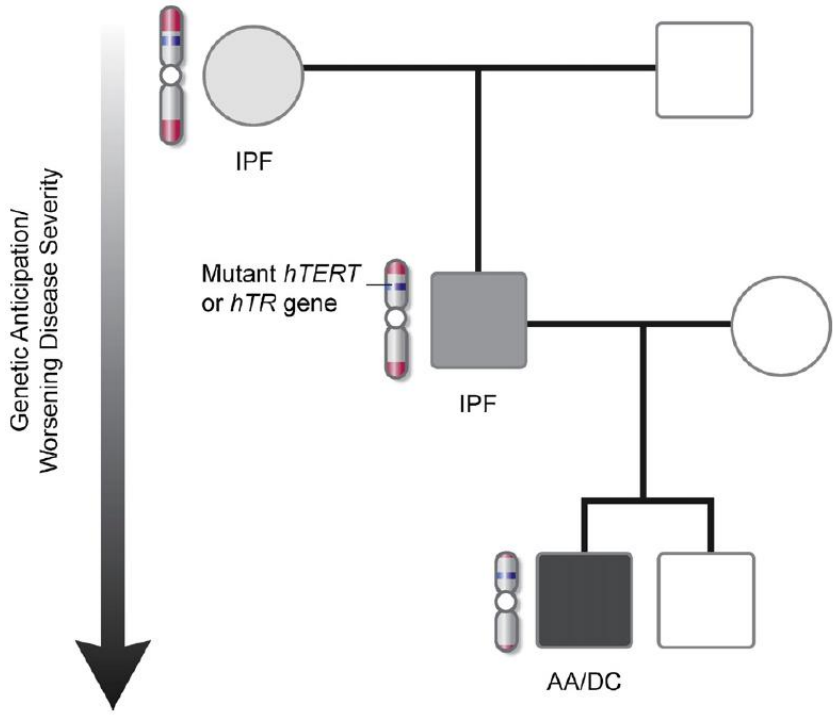

Figure 2. Model of genetic anticipation associated to telomerase mutations. (Armanios, 2012) Telomeres are represented at the extreme of the chromosome in red. IPF: Idiopathic Pulmonary Fibrosis; AA: Aplastic Anemia; DC: Dyskeratosis Congenita.

Disease anticipation is found in human families with telomere syndromes as well as in mice. Generally, the mutation first manifests in adults with pulmonary fibrosis and the more severe phenotypes appear in paediatric populations (immunodeficiency) and young adults (aplastic anaemia) from the next generations (Armanios, 2012, 2013) (**Fig. 2**).

In spite of pulmonary fibrosis and emphysema being the most frequent manifestations of telomere defects in humans, telomerase-deficient mice with critically short telomeres do not spontaneously develop pulmonary disease. Exposure to cigarette smoke, which is known to accelerate pulmonary fibrosis onset in humans, induces emphysema in telomerase-deficient mice, but no IPF was observed (Alder et al., 2011). It has recently been shown that alveolar progenitor senescence induced by telomere dysfunction is sufficient to recapitulate the regenerative defects, inflammatory responses and susceptibility to injury that are characteristic of human telomere-mediated lung disease although no fibrosis was reported in this mouse model (Alder et al., 2015). These findings suggest that additional damages, or a telomere damage of higher severity, may be required for IPF onset in mice with short telomeres.

III. Mouse models for pulmonary fibrosis

To study the fibrotic process in IPF and the evolution of the disease several animal models have been developed. They have been useful to identify an important number of key cells, mediators and mechanisms linked to pulmonary fibrosis. However, mouse models that faithfully recapitulate the molecular features of the human disease and that aid to find new therapeutic strategies have not yet been developed. Following, I will list the principal mouse models for pulmonary fibrosis existing to date:

- DNA damaging agents

Bleomycin inoculation is the most used and best characterized mouse model for pulmonary fibrosis. The drug was isolated from *Streptomyces verticillatus* and found to be effective against tumors (Umezawa, 1974; Umezawa et al., 1967). Bleomycin has been used in a wide variety of experimental animals and over a range of doses administrated either via intraperitoneal, intravenous, subcutaneous, or intratracheal. Intratracheal inoculation with bleomycin is the easiest and fastest way to provoke pulmonary fibrosis, reason why it is the most commonly used (Moore and Hogaboam, 2008). This model, however, posses the limitation that fibrosis regresses after 4-5 weeks (Mouratis and Aidinis, 2011). Bleomycin produces double strand breaks in the

DNA from alveolar cells leading to cell death, what induces the recruitment of the immune system and of activated fibroblasts, and ultimately leading to fibrosis.

Ionizing radiation is also used to produce fibrosis, which starts to appear as early as 20 weeks post-exposure (McDonald et al., 1993). Radiation, as bleomycin, provokes DNA damage directly into the lungs. However, its response is considerably slower than the induced by bleomycin.

Silica aerosol instillation induces fibrosis in the lungs, recapitulating fibrotic nodules seen in humans due to the focal inflammation where silica particles are located. Development of fibrosis takes around 15 weeks. In addition, special instrumentation for aerosol delivery is required, making this technique not very suitable for researchers (Davis et al., 1998).

- Transgenic mouse models

Transgenic models are based on the constitutive or conditional expression of a transgene. However, although they have aided to the study of the pulmonary fibrosis pathophysiology, none of them mimics the main characteristic of human pulmonary fibrosis which is the late adulthood onset (Moore and Hogaboam, 2008).

TGF-α mouse model: in this model, TGF-α over-expression specifically in ATII cells induces severe pulmonary fibrosis, located at peribronchiolar and perivascular regions. Alveolar architecture is disrupted owing to fibrotic lesions in the alveoli, which are induced by paracrine signalling (Korfhagen et al., 1994).

IL-11 mouse model: over-expression of IL-11 in club cells originates peribronchiolar inflammation mainly by mononuclear cell infiltrates, leading to airways remodelling with subepithelial fibrosis. These results suggested an important role of this interleukin in IPF (Tang et al., 1996).

Other transgenic mouse models: Over-expression of inflammation-related genes such as IL-13, IL-10, IL-1β or Fra-2/AP-1 have also been shown to originate fibrosis (Eferl et al., 2008; Kolb et al., 2001; Sun et al., 2011; Zhu et al., 1999).

In summary, mouse models that recapitulate more closely the molecular features of human disease, including telomere defects, are needed. These new models will aid in our understanding of the pathobiology of IPF and will allow more efficient preclinical testing of novel therapeutic strategies.

IV. Telomeres and the telomerase complex

Mammalian telomeres are protective structures at ends of chromosomes (Blackburn, 2001; de Lange, 2005) that consist of TTAGGG repeats bound by a six-protein complex known as shelterin (de Lange, 2005). Shelterin complex is composed of 6 core proteins: the telomere repeat factor 1 and 2 (Trf1 and Trf2), the TRF1-interacting factor 2 (Tin2), the protection of telomeres 1 (Pot1), the Pot1-Tin2 organizing protein Tpp1 (also known as Tint1, Ptop or Pip1), and the repressor/activator protein 1 (Rap1) (de Lange, 2005) (**Fig. 3**). A minimum length of telomeric repeats is necessary for shelterin binding and telomere protection (Blackburn, 2001; de Lange, 2005). Lately, it has been demonstrated that shelterin complex is essential for telomeric chromatin condensation, what restricts the accessibility of the DNA damage response machinery to the telomere (Bandaria et al., 2016). Shelterin also prevents the telomeres from degradation and the fusion with other chromosomes (de Lange, 2005). Generation of mouse models with ubiquitous deletion of shelterin components showed an early embryonic lethality, with the exception of *Rap1*-deficient mice, highlight the importance of shelterins for cell viability and tissue homeostasis (Celli and de Lange, 2005; Chiang et al., 2004; Hockemeyer et al., 2006; Karlseder et al., 2003; Kibe et al., 2010; Lazzerini Denchi et al., 2006; Martinez and Blasco, 2011; Martinez et al., 2010; Wu et al., 2006).

The catalytic subunit of telomerase, *Tert* (telomerase reverse transcriptase), is an enzyme capable of compensating the telomere attrition produced by telomere degradation and/or by the incomplete replication of telomeric repeats associated to each DNA replication cycle, through *de novo* addition of TTAGGG repeats to the chromosome ends. To this end, telomerase uses an associated RNA component as replication template (*Terc*, telomerase RNA component) (Greider and Blackburn, 1985) (**Fig. 3**).

In mice and humans, telomerase is silenced after birth leading to progressive telomere shortening associated to cell division throughout lifespan, with the exception of adult stem cells which maintain telomerase expression to slow down telomere attrition in the stem cell compartment (Canela et al., 2007; Flores et al., 2008; Harley et al., 1990; Vera et al., 2012). When telomeres reach a critically short length, this triggers activation of a persistent DNA damage response at telomeres and the subsequent induction of cellular senescence or apoptosis. In the case of adult stem cells, critical telomere shortening impairs their ability to regenerate tissues both in mice and humans, leading to several different age-related pathologies (Flores et al., 2005).

Interestingly, telomere shortening has been shown to be influenced both by genetic factors (i.e., mutations in genes necessary for telomere maintenance) and environmental factors (e.g., cigarette smoke has a negative effect) (Armanios, 2013; King et al., 2011).

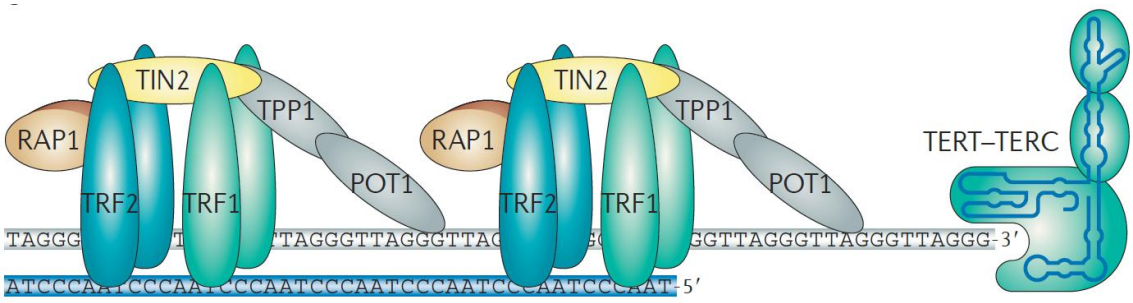

Figure 3. Telomere and shelterin complex structure. (Martinez and Blasco, 2011)

In this regard, proper telomere capping requires not only a minimum length of telomere repeats, but also the integrity of the 6 proteins shelterin complex, binding the telomeric repeats (de Lange, 2005). Out of these six shelterin components TRF1 was the first to be identified (Chong et al., 1995). Extensive work using genetically modified mouse models has shown that TRF1 deletion leads to an immediate and persistent DNA damage response at chromosome ends. Thus, TRF1 abrogation leads to severe proliferative defects in all the tissues studied, including stem cell compartments, recapitulating some of the pathologies associated to telomere syndromes (Beier et al., 2012; Martinez et al., 2009; Povedano et al., 2015; Schneider et al., 2013).

Regarding the topic of this thesis, it is interesting that TRF1-interacting shelterin protein TIN2 has also been found mutated in telomeres syndromes, suggesting that telomere uncapping could also leads to disease. However, the role of shelterin dysfunction in pulmonary fibrosis has not been formally addressed.

V. Telomerase gene therapy to delay aging and age-related diseases

Critical telomere shortening has been a determinant of aging and longevity. In agreement with this, increased TERT expression in the context of cancer resistant transgenic mice was sufficient to delay aging and extend mouse longevity by 40% (Tomas-Loba et al., 2008). Recently, these findings have been translated into a potential therapeutic strategy by using adeno-associated vectors (AAV) to transiently activate telomerase in adult tissues (Bar et al., 2014; Bernardes de Jesus et al., 2012). In particular, treatment with *Tert* gene therapy using non-integrative AAV9 vectors in

adult mice was able to delay aging and increase longevity by decreasing age-related pathologies such as osteoporosis, glucose intolerance, as well as neuromuscular and cognitive decline. Furthermore, cancer incidence was not increased in the *Tert* treated mice (Bernardes de Jesus et al., 2012) (**Fig. 4**). More recently, AAV9-*Tert* delivery specifically to the heart was sufficient to significantly increase mouse survival and heart function upon myocardial infarction, which was concomitant with decreased fibrosis and increased cardiac myocyte proliferation (Bar et al., 2014). In the case of aplastic anemia, AAV9-*Tert* gene therapy was able to improve survival increasing blood counts associated to telomere elongation in bone marrow and peripheral blood mononuclear cells in two different mouse models (Bar et al., 2016). All these findings together support the notion that telomere shortening is at the origin of age-related diseases and that, by delaying or reverting this process with telomerase expression, it is possible to postpone and treat more effectively age-associated diseases, such as heart infarct, aplastic anemia, and pulmonary fibrosis.

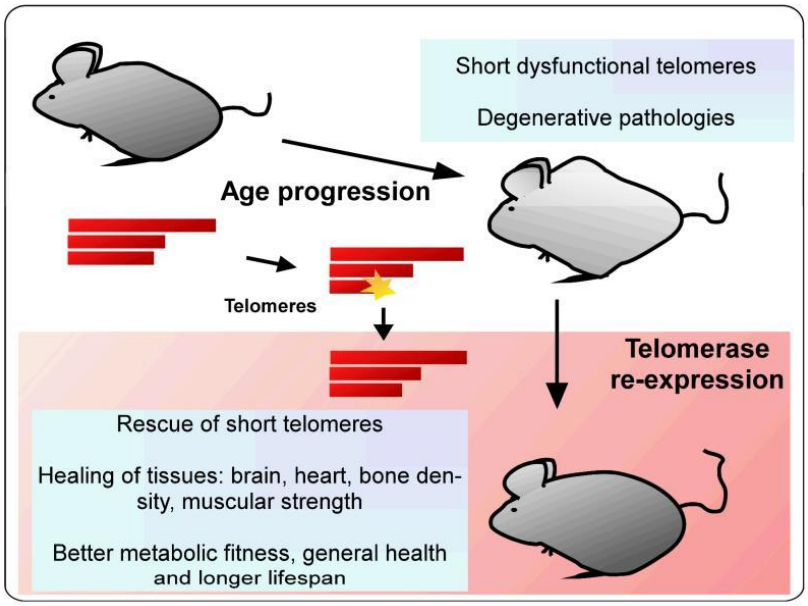

Figure 4. Rescue of age-related tissue regeneration in mice upon telomerase re-expression. (Bernardes de Jesus and Blasco, 2012)

VI. Current treatments for IPF

Idiopathic pulmonary fibrosis has few available therapeutic options, despite being a life-threatening lung degenerative disease (King et al., 2011). For the last decades, several treatments have been tested to cure IPF patients with no success, i.e. prednisone, azathioprine, N-acetylcysteine, anti-inflammatory, and anti-coagulation drugs. Strikingly, some of them turn to be harmful for IPF patients when used in combination.

This is the case of prednisone, azathioprine and N-acetylcysteine combined treatment, what led to the National Heart, Lung, and Blood Institute (NHLBI) to discontinue after observing an increase of deaths from 1% in placebo-treated patients to 11% in triple therapy patients (Wells et al., 2012). Moreover, anticoagulant drugs were also found to be no beneficial and potentially harmful (Noth et al., 2012). On the other hand, based on the inflammatory nature of the disease, current anti-inflammatory drugs resulted to have no or little success for IPF patients (Ahluwalia et al., 2014; Raghu, 2006).

Nintedanib and pirfenidone are two recently FDA-approved drugs that have anti-inflammatory and anti-fibrotic activity. Nintedanib is a small molecule tyrosine kinase inhibitor. It targets vascular endothelial growth factor receptor (VEGFR), fibroblast growth factor receptor (FGFR), and platelet derived growth factor receptor (PDGFR), blocking signalling pathways involved in the fibrotic process (Ahluwalia et al., 2014). In the case of pirfenidone, down-regulates the production of growth factors and collagen, and thereby reducing fibers deposition. In bleomycin-induced fibrosis mouse models displayed an antifibrotic activity when administered in a prophylactic treatment regimen (Ahluwalia et al., 2014; Inomata et al., 2014; Oku et al., 2008; Tanaka et al., 2012).

These drugs are the only two efficient drugs for IPF (Ahluwalia et al., 2014; Karimi-Shah and Chowdhury, 2015; King et al., 2014). However, they only slow down IPF progression with no curative capacity (Hunninghake, 2014; Karimi-Shah and Chowdhury, 2015; King et al., 2014).

Indeed, to date, lung transplantation is the only curative therapeutic option in less than 5% of IPF patients with severe disease (Lama, 2009). This method is very complicated due to the intervention complexity and the post-surgical complications, and it is only available to a small minority of IPF patients (Raghu et al., 2011). Thus, development of novel and more effective therapeutic strategies to treat the disease are urgently needed.

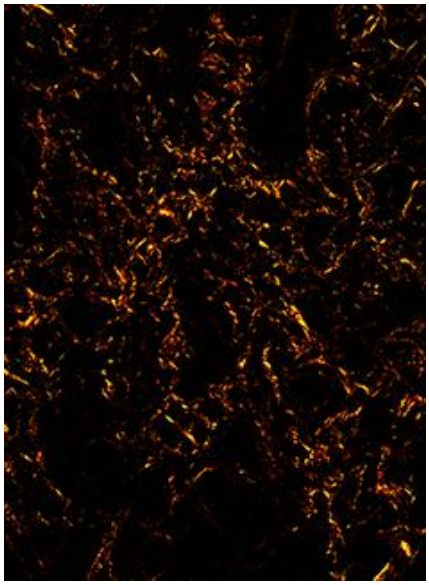

Objectives

The objective of this Thesis is to generate mouse models that recapitulate human IPF to be used for the development of novel therapeutic strategies for IPF treatment. I had the following specific aims:

1.- Generation of a mouse model of pulmonary fibrosis due to telomere dysfunction by *Trf1* deletion.

2.- Generation of a mouse model of pulmonary fibrosis due to short telomeres and telomerase deficiency.

3.- To test *Tert* gene therapy as a potential treatment of idiopathic pulmonary fibrosis due to short telomeres.

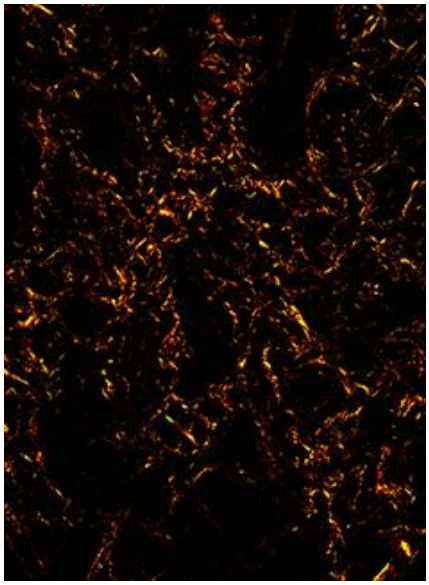

Material and Methods

Mice and animal procedures

Trf1$^{flox/flox}$ mice were generated as described (Martinez et al., 2009). To conditionally delete *Trf1* from alveolar epithelial type II (AT II) cells, homozygous *Trf1*$^{flox/flox}$ mice were crossed with transgenic mice expressing Cre-ER^{T2} under the control of *surfactant protein C* (SPC) promotor (Rock et al., 2011) as well as with transgenic mice harbouring the fluorescence katushka (KFP) protein encoding gene that contains a stop cassette flanked by lox sequences, the *KFP*$^{CAG\text{-}lox\text{-}STOP\text{-}lox}$ allele (Diéguez-Hurtado R *et al*, 2011). Heterozygous *Trf1*$^{flox/+}$ *SPC-Cre*^{ERT2} *KFP*$^{CAG\text{-}lox\text{-}STOP\text{-}lox}$ mice were crossed with *Trf1*$^{+/flox}$ mice to obtain *Trf1*$^{+/+}$ *SPC-Cre-*^{ERT2} *KFP*$^{CAG\text{-}lox\text{-}STOP\text{-}lox}$ and *Trf1*$^{flox/flox}$ *SPC-Cre*^{ERT2} *KFP*$^{CAG\text{-}lox\text{-}STOP\text{-}lox}$ mice.

Tert knock-out and wild-type mice:

Wild-type mice and *Tert*$^{-/-}$ of pure C57/BL6 background were used for bleomycin intratracheal inoculation procedure. *Tert* heterozygous mice generated as previously described (Liu et al., 2000) were backcrossed to >98% C57/BL6 background. *Tert*$^{+/-}$ mice were intercrossed to generate first generation (G1) homozygous *Tert*$^{-/-}$ knock-out mice. G2 and G4 *Tert*$^{-/-}$ mice were generated by successive breeding of G1*Tert*$^{-/-}$ and G3*Tert*$^{-/-}$ mice, respectively

All mice were produced and housed at the *specific pathogen-free* barrier area of the CNIO, Madrid. All animal procedures were approved by the CNIO-ISCIII Ethics Committee for Research and Animal Welfare (CEIyBA) and conducted in accordance to the recommendations of the Federation of European Laboratory Animal Science Associations (FELASA).

Tamoxifen treatment

Tamoxifen was dissolved in corn oil to a concentration of 20 µg/µL. Eighth to ten week old *Trf1*$^{flox/flox}$ *SPC-Cre-*^{ERT2} *KFP*$^{T/+}$ and *Trf1*$^{+/+}$ *SPC-Cre-*^{ERT2} *KFP*$^{T/+}$ mice were intraperitoneally inoculated with 50 µL (1 mg per injection) of tamoxifen solution 3 times per week during 6 weeks.

Bleomycin titration and inoculation

Decreasing bleomycin concentrations (2.5 mg/kg body weight, 1 mg/kg body weight, 0.5 mg/kg body weight and 0.1 mg/kg body weight) were intratracheally inoculated to 8-

10 weeks old wild-type mice. 2 weeks after the inoculation mice were sacrificed and analyzed by immunohistochemistry for pulmonary fibrosis.

Low dose of bleomycin (0.5 mg/kg body weight) or PBS were inoculated to 8-10 weeks old wild-type, G2 *Tert*$^{-/-}$ and G4 *Tert*$^{-/-}$ mice.

Viral particle production

Viral vectors were generated as described (Matsushita *et al*.) and purified as previously described(Ayuso et al., 2014). Vectors were produced through triple transfection of HEK293T. Cells were grown in roller bottles (Corning, NY, USA) in DMEM medium supplemented with fetal bovine serum (10% v/v) to 80% confluence and then co-transfected with the following plasmids: plasmid_1 carrying the expression cassette for gene of interest flanked by the AAV2 viral ITRs; plasmid_2 carrying the AAV *rep2* and *cap9* genes; plasmid_3 carrying the adenovirus helper functions (plasmids were kindly provided by K.A. High, Children's Hospital of Philadelphia). The expression cassettes were under the control of the cytomegalovirus (CMV) promoter and contained a SV40 polyA signal for *EGFP* and the CMV promoter and the 3'-untranslated region of the *Tert* gene as polyA signal for Tert. AAV9 particles were purified following an optimized method using two caesium chloride gradients, dialysed against PBS, filtered and stored at 80°C until use. Mice were treated with viral genome particle in a concentration per mouse of $2.5*10^{12}$ vg/mL.

Histopathology, immunohistochemistry and immunofluorescence analysis

Histopathological analysis of paraffin-embedded lungs was performed in lung sections stained with haematoxylin and eosin and Masson's trichrome using standard procedures. To quantify collagen deposition Sirius red staining was performed on deparaffinised slides with Picro-Sirius red solution for 1 h.(Broytman et al., 2015)

Immunohistochemistry stainings were performed with the following primary antibodies: rat monoclonal to p53 (POE316A/E9; CNIO histopathology core unit), rat monoclonal to p21 (HUGO-291H/B5; CNIO histopathology core unit), mouse monoclonal to phospho–Histone H2AX (Ser139) (Millipore), rat monoclonal to F4/80 (ABD serotec), p19ARF (5-C3-1 Santa Cruz Biotechnology), activated-caspase-3 (RyD systems), Interleukin 6 (ab6672, Abcam) and rabbit polyclonal turbo-RFP (Evrogen).

For immunofluorescence, the antibodies used were a rabbit polyclonal anti-TRF1 (homemade), phospho-H2AX Ser 139 (05-636, Millipore), goat polyclonal anti SPC (C-19; Santa Cruz Biotechnology), αSMA (CME 305; Biocare Medical) and mouse monoclonal, *KFP* (RF5R; Abcam), and rabbit monoclonal anti Ki67 (0003110QD; Master Diagnostica). Images were obtained using a confocal ultraspectral microscope (Leica TCS-SP5). Fluorescence intensities were analyzed with Definiens software.

Lung *in-vivo* imaging by computerized tomography (CT)

The acquisition was made on a high-resolution CT system (CT Locus, GE Healthcare) specially designed for small laboratory animals. Mice were anesthetized with a 4% rate of isoflurane (IsoVet Braun) during the induction and 2% during the maintenance period (scanning time). Micro-CT image acquisition consisted of 400 projections collected in one full rotation of the gantry in approximately 14 min in a single bed focused on the legs, with a 450 μA/80kV X-ray tube. 2-D and 3-D images were obtained and analysed using the software program MicroView (GE Healthcare). All procedures were carried out according to the European Normative of Welfare and Good Practice (2010/63/UE)

Spirometry analysis

Wild-type and G2 *Tert*$^{-/-}$ mice were placed into a head-out single chamber plethysmograph (Harvard Apparatus) for 3-5 min. Data acquisition was performed by Pulmodyn W software (from Hugo Sachs Elektronic Harvard Apparatus).

Transcriptional analysis in paraffin included lungs

RNA was extracted from two lung paraffin block sections of 20 mm with RNeasy FFPE kit following manufacturer instruction (Qiagen, cat. Nº 73504). cDNA was synthesised and collagen I and III expression was analysed by qPCR. The primers used for Col1a1 were Col1a-F (5'-GCCACTCTGACTGGAAGAGC-3') and Col1a-R (5'-CAGCCTTGGTTAGGGTCGAT-3'). The primers used for Col3a1 were Col3a1-F (5'-AAATTCTGCCACCCCGAACT-3') and Col3a-R (5'- AGCCTTGGTTAGGATCAACCC-3').

Telomere analysis

Q-FISH determination on paraffin-embedded tissue sections was performed as described previously (Gonzalez-Suarez et al., 2000). After deparaffinization, tissues were post-fixed in 4% Formaldehyde 5min, washed 3x5min in PBS and incubated at 37ºC 15 min in pepsin solution (0.1% Porcine Pepsin, Sigma; 0.01M HCl, Merck). After another round of washes and fixation as above-mentioned, slides were dehydrated in a 70% - 90% - 100% ethanol series (5min each). After 10 min of air drying, 30μl of telomere probe mix (10mM TrisCl pH7, 25mM MgCl2, 9mM Citric Acid, 82 mM Na2HPO4, 70% Deionised Formamide –Sigma-, 0.25% Blocking Reagent –Roche- and 0.5μg/ml Telomeric PNA probe -Panagene) were added to each slide. A cover slip was added and slides incubated for 3min at 85ºC, and for further 2h at RT in a wet chamber in the dark. Slides were washed 2x15 min in 10 mM TrisCl pH7, 0.1% BSA in 70% formamide under vigorous shaking, then 3x5min in TBS 0.08% Tween20 and then incubated in a 4`,6-diamidino-2-phenylindole (DAPI) bath (4μg/ml DAPI (Sigma) in PBS) before mounting samples in Vectashield (VectorTM). Confocal image were acquired as stacks every 1 μm for a total of 3 μm using a Leica SP5-MP confocal microscope and maximum projections were done with the LAS-AF software. Telomere signal intensity was quantified using Definiens software.

In the case of immuno-FISH, immunofluorescence against SPC was performed as described above before start QFISH. Next to secondary antibody incubation tissues were post-fixed in 4% Formaldehyde 5min, washed 3x5min in PBS, and after another round of fixation as above-mentioned, slides were dehydrated in a 70% - 90% - 100% ethanol series (5min each). After 10 min of air drying, 30μl of telomere probe mix (10mM TrisCl pH7, 25mM MgCl2, 9mM Citric Acid, 82 mM Na2HPO4, 50% Deionised Formamide –Sigma-, 0.25% Blocking Reagent –Roche- and 0.5μg/ml Telomeric PNA probe -Panagene) were added to each slide. A cover slip was added and slides incubated for 3min at 85ºC, and for further 2h at RT in a wet chamber in the dark. Slides were washed 2x15 min in 10 mM TrisCl pH7, 0.1% BSA in 50% formamide under vigorous shaking, then 3x5min in TBS 0.08% Tween20 and then incubated in a 4`,6-diamidino-2-phenylindole (DAPI) bath (4μg/ml DAPI (Sigma) in PBS) before mounting samples in Vectashield (VectorTM). Confocal image were acquired as stacks every 1 μm for a total of 3 μm using a Leica SP5-MP confocal microscope and maximum projections were done with the LAS-AF software. Telomere signal intensity was quantified using Definiens software.

Gene expression analysis

RNA was extracted from post-caval lobe frozen lungs with RNeasy kit following manufacturer instruction (Qiagen, cat. Nº 73504) and RNA integrity analyzed in an Agilent Bioanalyzer. cDNA was synthesized and analyzed on Agilent´s Mouse Genome DNA microarray, following the manufacturer's instructions.

Validation by qPCR for several hits was performed. The primers used were the following.

Table 2. Primer list.

Gene		Sequence (5' -> 3')	Length	Tm
FLIP	FWD Primer	GCTCCAGAATGGGCGAAGTAA	21	62
	RV Primer	ACGGATGTGCGGAGGTAAAAA	21	62
MMP-9	FWD Primer	TGG CTT TTG TGA CAG GCA CTT		
	RV Primer	CCC GAC ACA CAG TAA GCA TTC		
Lrp5	FWD Primer	AAGGGTGCTGTGTACTGGAC	20	62
	RV Primer	AGAAGAGAACCTTACGGGACG	21	61
Bid	FWD Primer	GCCGAGCACATCACAGACC	19	63
	RV Primer	TGGCAATGTTGTGGATGATTTCT	23	61
Bax	FWD Primer	TGAAGACAGGGGCCTTTTTG	20	60
	RV Primer	AATTCGCCGGAGACACTCG	19	62
Lrp6	FWD Primer	TTGTTGCTTTATGCAAACAGACG	23	61
	RV Primer	GTTCGTTTAATGGCTTCTTCGC	22	60
APC	FWD Primer	CTTGTGGCCCAGTTAAAATCTGA	23	61
	RV Primer	CGCTTTTGAGGGTTGATTCCT	21	61
Fzd5	FWD Primer	GGTGTGCCAGGAAATCACG	19	61
	RV Primer	CACAAGCGGCCAGAATTGG	19	62
Ctnnb1	FWD Primer	ATGGAGCCGGACAGAAAAGC	20	63
	RV Primer	CTTGCCACTCAGGGAAGGA	19	61
MCL1 P3	FWD Primer	CAAAGATGGCGTAACAAACTGG	22	60
	RV Primer	CCGTTTCGTCCTTACAAGAACA	22	61
CenpQ	FWD Primer	AATGTGCAACACTGAAAGTCCC	22	61
	RV Primer	ATTCTGGTTTGGAATTAGTGCCA	23	60

Microarray analysis

Microarray background subtraction was carried out using normexp method. To normalize the dataset, we performed loess within arrays normalization and quintiles between arrays normalization. Differentially expressed genes were obtained by applying linear models with R limma package (Smyth GK) (Bioconductor project, http://www.bioconductor.org). To account for multiple hypotheses testing, the estimated significance level (p value) was adjusted using Benjamini & Hochberg False Discovery Rate (FDR) correction. Those genes with FDR <0.05 were selected as differentially expressed between controls and tumors.

Gene set enrichment analysis

Gene set enrichment analysis (GSEA) was applied using annotations from Biocarta, KEGG, NCI pathways and Reactome. Genes were ranked based on limma moderated t statistic. After Kolmogorov-Smirnoff testing, those gene sets showing FDR <0.05, a well-established cut-off for the identification of biologically relevant gene sets (Subramanian et al., 2005), were considered enriched between classes under comparison.

Flow cytometry

Cells were isolated from mouse lungs of both groups AAV9-*Tert* and AAV9-empty vector. Lungs were extracted and introduced in HBBS buffer with antibiotic and 1% BSA. Separate the lobules of the lung on a dish mince them with a scalpel. Transfer them to a GentleMacs tube with HBBS, antibiotics,, 1% BSA, DNAse I (60 units/mL) (Sigma, DN25) and collagenase type I (70 units/mL) (GIBCO, Cat. Number 17100). Then we run the GentleMac program “lung 1”, after the program incubate the sample at 37ºC for 30 minutes and at the end we run the GentleMac program “lung 2”. Cell suspension was filtered through a 40µm strainer and then centrifuge 1200 rpm 5 min. Cells were resuspended in 2 mL ACK Lysis Buffer to lyse red blood cells. Incubated for 4 min. at room temperature. We added DMEM without serum to wash, centrifuged cells and discarded the supernatant. Cells were resuspended in PBS with EDTA (1mM), Hepes (25 mM) and 3% FBS and stained with LysoTracker as described in commercial protocol (Molecular Probes, LysoTracker Green DND-26, Cat. Num. L7526) and the following antibodies from Pharmingen (BD Biosciences, San Jose CA): PE anti-mouse CD45, PE anti-mouse CD31, APC anti-mouse EpCAM. DAPI (Sigma, St Louis MO)

was used to identify dead cells. Data was collected and the defined populations (CD45-CD31-EpCAM+ LysoTracker+ and LysoTracker-) were sorted using an InFlux cell sorted (BD, San Jose CA), we excluded cell aggregates by using pulse processing in the scatter signals and dead cells in the basis of DAPI staining. All data was analyzed using FlowJo software v9.8.5 (Treestar, Ahsland OR).

Statistical analysis

An unpaired t-student test was used to calculate statistical significance of p21, p53, p19, C3a and γH2AX markers by immunohistochemistry and interstitial fibrosis by Sirius red staining. A Log Rank test was used to calculate the statistical differences in the survival curves of the different mice cohorts.

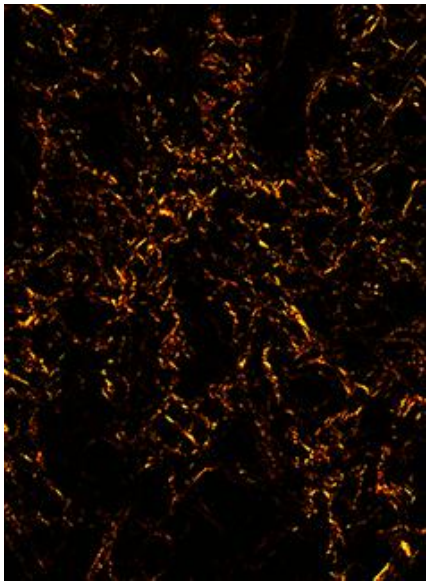

Results

Generation of *Trf1* conditional knock-out mouse model

To generate a *Trf1* conditional knock-out mouse model we took advantage of previous work from our lab (Martinez et al., 2009). The *Trf1*$^{flox/flox}$ locus contains two *loxP sites* flanking the exon 1 of the gene (**Fig. 5**). Mice were crossed with a mouse strain carrying an inducible *Cre*^{ERT2} recombinase that is expressed under the control of surfactant protein C promoter (*Sftpc*), a specific marker for ATII cells (**Fig. 5**). This Cre recombinase is fused to an estrogen receptor (ERT2) which sequesters Cre into the cytoplasm until an agonist is provided (i.e., tamoxifen) and relocates Cre into the nucleus, where it can produce direct recombination. We also introduced a fluorescence reporter gene to control Cre activity and to identify cells undergoing *Trf1* deletion. In particular, transgenic mice harboring the katushka fluorescence protein (KFP) whose expression is regulated by a transcriptional stop cassette flanked by *loxP* sequences *KFP*$^{CAG\text{-}lox\text{-}STOP\text{-}lox}$ were used (Dieguez-Hurtado et al., 2011) (**Fig. 5**). Upon intraperitoneal injection of tamoxifen (TMX) we induced Cre relocation and the subsequent TRF1 abrogation and KFP expression specifically in ATII cells.

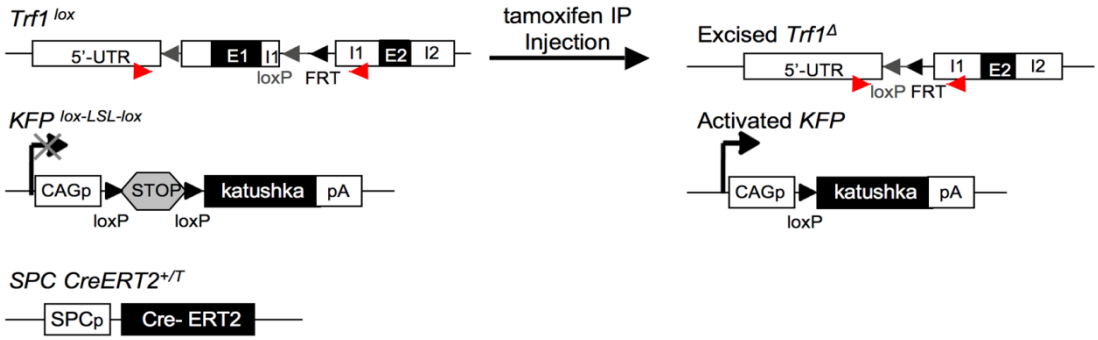

Figure 5. Genetic mouse model. *Trf1*$^{lox/lox}$, *KFP* $^{Lox\text{-}STOP\text{-}Lox}$ and *SPC-Cre*^{ERT2} alleles are depicted before and after Cre-mediated excision.

Trf1 deletion in the lung induces pulmonary fibrosis and decreases mouse survival

First, we validated the model by inducing Cre^{ERT2} activation by intraperitoneal TMX administration three times per week (**Fig. 6A**). After two weeks of tamoxifen-treatment, we quantified the amount of KFP positive cells in the lungs of *Trf1*$^{lox/lox}$ *SPC-Cre*^{ERT2} *KFP*$^{lox\text{-}STOP\text{-}lox}$ mice and of *Trf1*$^{+/+}$ *SPC-Cre*^{ERT2} *KFP*$^{lox\text{-}STOP\text{-}lox}$ control mice by immunohistochemistry. In both genotypes, we found that 1 week after TMX treatment approximately 14% of the total lung cells were KFP positive (**Fig. 6B;** see also **Fig. 10A**) what is in agreement with the previously reported abundance of ATII cells

(12-15%) in whole lung cell population (Dobbs, 1990; Van der Velden et al., 2013). We next confirmed *Trf1* deletion in the lungs of *Trf1*$^{lox/lox}$ *SPC-Cre*^{ERT2} *KFP*$^{lox\text{-}STOP\text{-}lox}$ mice by PCR amplification of the *Trf1*$^{\Delta/\Delta}$ alleles (**Fig. 6C**). In addition, triple immunofluorescence staining against SPC, KFP and TRF1 clearly demonstrated that the totality of the SPC positive cells were also KFP positive, as well as these cells stained negative for TRF1 in the lungs of *Trf1*$^{lox/lox}$ mice (**Fig. 6D,E**). These results indicate efficient Cre expression in ATII cells and *Trf1* deletion in the lungs of *Trf1*$^{lox/lox}$ *SPC-Cre*^{ERT2} *KFP*$^{lox\text{-}STOP\text{-}lox}$ mice.

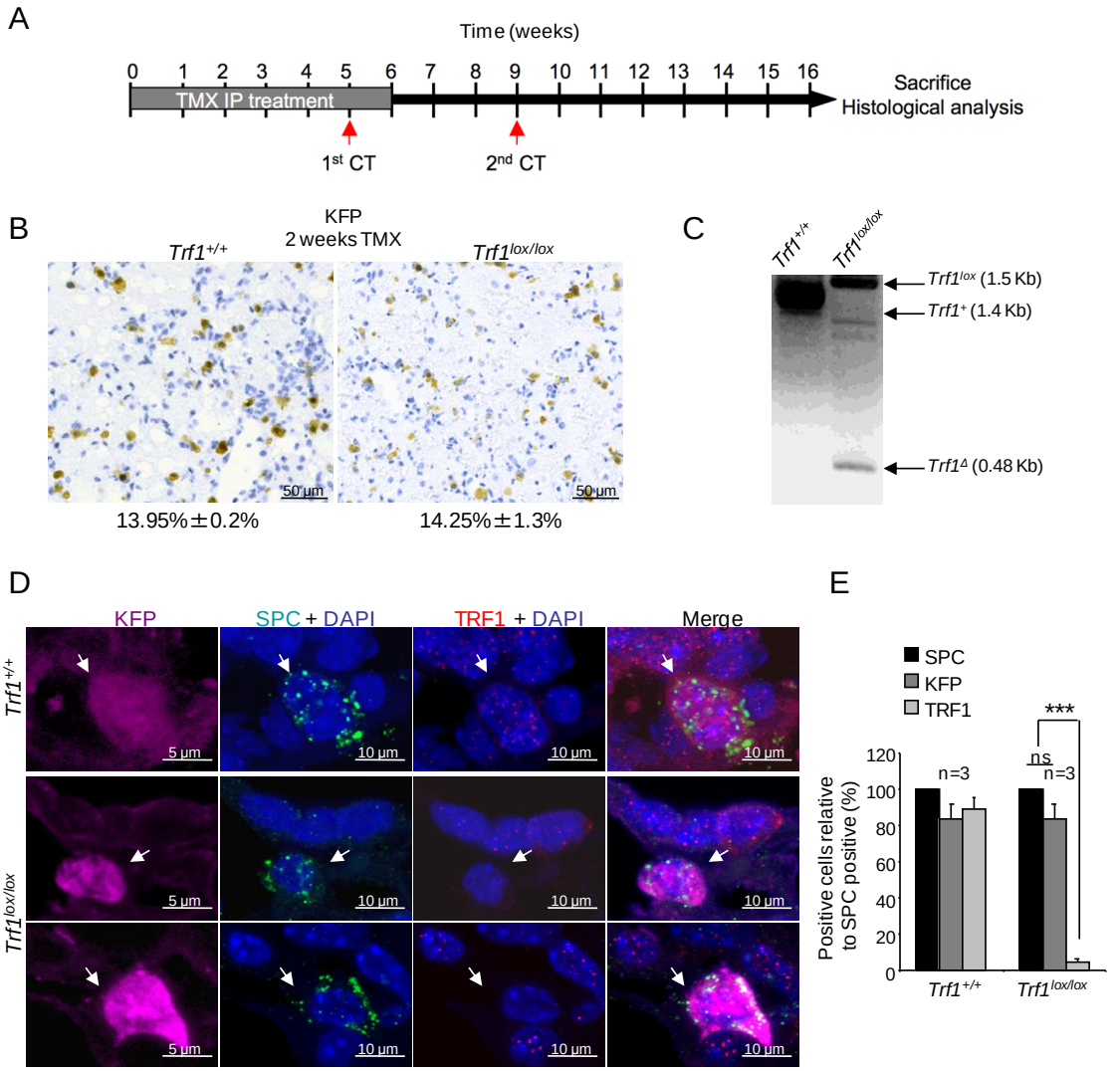

Figure 6. Efficient *Trf1* deletion in alveolar type II cells upon tamoxifen administration. (A) Intraperitoneal TMX treatment and *in vivo* imaging schedule. 8-10 week old mice were IP injected with TMX three times a week during six consecutive weeks. At week 5 and 9 from the beginning of the TMX treatment, mice were analyzed by computerized tomography (CT) and at week 16 the remaining alive mice were sacrificed for histological analysis. **(B)** Representative images of immunohistochemistry for KFP staining of *Trf1*$^{+/+}$ *SPC-Cre-*^{ERT2} *KFP*$^{CAG\text{-}lox\text{-}STOP\text{-}lox}$ and *Trf1*$^{flox/flox}$ *SPC-Cre*^{ERT2} *KFP*$^{CAG\text{-}lox\text{-}STOP\text{-}lox}$ lung sections after one week of TMX treatment. The percent of KFP positive cells with regards to the total lung cell population is indicated. **(C)** Analysis of *Trf1* excision by PCR in lung samples. Notice that lung cell

populations that are not alveolar type II give rise to *TRF1*^{lox} allele amplification. **(D)** Representative images of triple immunofluorescence staining of KFP (purple), SPC (green) and TRF1 (red) in *Trf1*$^{+/+}$ *SPC-Cre*^{ERT2} *KFP*$^{CAG\text{-}lox\text{-}STOP\text{-}lox}$ and *Trf1*$^{flox/flox}$ *SPC-Cre*^{ERT2} *KFP*$^{CAG\text{-}lox\text{-}STOP\text{-}lox}$ lung sections after two weeks of TMX treatment. **(E)** Quantification of the percent KFP and TRF1 positive cells with regards to SPC positive cells.

Interestingly, 4 to 8 weeks after TMX treatment, we observed that 42% of the TRF1-deficient mice of both genders (this increased up to 65% in male mice) showed an abnormal CT pattern compatible with fibrosis, while none of the wild-type animals showed this CT pattern (**Fig. 7A,B**). This abnormal radiological pattern is characterized by presence of reticular opacities with honeycombing, also typically found in human pulmonary fibrosis patients (**Fig. 7A**) (Ryu et al., 2014). Notably, the radiologic lesions detected by CT occupied the large majority of the lungs (up to 100% of the lung area), indicative of very severe lesions (**Fig. 7C**). In agreement with this severity, TRF1-deficient mice showing these lesions had to be sacrificed during the first 8 weeks after the TMX treatment owing to severe respiratory defects, i.e. laboured and heavy breathing, leading to a significantly decreased survival compared to the wild-type mice (**Fig. 7D**).

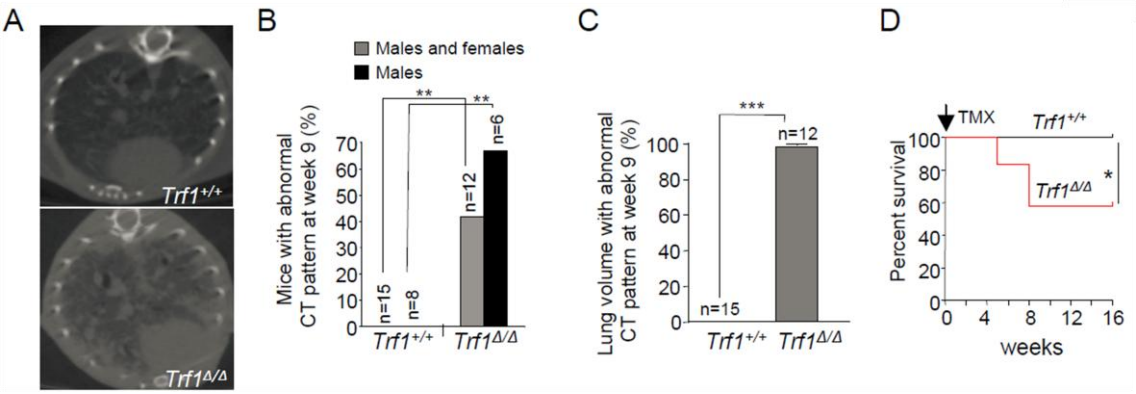

Figure 7. *Trf1* deletion in ATII cells provokes abnormal CT pattern in lungs and affects mouse survival within 8 weeks. (A) Representative CT images of *Trf1*$^{+/+}$ and affected *Trf1*$^{\Delta/\Delta}$ lungs. **(B)** Percent of mice of both genders or only males with abnormal CT pattern at week 9 post beginning of TMX treatment. χ^2 test was used for statistical analysis. **(C)** Quantification of the affected lung volume. T-test was used for statistical analysis. **(D)** Survival curve of *Trf1*$^{+/+}$ (n=15) and *Trf1*$^{\Delta/\Delta}$ (n=12) mice. Log-Rank test was used for statistical analysis of survival curve.

To confirm pulmonary fibrosis as the cause of abnormal radiological pattern observed in TRF1-depleted lungs, we performed full histopathology of the lungs upon mouse sacrifice. As pulmonary fibrosis is characterized by formation of fibrotic scars, we determined the presence of collagen fiber deposits by using Masson´s trichrome

staining (Methods). We observed that more than 40% of the TRF1-deficient mice of both genders and 65% of male mice showed pathological findings characteristic of pulmonary fibrosis (**Fig. 8A,B**). In particular, these mice showed extensive pneumonia (between 40-50% of the lung parenchyma affected), inflammatory infiltrates consisting mainly of macrophages with hemosiderin content indicative of traumatic haemorrhage and intense inflammation that were absent in wild-type lungs (**Fig. 8A**). In agreement with human findings, we also detected increased presence of macrophage infiltrates and the activation of an inflammatory response as indicated by specific staining against F4/80 and against interleukin 6, respectively (**Fig. 8A**). Deposition of collagen fibers is also visualised by Sirius red staining using polarized light for detection (Methods) (Broytman et al., 2015). We detected six-fold higher amount of collagen fibers in the *Trf1* deleted fibrotic lungs compared to the wild-type controls (**Fig. 8C,D**). This was also confirmed by higher collagen expression levels in TRF1-depleted lungs (**Fig. 8E**). In addition, we also observed increased number of α-smooth muscle actin (αSMA) positive myofibroblast, which have been associated to fibrotic foci (Zhang et al., 1996) (**Fig. 8F,G**). Together, these findings confirm extensive fibrosis as the consequence of TRF1 depletion in ATII cells.

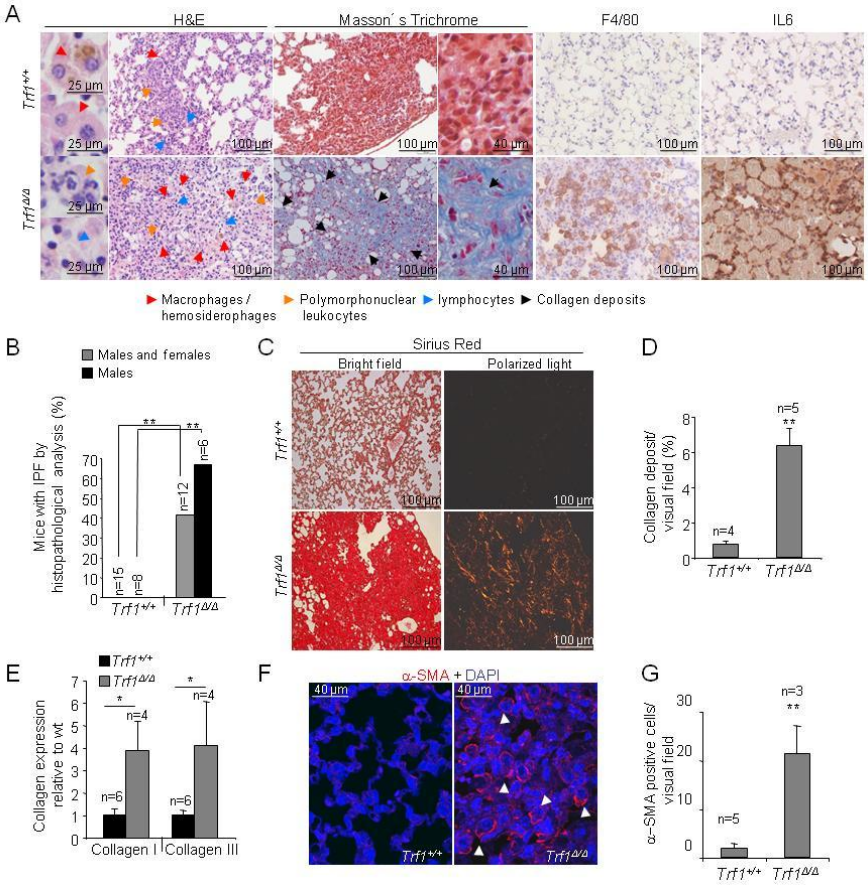

Figure 8 (previous page). Histopathological confirmation of pulmonary fibrosis and inflammatory phenotype in affected *Trf1* $^{\Delta/\Delta}$ mice. (A) Representative hematoxylin & eosin, Masson's trichrome, F4/80 and interleukin 6 staining images of *Trf1*$^{+/+}$ and affected *Trf1*$^{\Delta/\Delta}$ lungs. Different types of infiltrates; macrophages and hemosiderophages (red arrow heads), polymorphonuclear leukocytes (orange arrow heads), lymphocytes (blue arrow heads) and collagen deposits (black arrow heads) are indicated. Amplification of Masson's trichrome images is shown. **(B)** Percentage of mice of both genders or only males diagnosed with pulmonary fibrosis by histopathological analysis. T-test was used for statistical analysis **(C)** Representative images of *Trf1*$^{+/+}$ and affected *Trf1*$^{\Delta/\Delta}$ lung sections stained with Sirius red and visualized by bright field and polarized light where collagen fibers are bright orange. **(D)** Percent of lung area filled with collagen fibers. **(E)** Transcriptional levels of collagen expression of collagen in *Trf1*$^{+/+}$ and affected *Trf1*$^{\Delta/\Delta}$ lungs. **(F-G)** Representative image and quantification of αSMA positive myocytes staining.

Trf1 deletion in alveolar type II cells leads to cell death without inducing telomere length changes in lung cells

We investigated the underlying molecular consequences of *Trf1* deletion in the lung that trigger the disease. First, we considered the hypothesis that TRF1 deficiency may lead to decreased telomere length by forcing extra proliferation of the remaining non-deleted *Trf1* lung epithelial cells. In particular, we recently described that *Trf1* deletion in the bone marrow led to depletion of the stem cell compartment and to extra proliferation of the remaining non-deleted *Trf1* progenitor cells, leading to very rapid telomere shortening in the bone marrow (Beier et al., 2012). To this end, we performed Q-FISH directly on lung sections (Methods). However, we did not observe differences either in the mean telomere fluorescence intensity or in the mean nuclear telomere fluorescence between tamoxifen treated *Trf1*$^{lox/lox}$ *SPC-Cre*^{ERT2} *KFP*$^{lox\text{-}STOP\text{-}lox}$ mice and wild-type controls (**Fig. 9A-B,E**). Similarly, we did not see increased frequency of telomere spots with low fluorescence (<50 and <60 arbitrary units of fluorescence) corresponding to the 10th and 20th percentile of the wild-type telomere fluorescence distribution in the *Trf1*-deficient lungs, which are indicative of presence of very short telomeres (**Fig. 9C-E**). These results are in agreement with the fact that lung is a low proliferative compartment with a cell turnover estimated to be less than 2% per week in alveolar epithelial cells (Alder et al., 2011).

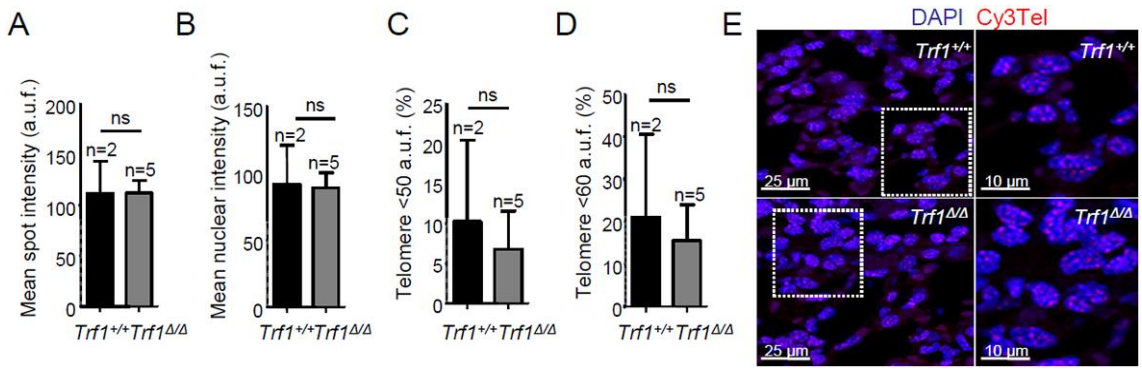

Figure 9. *Trf1* deletion in alveolar type II cells does not induce telomere length changes in lung cells. (A-D) Individual mean telomere length (A), total mean nuclear telomere length (B), percent of short telomeres <50 a.u.f corresponding to 10th percentile of wild-type telomere distribution (C) and percent of short telomeres < 60 a.u.f. corresponding to 20th percentile of wild-type telomere distribution (D) in *Trf1*$^{+/+}$ and *Trf1*$^{\Delta/\Delta}$ lungs. **(E)** Representative images of telomere Q-fish analysis.

Interestingly, we observed that the initial amount of KFP-positive cells (15% for both genotypes) dramatically decreased in *Trf1* deleted lungs compared to wild-type lungs around 6 to 8 weeks after TMX treatment (**Fig. 10A,D**), which strongly suggests elimination of ATII cells as a consequence of *Trf1* deletion. Indeed, at death point, while *Trf1* wild-type lungs showed a 12% of cells being KFP-positive corresponding to the totality of ATII cells (Dobbs, 1990; Van der Velden et al., 2013), *Trf1*-deleted fibrotic lungs presented less than 5% of ATII cells indicating that two third of these cells have been eliminated in the course of the experiment (**Fig. 10A,D**).

Abrogation of TRF1 in proliferative tissues such as the stratified epithelia induces telomeric DNA damage and a rapid DNA damage response characterized by the activation of p53/p21 pathways (Martinez et al., 2009). Thus, we set to investigate these pathways in the lung. Immunohistochemistry analysis of lung sections readily revealed that TRF1-depleted ATII cells presented a significant increase in the amount of p53 and p21 positive cells, indicative of cellular senescence (**Fig. 10B-D**). The number of p21 positive cells relative to KFP positive cells was progressively increasing throughout the course of the experiment. Further supporting the induction of cellular senescence, we also detected increased numbers of the p19 protein in TRF1-depleted lungs (**Fig. 10C-D**) (Collado et al., 2007). In addition, we also detected increased numbers of cells positive for active caspase 3 (C3a) in TRF1-depleted lungs, indicative of apoptosis (**Fig. 10C-D**). Thus, both senescence and apoptosis are induced as the consequence of TRF1 ablation in ATII cells.

Double immunofluorescence staining against γH2AX and TRF1 antibodies showed a significant progressive increase in the number of γH2AX-positive damaged cells reaching 10% of the total lung cell population at 6-8 weeks after the beginning of TMX treatment (**Fig. 10E-F**). Those cells were negative for TRF1 staining demonstrating that TRF1 abrogation results in telomeric DNA damage (**Fig. 10E-F**). Given that wild-type lungs did not show damaged cells (<1% of total lung cells) and that the percent of damaged cells out of the total lung cells in *Trf1*-deleted lungs (10%) correspond approximately with the number of the totality of alveolar type ATII cells (10-15%) (Dobbs, 1990; Van der Velden et al., 2013), our observations suggests that at least 90% of the total alveolar type II cells lacking TRF1 show DNA damage. This increase in γH2AX positive cells could also be a consequence of the anticipated inflammatory response observed in *Trf1*-deficient lungs (**Fig. 8A**).

In summary, these findings demonstrate that acute telomere dysfunction in lung epithelial cells, such as that triggered by abrogation of the TRF1 shelterin component in ATII cells, is sufficient to rapidly induce massive pulmonary fibrosis in mice through induction of DNA damage, p21/p53 cell cycle inhibitors, and elimination of ATII cells. Thus, we have generated a mouse model that develops IPF induced by telomere dysfunction and in the absence of additional damaging agents. These findings also highlight the involvement of ATII cells in the development of pulmonary fibrosis.

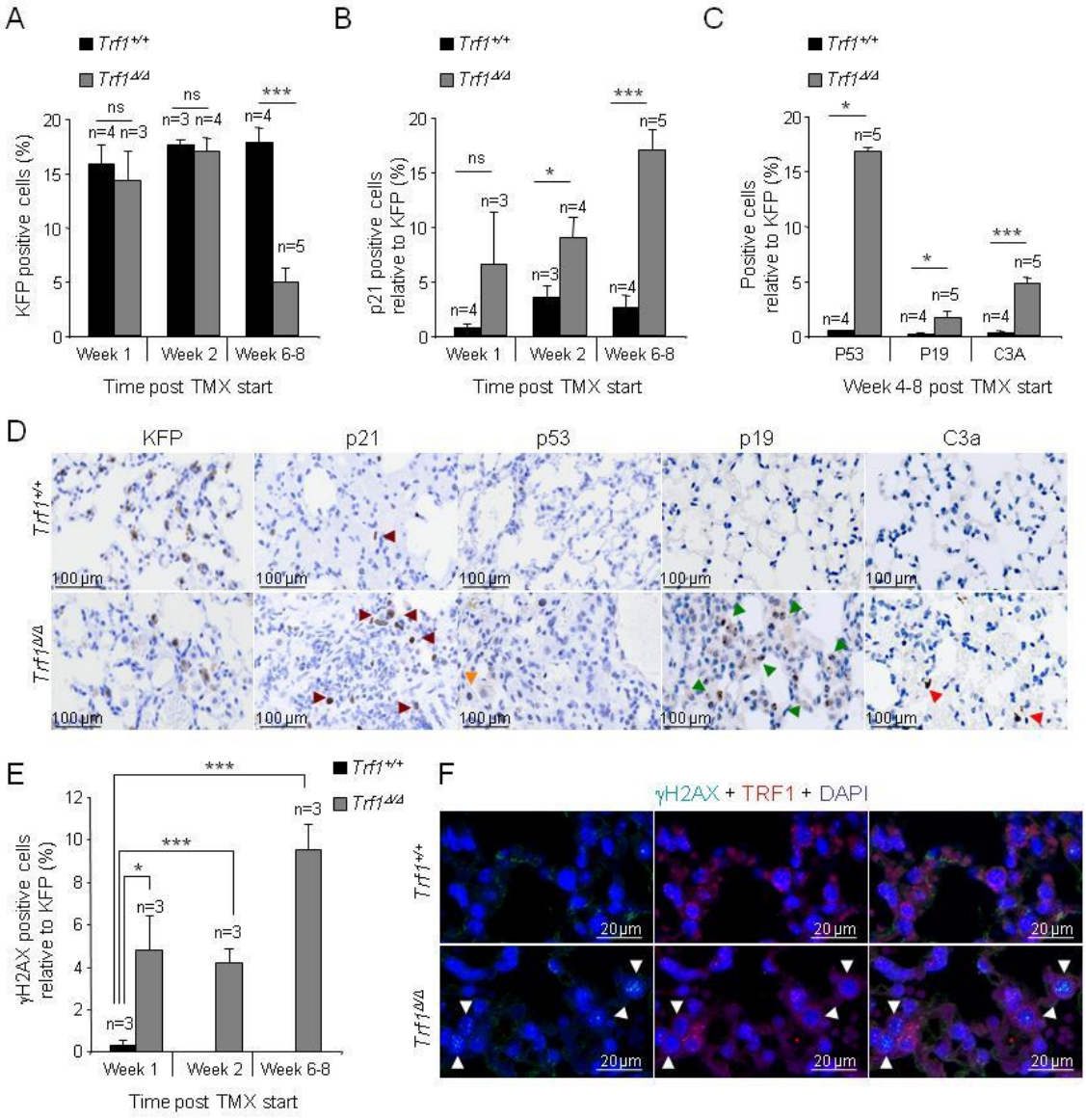

Figure 10. *Trf1* deletion in ATII cells leads to cell death. (A) Quantification of KFP positive cells in *Trf1*$^{+/+}$ and *Trf1*$^{\Delta/\Delta}$ lungs after 1, 2 and 6-8 weeks from the beginning of the tamoxifen (TMX) treatment. **(B)** Quantification of p21 positive cells in *Trf1*$^{+/+}$ and *Trf1*$^{\Delta/\Delta}$ lungs after 1, 2 and 6-8 weeks from the beginning of the TMX. **(C)** Quantification of p53, p19 and C3a positive cells in *Trf1*$^{+/+}$ and *Trf1*$^{\Delta/\Delta}$ lungs after 4-8 weeks from the beginning of the TMX treatment. **(D)** Representative images of KFP (black arrow heads), p21 (purple arrow heads), p53 (orange arrow heads), p19 (green arrow heads) and C3a (red arrow heads) immunohistochemistry analysis of *Trf1*$^{+/+}$ and *Trf1*$^{\Delta/\Delta}$ lungs at 6-8 weeks after the beginning of TMX treatment. **(E)** Quantification of γH2AX positive cells in *Trf1*$^{+/+}$ after 1 week TMX treatment and in *Trf1*$^{\Delta/\Delta}$ lungs after 1, 2 and 6-8 weeks from the beginning of the TMX treatment. **(F)** Representative images of double immunofluorescence against γH2AX and TRF1 in *Trf1*$^{+/+}$ and *Trf1*$^{\Delta/\Delta}$ lungs after 6-8 weeks from the beginning of the TMX treatment. Notice that γH2AX positive cells stain negative for TRF1 in *Trf1*$^{\Delta/\Delta}$ lung sections (white arrow heads). p21, p53 and γH2AX positive cells in B, C and E are normalized to the number of KFP positive cells.

A low bleomycin dose synergizes with short telomeres to trigger pulmonary fibrosis

As pulmonary fibrosis induced by *Trf1* deletion does not lead to short telomeres, which are characteristic of familiar and sporadic case of human IPF, we next set to develop a mouse model for IPF based on telomerase deficiency and short telomeres. This mouse model may recapitulate the short telomere phenotype of human patients. However, previous reports showed that mice deficient for the telomerase RNA component *Terc* (*Terc*$^{-/-}$), which lack telomerase activity, do not develop IPF. Even when these mice are subjected to additional cellular damaging agents like cigarette smoke, emphysema is the only pulmonary pathology that develops (Alder et al., 2011).

Bleomycin is widely used to induce acute pulmonary fibrosis in mice (Mouratis and Aidinis, 2011). In particular, intratracheal inoculation in wild-type mice with a single 2.5 g/kg body weight (BW) dose of bleomycin, leads to development of severe fibrotic lesions in the lung as early as two weeks post-inoculation. However, these lesions do not progress in time and many of them sporadically regress after 4-5 weeks after bleomycin inoculation, most likely owing to lung regeneration by the non-affected cells (Mouratis and Aidinis, 2011). This fact has been an important shortcoming for the use of bleomycin-induced pulmonary fibrosis mouse models for development of new treatments.

To recapitulate the short telomeres phenotype in IPF development in humans, during following experiment of this Thesis, we used a low dose of bleomycin which is not sufficient to induce pulmonary fibrosis in wild-type mice but may synergize with short telomeres in the context of telomerase-deficient mice (Blasco et al., 1997) (**Fig. 11A-C**). To determine the highest bleomycin dose that does not induce pulmonary fibrosis in wild-type mice, we subjected wild-type mice to 2.5 mg/kg BW, 1 mg/kg weight, 0.5 mg/kg BW and 0.1 mg/kg BW of bleomycin. We found that the maximum dose that did not induce pulmonary fibrosis in wild-type mice was 0.5 mg/kg BW (**Fig. 11C**). Thus, we selected this low dose of bleomycin for further experiments. In particular, we subjected G2 and G4 *Tert*$^{-/-}$ mice as well as wild-type mice as controls, to 0.5 mg/kg BW of bleomycin and followed by CT (**Fig. 11B**).

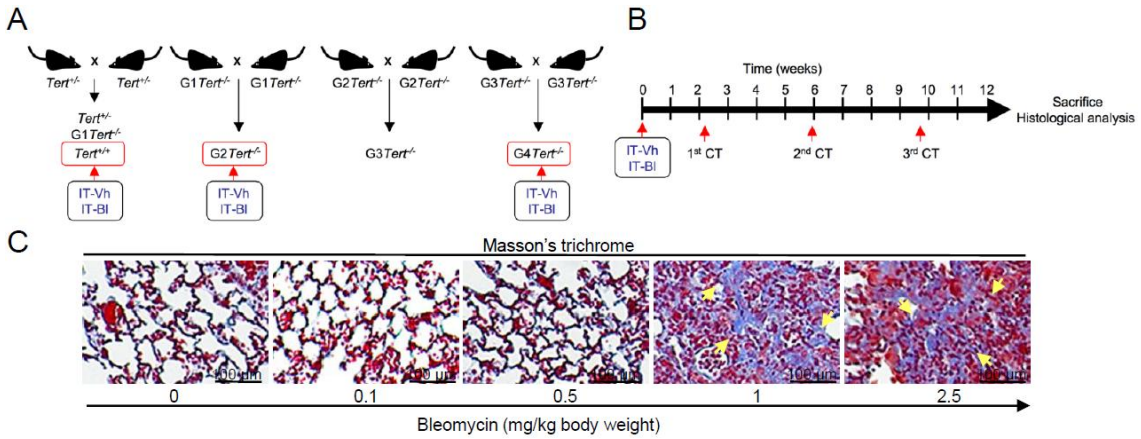

Figure 11. Bleomycin dose titration in wild-type mice that does not trigger pulmonary fibrosis. (A) Heterozygous *Tert*$^{+/-}$ mice were intercrossed to generate *Tert*$^{+/+}$ and G1*Tert*$^{-/-}$ mice. Successive crosses between G1*Tert*$^{-/-}$ and between G3*Tert*$^{-/-}$ were set to generate *G2 Tert*$^{-/-}$ and G4*Tert*$^{-/-}$ cohorts, respectively. 8-10 week old *Tert*$^{+/+}$, G2*Tert*$^{-/-}$ and G4*Tert*$^{-/-}$ mice were intratracheally inoculated either with vehicle (PBS) (IT-Vh) or with 0.5 mg/kg BW bleomycin (IT-Bl). **(B)** *in vivo* follow-up of different mouse cohorts. At week 2, 6, and 10 mice were analyzed by computerized tomography (CT) and at week 12 mice were sacrificed for histological analysis. **(C)** Determination of the maximum bleomycin dose that does not induce pulmonary fibrosis in wild-type mice. Representative image of wild-type lung sections two weeks after intratracheal inoculation of bleomycin at a dose of either 2.5mg/kg BW, 1 mg/kg BW, 0.5 mg/kg BW, 0.1 mg/kg BW or 0.0 mg/kg BW.

Two to four weeks after inoculation with a low dose of bleomycin, we observed that 30% and 25% of G2 and G4 *Tert*$^{-/-}$ mice, respectively, in contrast to 10% of wild-type control mice presented abnormal radiological images of the lung (**Fig. 12A-B**). When only males were taken into account, we observed that 50% and 45% of G2 and G4 *Tert*$^{-/-}$ mice, respectively, compared to 20% of wild-type control mice presented abnormal radiological images of the lung, indicating a tendency towards more *Tert*$^{-/-}$ males than females presenting abnormal CT patterns (**Fig. 12A-B**). Interestingly, we noted that these abnormal CT pattern disappeared with time in the case of wild-type mice, indicating that they could correspond to an inflammatory reaction trigger by bleomycin inoculation. In contrast, after 10 weeks both G2 and G4 *Tert*$^{-/-}$ mice were still showing an abnormal CT pattern, and lesions were approximately 50% of the affected initial lung volume (**Fig. 12C-D**).

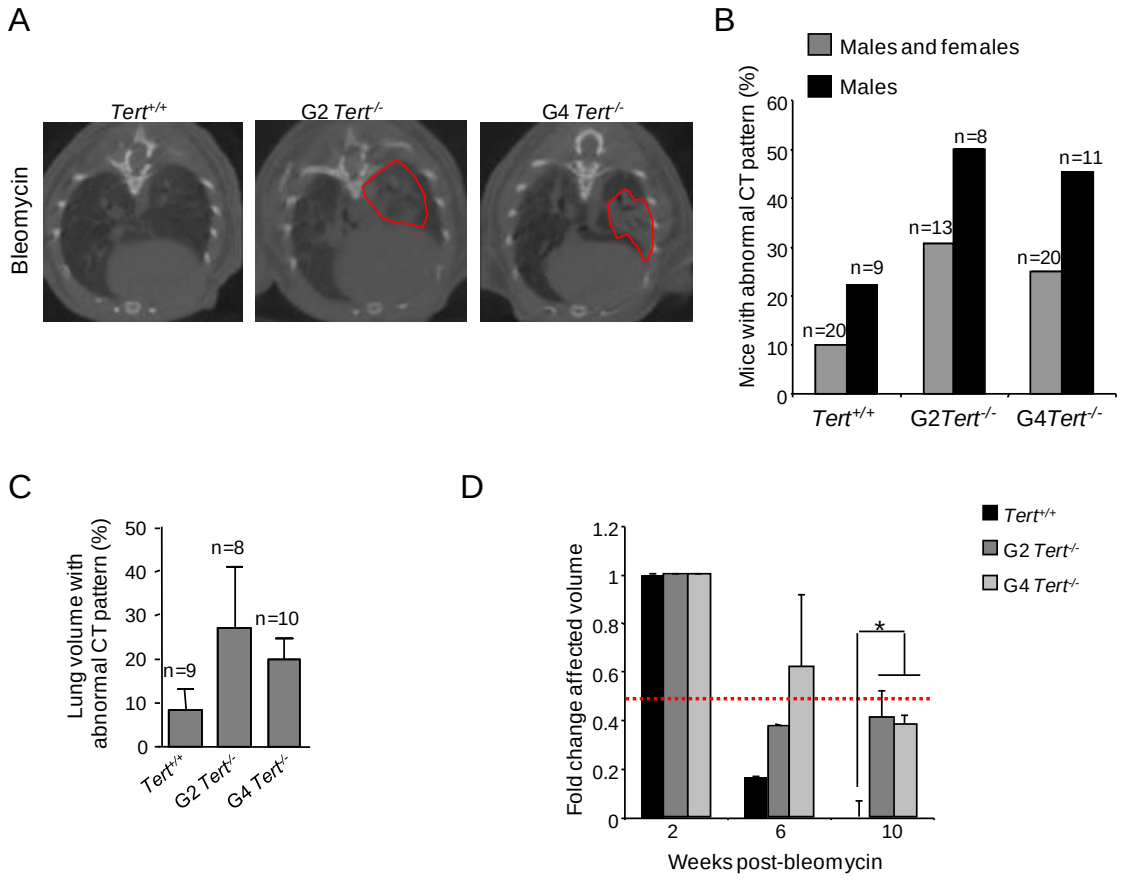

Figure 12. Bleomycin low dose provokes abnormal CT pattern with a higher impact for G2 and G4 *Tert*$^{-/-}$. (A) Representative CT images of wild-type, G2 and G4 *Tert*$^{-/-}$ lungs. **(B)** Percentage of mice of both genders or only males with abnormal CT pattern at 10 weeks after bleomycin inoculation. **(C)** Quantification of the abnormal lung volume of affected mice. **(D)** Longitudinal study of affected lung volume behavior in the three groups of study. T-test was used for statistical analysis.

To confirm the presence of lung disease, we performed full histopathological analysis of the lungs from four to ten weeks post-inoculation, using Masson´s trichrome staining to visualize fibrotic areas. Strikingly, 50-25% of G2 and G4 *Tert*$^{-/-}$ mice subjected to low dose of bleomycin presented with chronic multifocal pneumonia and extensive moderate fibrosis, while none of the vehicle-inoculated G2 and G4 *Tert*$^{-/-}$ male mice, and none of the examined wild-type mice (both bleomycin and vehicle-inoculated) showed lung fibrosis (**Fig. 13A-B**). As observed in the *Trf1*-deficient model, we observed a gender bias towards more males than females showing pulmonary fibrosis. In addition, macrophage infiltrates and the induction of an inflammatory response, as determined by F4/80 and interleukin 6 stainings, respectively, were readily revealed in G2 *Tert*$^{-/-}$ and G4 *Tert*$^{-/-}$ lungs inoculated with bleomycin. Both markers were absent in wild-type controls (**Fig. 13C**). These findings were further validated by determination of collagen fiber deposition using Sirius red staining visualized by polarized light, which

revealed approximately 3-fold increase in collagen deposition in the bleomycin-inoculated G2 and G4 *Tert*$^{-/-}$ mice compared to vehicle inoculated controls or to wild-type mice (both bleomycin and vehicle-inoculated) (**Fig. 13D-E**). Higher collagen expression levels were also confirmed by RT-PCR in the bleomycin-inoculated *Tert*-deficient lungs compared to bleomycin-inoculated wild-type lungs (**Fig. 13F**). Furthermore, we detected increased numbers of αSMA positive myofibroblast in telomerase-deficient mice inoculated with bleomycin, which are indicative of lung fibrosis (Zhang et al., 1996) (**Fig. 13G-H**).

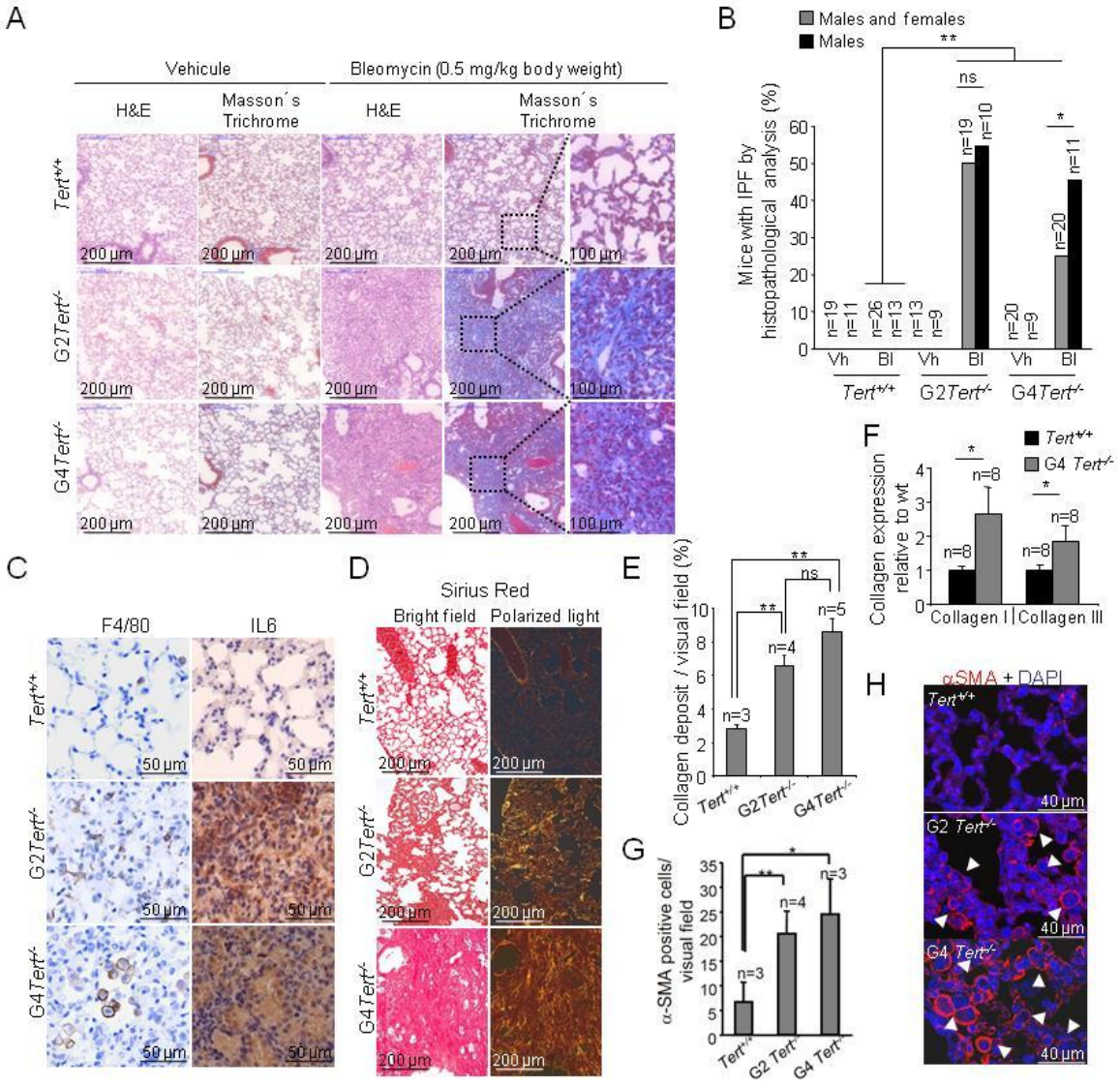

Figure 13. Low bleomycin dose synergizes with short telomeres to trigger pulmonary fibrosis. **(A)** Representative hematoxylin & eosin and Masson's trichrome staining images of *Tert*$^{+/+}$, G2*Tert*$^{-/-}$ and G4 *Tert*$^{-/-}$ mice inoculated with either vehicle or 0.5 mg/kg BW bleomycin. To the right, amplification Masson's trichrome images are shown. **(B)** Percentage of mice of either genders or only males diagnosed with pulmonary fibrosis by histopathological analysis. **(C-D)** Representative images of *Tert*$^{+/+}$, G2*Tert*$^{-/-}$ and G4*Tert*$^{-/-}$ lung sections inoculated with 0.5 mg/kg BW bleomycin stained against F4/80 and Interleukin 6

(C), and Sirius red visualized by bright field and polarized light where collagen fibers are bright orange (D). **(E)** Percent of lung area filled with collagen fibers. **(F)** Transcriptional levels of collagen expression in *Tert*$^{+/+}$, G2*Tert*$^{-/-}$ and G4*Tert*$^{-/-}$ bleomycin treated lungs. **(G-H)** Quantification of αSMA positive myofibroblasts (G) and representative images of wild-type, G2 *Tert*$^{-/-}$ and G4 *Tert*$^{-/-}$ lungs treated with bleomycin (H).

The presence of pulmonary fibrosis in the bleomycin-inoculated *Tert*$^{-/-}$ mice, G2 and G4 *Tert*$^{-/-}$ mice are concomitant with the significantly altered respiratory parameters when subjected to spirometry compared with their corresponding vehicle-inoculated controls or to treated wild-type mice (Methods). In particular, prior to sacrifice G2 *Tert*$^{-/-}$ mice showed significantly decreased tidal volume, inhaled minute volume, and expiration influx compared to their corresponding vehicle-inoculated controls or to both bleomycin and vehicle-inoculated wild-type mice (**Fig. 14A-C**).

To further investigate whether pulmonary fibrosis and lung function impairment in G2 and G4 *Tert*$^{-/-}$ mice was accompanied by presence of short telomeres, we performed telomere Q-FISH directly on lung sections (Methods). As expected, G2 and G4 *Tert*$^{-/-}$ mice showed significantly lower mean telomere fluorescence as well as a lower mean telomere nuclear intensity compared with wild-type controls. In addition, we observed higher percentage of telomeres showing low fluorescence (<20 and <25 arbitrary units of fluorescence, corresponding to 10th and 20th percentile of the G2 *Tert*$^{-/-}$ telomere distribution) in G2 and G4 *Tert*$^{-/-}$ cohorts compared with wild-type mice (**Fig. 14D-H**). Interestingly, inoculation with low dose of bleomycin did not affect either mean telomere fluorescence or the percent of telomeres with low fluorescence in wild-type mice, indicating that this cellular damaging agent does not provoke telomere shortening (**Fig. 14D-H**). Bleomycin-inoculated G2 and G4 *Tert*$^{-/-}$ mice showed a tendency to lower telomere fluorescence than the untreated controls, most likely as the consequence of additional cell divisions to regenerate the damage lung in the absence of telomerase, but this trend did not reach statistical significance (**Fig. 14D-H**). These results indicate that development of pulmonary fibrosis in G2 and G4 *Tert*$^{-/-}$ mice inoculated with a low dose of bleomycin require the presence of short telomeres, as inoculated wild-type mice do not develop the disease. These results also suggest that the feature of having short telomeres is not sufficient for disease onset, and requires of additional damage in mice (i.e., bleomycin inoculation). Our results are in line with human findings showing that damaging agents such as smoking increases the risk of developing pulmonary fibrosis associated with aging or with telomerase mutations (Armanios, 2013).

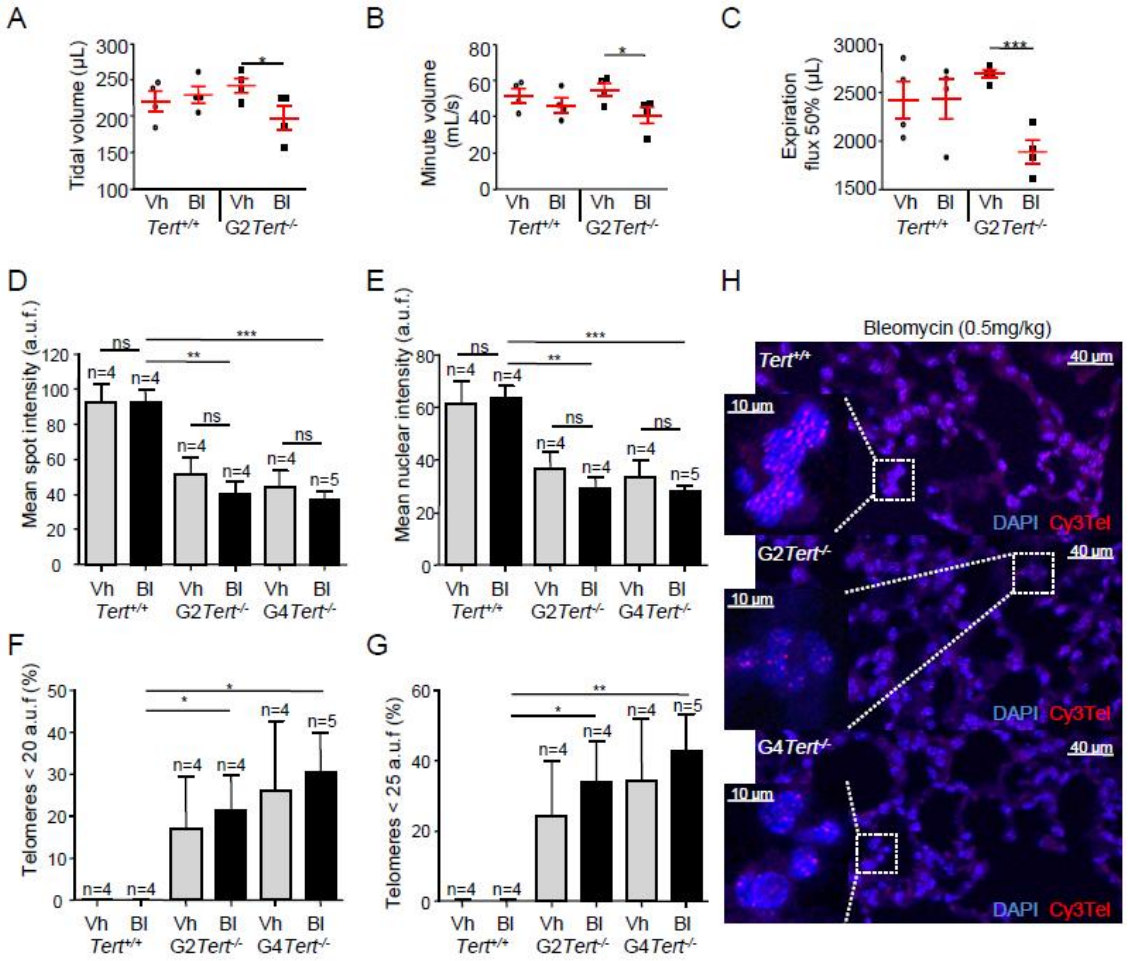

Figure 14. Decreased pulmonary capacity and telomere shortening in lung tissues of telomerase deficient mice. (A-C) Analysis of tidal volume (A), minute volume (B) and expiration flux at 50% (C) in *Tert*$^{+/+}$ and G2*Tert*$^{-/-}$ mice inoculated with either vehicle or with 0.5 mg/kg BW bleomycin. **(D-G)** Individual mean telomere length (D), total mean nuclear telomere length (E), percent of short telomeres <20 a.u.f corresponding to 10th percentile of G2 *Tert*$^{-/-}$ telomere distribution (E) and percent of short telomeres < 25 a.u.f. corresponding to the 20th percentile of G2 *Tert*$^{-/-}$ telomere distribution (G) in *Tert*$^{+/+}$, G2*Tert*$^{-/-}$ and G4 *Tert*$^{-/-}$ mice intratracheally inoculated either with vehicle (PBS) or with 0.5 mg/kg BW bleomycin. **(H)** Representative images of telomere Q-FISH analysis in *Tert*$^{+/+}$, G2*Tert*$^{-/-}$ and G4*Tert*$^{-/-}$ bleomycin treated lungs. Amplified images are shown in the insets.

Bleomycin enhances the DNA damage response in the lungs of telomerase deficient mice

To determine the amount of DNA damage induced by *Tert* deficiency *per se* compared to combination of *Tert* deficiency and bleomycin, we first measured DNA damage foci by γH2AX on lung sections, as well as the presence of senescence-associated markers p21, p53 and p19 as well as the apoptotic marker active caspase-3 (C3a). Of note, bleomycin inoculation induces DNA damage in all three genotypes (**Fig. 15A,F**).

Interestingly, the burden of DNA damage was much higher in the G2 and G4 *Tert*$^{-/-}$ mice inoculated with bleomycin (approximately 5% of total lung cells in both cases) compared to the vehicle-inoculated controls (around 1-2% in G2-G4 *Tert*$^{-/-}$, respectively), and also higher than in the treated wild-type mice (less than 1%) (**Fig. 15A,F**). The increase in DNA damage burden in bleomycin-treated G2-G4 *Tert*-deficient mice was accompanied by increased percentage of positive cells for p53, p21 and p19, three well-established markers of cell cycle arrest and cellular senescence (**Fig. 15B-D,F**). Similar to TRF1-depleted lungs, we also found increased number of active caspase-3 (C3a) positive cells in bleomycin-inoculated *Tert*-deficient lungs compared to wild-type mice (**Fig. 15E-F**).

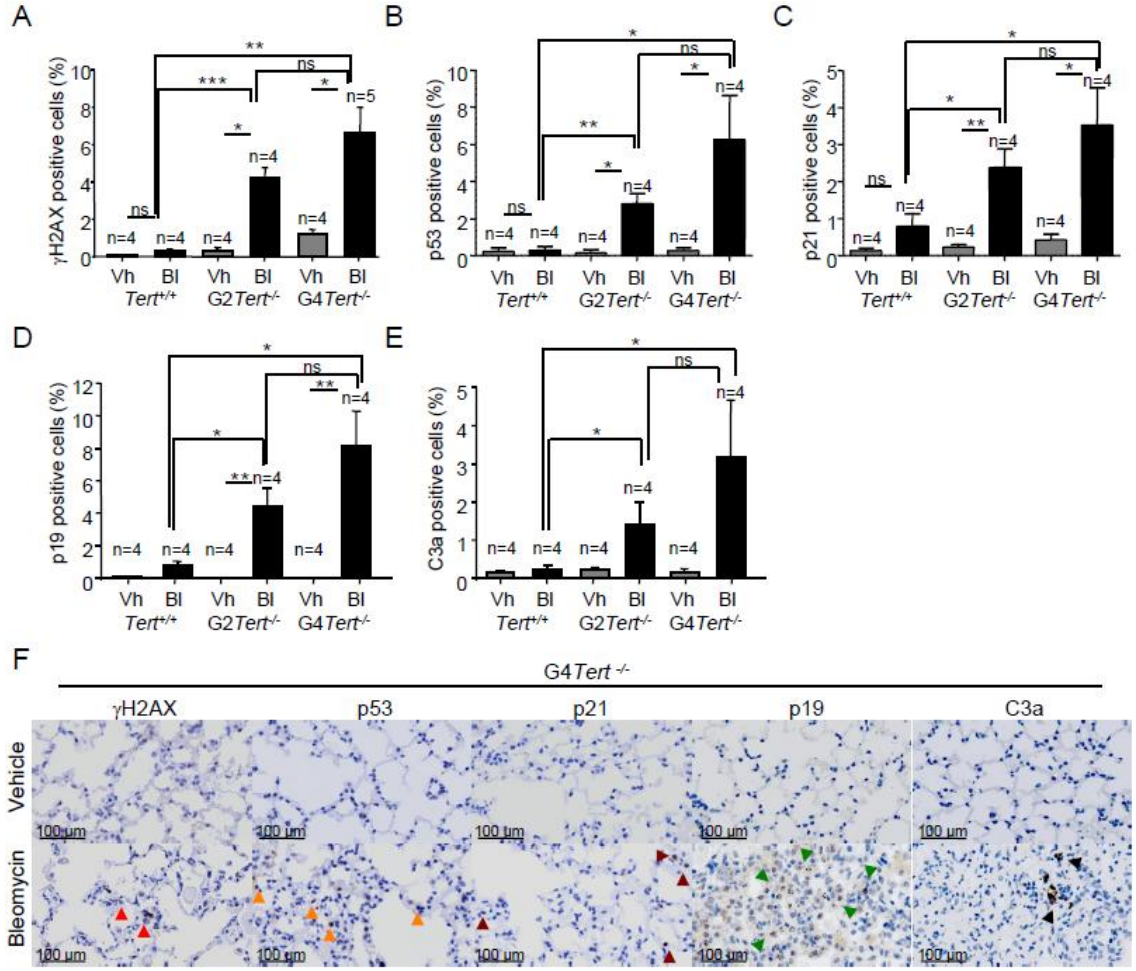

Figure 15. Bleomycin enhances the DNA damage response in telomerase-deficient mouse lungs. **(A-E)** Quantification at time of death of γH2AX (A), p53 (B), p21 (C), p19 (D) and C3a (E) positive cells in *Tert*$^{+/+}$, G2 and G4*Tert*$^{-/-}$ lungs inoculated either with vehicle (PBS) or with 0.5 mg/kg BW bleomycin. **(F)** Representative images at time of death of γH2AX, p53, p21, p19 and C3a immunohistochemistry staining in G4*Tert*$^{-/-}$ lungs inoculated either with vehicle (PBS) or with 0.5 mg/kg BW bleomycin.

Targeting alveolar type II cells by *Tert* gene therapy reverses pulmonary fibrosis induced by telomere shortening

We decided to test the potential of the mouse model generated in the first part this thesis. To do so, we set to address whether telomerase re-expression in the adult lung by using AAV9-*Tert* vectors could be an effective treatment for pulmonary fibrosis associated to critical telomere shortening in mice (Povedano et al., 2015). To this end, we used the G2 *Tert*-deficient mouse model of pulmonary fibrosis induced by critically short telomeres and a low bleomycin dose (Povedano et al., 2015).

We first analyzed which lung cell types were transduced by the AAV9 vectors in adult mice. To this end, we intravenously (IV) injected adult wild-type mice with AAV9-eGFP and determined the expression of eGFP in the lungs at 2 weeks after inoculation. As ATII cells have been previously described by us to be a key target for the induction of pulmonary fibrosis owing to dysfunctional telomeres (Povedano et al., 2015), we first performed double immunofluorescence against eGFP and surfactant protein C (Sftpc) a marker of ATII cells. Strikingly, around 80% of all lung cells positive for eGFP cells were indeed ATII cells (**Fig. 16A-B**), demonstrating that AAV9 has a specific tropism for this cell type in the lung. At the virus dosage used ($2.5*10^{12}$ vg/mL), 17% of the total ATII cells were transduced with AAV9 vectors (**Fig 16A-B**).

A

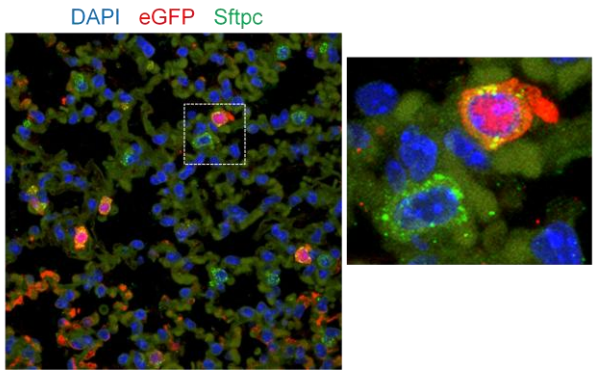

B

	GFP⁺Sftpc⁺cells /GFP⁺cells	GFP⁺Sftpc⁺cells /Sftpc⁺cells
Mean	79.5 (± 10.5)	17.6 (± 4.2)

Figure 16. Intravenous AAV9-*Tert* treatment targets ATII cells. (A) Representative image of immunofluorescence against GFP (in red) and Sftpc (in green). Mice were injected intravenously in the tail with AAV9-eGFP and two weeks later were sacrificed to localize virus cell type target. **(B)** Quantification of percentage of GFP^+ $Sftpc^+$ cells relative to total GFP^+ cells and to total $Sftpc^+$ cells.

We inoculated telomerase-deficient male mice from the second generation, G2 *Tert*$^{-/-}$ mice, with low doses of bleomycin (0.5 mg/kg BW) to induce pulmonary fibrosis (Povedano et al., 2015) to later explore the efficacy of AAV9-*Tert* therapy in this mouse model. Two weeks after bleomycin inoculation, mice were examined by CT to identify

those individuals with abnormal lung radiological pattern indicative of pulmonary fibrosis (**Fig. 17A**). In agreement with previous results, approximately 50% of the mice showed a radiological pattern consistent with pulmonary fibrosis, including presence of reticular opacities with honeycombing, typically found in pulmonary fibrosis patients (Povedano et al., 2015). Out of the mice diagnosed with pulmonary fibrosis, half were intravenously (IV) injected with AAV9-*Tert* and the other half with the AAV9-empty vector as controls. Upon treatment, all mice were longitudinally followed by thoracic CT scan at 1, 2, 4, and 7 weeks after gene therapy treatment (**Fig. 17A**). One week after treatment, all fibrotic lesions in AAV9-*Tert* treated animals regressed in size while they further increased in mice treated with empty vector (**Fig. 17B-D**). Furthermore, from the second week after treatment onwards we observed a significantly faster regression of fibrotic lesions at all time-points in the in AAV9-*Tert* mice compared to those treated with the empty vector (**Fig. 17B**). Indeed, 22% of the *Tert* treated mice appeared to be free of the disease as no abnormal images were detected by CT (**Fig. 17C**). Importantly, 7 weeks after treatment, full regression of fibrotic lesions as detected by CT were observed in the AAV9-*Tert* treated group, while at this time point mice treated with the empty vector still exhibited 40% of the original fibrotic volume diagnosed by CT (**Fig. 17B-D**).

At week 8 after treatment, all mice where sacrificed for full histopathological and molecular analysis of the lungs. At this point, we also confirmed *Tert* overexpression by RT-PCR in lungs (**Fig. 17E**) (Bar et al., 2014; Bernardes de Jesus et al., 2012). As control, *Tert* expression was not detected in the lungs of mice inoculated with empty vector (**Fig 17E**).

Histopathological diagnosis of fibrosis was performed by Masson´s trichome staining. We considered “severe fibrosis” when more than 30% of the lung parenchyma was affected by fibrosis; “mild fibrosis” when less than 10% of the lung parenchyma was affected; and “cured or non-fibrotic lungs” when no signs of fibrosis were found. Histopathologic analysis revealed that at week 8 after treatment, all mice treated with the empty vector showed severe fibrosis as indicated by more than 30% of the lung parenchyma affected by fibrosis (**Fig. 17F-G**). In contrast, none of the AAV-*Tert* treated mice showed severe fibrosis at this point. Instead, 50% of *Tert*-treated mice presented mild fibrosis lesions and 50% were completely free of fibrotic lesions (**Fig 17F-H**). Thus, 50% of AAV9-*Tert* treated mice were cured of lung fibrosis 8 weeks post-treatment while none of the empty vector treated mice were cured and notice that all of them showed severe fibrotic lesions (**Fig. 17H**).

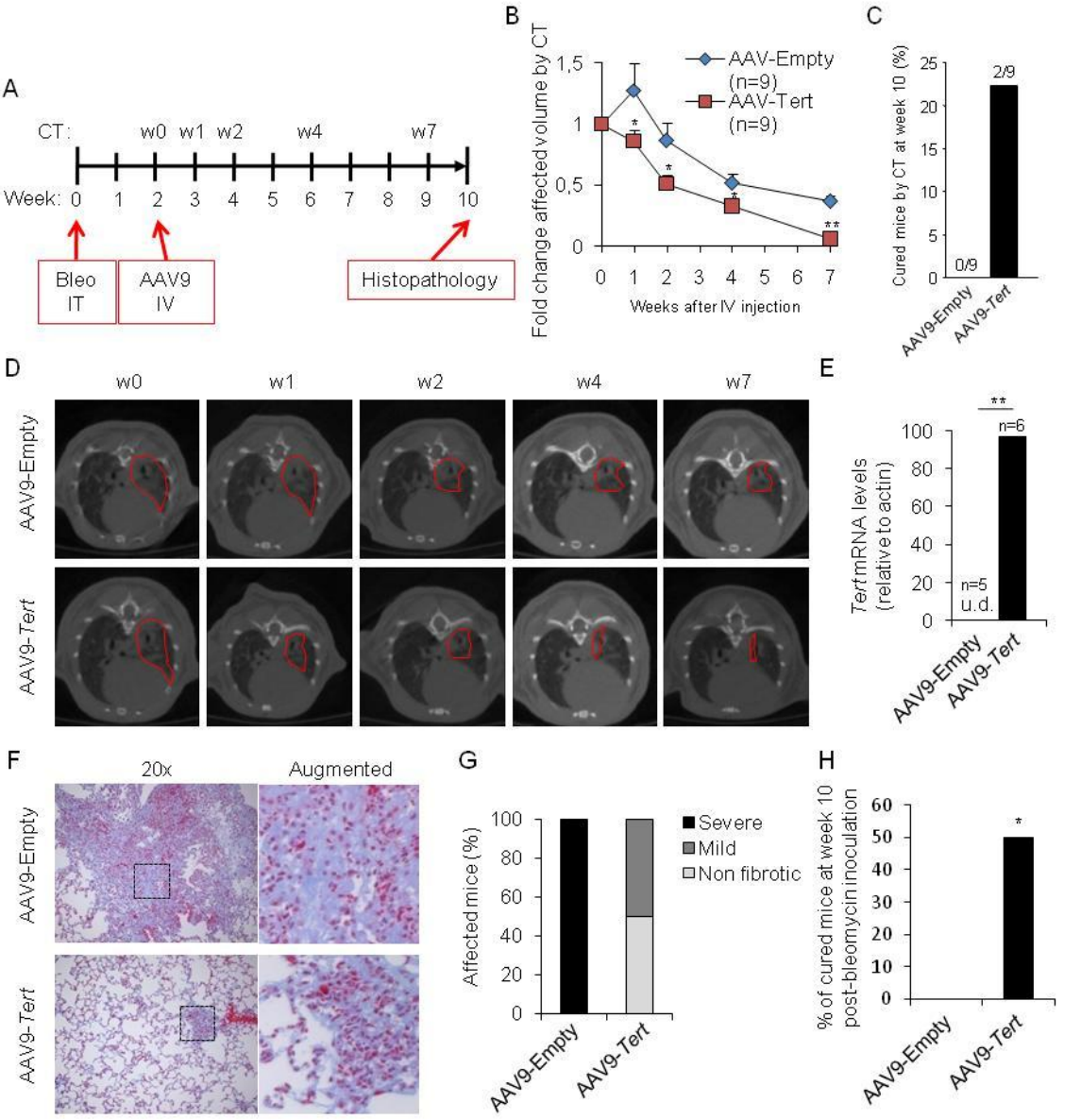

Figure 17. Intravenous AAV9-*Tert* treatment leads to reversal and remission of pulmonary fibrosis
(A) 8-10 week old G2*Tert*$^{-/-}$ mice were intratracheally inoculated with 0.5 mg/kg BW bleomycin and two weeks after were diagnosed by CT with pulmonary fibrosis. From those affected mice half of them were treated intravenously either with AAV9- empty or AAV9-*Tert*. **(B)** CT follow-up was performed at 1, 2, 4, and 7 weeks post-treatment and quantify as fold change affected lung volume. **(C)** Percentage of cured mice by CT at week 9 post bleomycin inoculation. **(D)** CT representative images for every time point of the treatment (fibrotic area in red). **(E)** Transcriptional levels of *Tert* in lung upon IV tail injection after 8 weeks. **(F)** Masson´s trichrome staining from lung sections to evaluate fibrotic regions at end point (collagen fibers in blue; nuclei and erythrocytes in red). **(G)** Histopathological analysis and fibrosis score from lung sections. **(H)** Percentage of cured mice confirmed by histopathological analysis from AAV9-*Tert* treated mice (n=6) and mice inoculated with empty vector (n=6).

In addition, collagen deposition analyzed by Sirius red staining of lung sections at week 8 after treatment confirmed that AAV9-*Tert* treated mice presented one-third less collagen deposition as compared to empty vector treated animals (**Fig 18A-B**). In agreement with lower collagen deposition and remission of fibrosis, AAV9-*Tert* treated mice also showed significantly reduced number of positive αSMA myofibroblasts, which are associated with collagen deposition in human IPF patients (**Fig 18C-D**), suggesting an inactivation of fibrotic foci upon *Tert* treatment.

In line with fibrosis regression and healing, we also found a significant decrease in F4/80 positive cells indicative of macrophages infiltrates reduction in the remaining fibrotic areas from AAV9-*Tert* treated mice compared with the fibrotic areas from AAV9-empty treated mice (**Fig 18E-F**), what suggests lower inflammation upon *Tert* treatment.

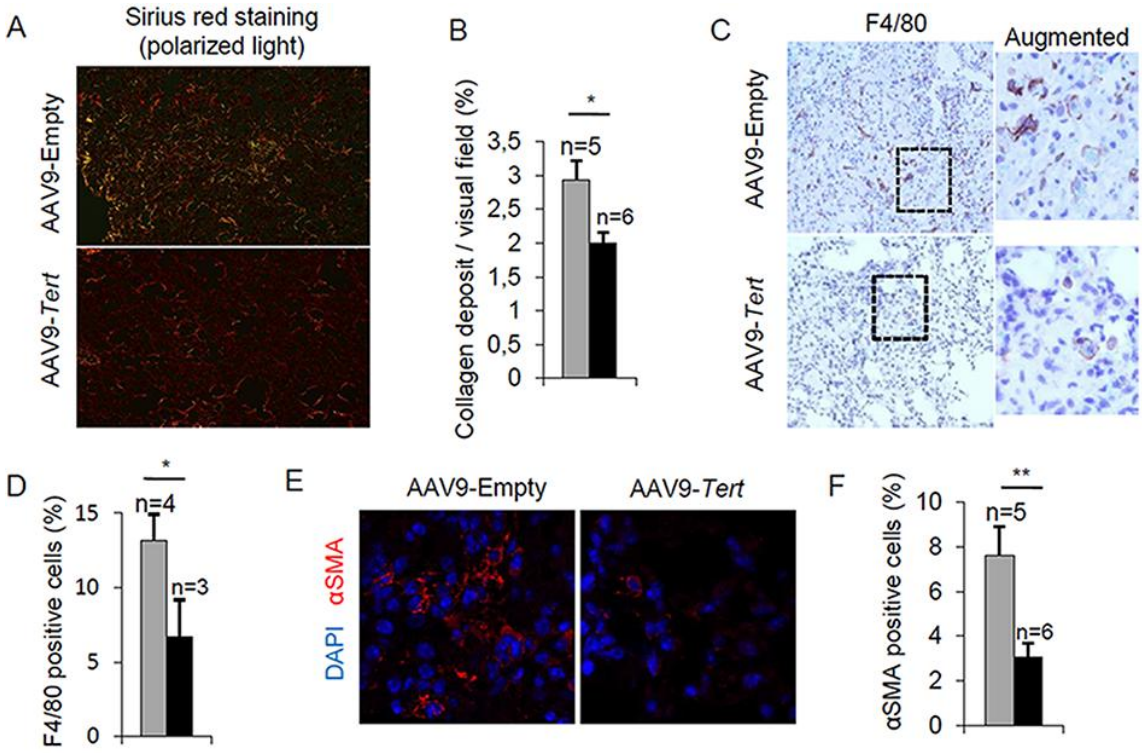

Figure 18. *Tert* treated mice show lower collagen deposition, less inflammation and decreased active fibrotic foci. (A) Representative images of Sirius red staining visualized by polarized light where collagen fibers are bright orange from mice treated with AAV9-*Tert* or empty vector. **(B)** Percent of lung area filled with collagen fibers. **(C)** Representative images of F4/80 (macrophage specific marker) immunohistochemistry staining in AAV9-empty and AAV9-*Tert* treated mice. **(D)** Quantification of F4/80 positive cells from *Tert* and empty-treated mice lung sections. **(E)** Representative images of immunofluorescence for αSMA (in red) and DAPI (in blue). **(F)** Quantification of αSMA positive cells.

Tert overexpression rescues apoptosis and cellular senescence in fibrotic lungs

Short dysfunctional telomeres have been previously shown to trigger a persistent DNA damage response (DDR) characterized by increased γH2AX foci, increased expression of p21 and p53 cell cycle arrest and senescence markers, as well as induction of apoptosis (Hemann et al., 2000; Meier et al., 2007). Indeed, we previously described that mice with pulmonary fibrosis owing to short telomeres also show increased γH2AX foci, increased expression of p21 and p53, as well as induction of apoptosis in the lungs (Povedano et al., 2015). Interestingly, we found that mice with pulmonary fibrosis treated with AAV9-*Tert* showed a significantly reduction of DNA damage markers as indicated by lower percentage of positive cells for γH2AX in the lung compared to mice treated with empty vector (**Fig. 19A-B**). We also found a significant reduction in the abundance of p21 and p53 positive cells in the AAV9-*Tert* treated mice compared to those treated with empty vector (**Fig. 19A,C-D**), as well as a significant decrease in apoptosis as indicated by percentage of cells positive for caspase-3 in the *Tert*-treated mice (**Fig 19A,E**). These results indicate that *Tert* re-expression in the adult lungs of mice with pulmonary fibrosis leads to decreased DNA damage and apoptosis, as well as a reduction in the percentage of cells positive for p53 and p21, suggestive of decreased cell death and senescence in the lung.

In order to specifically determine senescence cells in the lungs, we performed whole mount staining for SA-β-galactosidase assay in mice diagnosed with pulmonary fibrosis and treated with either AAV9-*Tert* or empty vectors. While senescence cells were readily detected in mice diagnosed with pulmonary fibrosis and treated with the empty-vector, they were undetectable in the residual fibrotic areas present in few AAV9-*Tert* treated lungs at the end of the experiment (**Fig 19F-G**). These findings indicate that *Tert* treatment rescues DNA damage, apoptosis and cellular senescence in mice diagnosed with pulmonary fibrosis owing to critically short telomeres.

Figure 19 (next page). *Tert*-treated mice show reduced DNA damage and subsequent decreased senescence and apoptosis. (A) Representative images for the markers γH2AX, p53, p21, p19 and Caspase-3 active (C3a) from both groups. **(B-E)** Quantification of γH2AX (B), p53 (C), p21 (D) and C3a (E) positive cells in lungs treated either with *Tert* or empty vector. **(F)** Representative pictures from fast red staining in whole mount SA-β-Gal tissue sections. **(G)** Quantification of SA-β-Gal positive cells per visual field.

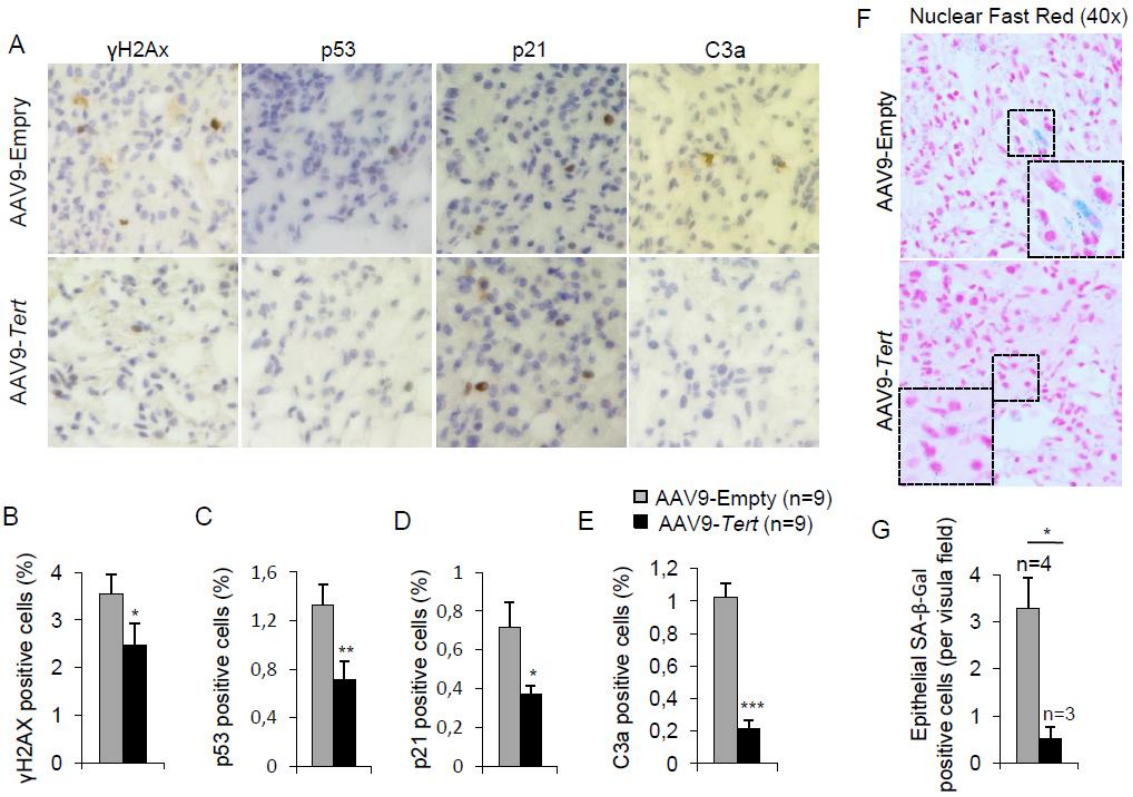

AAV9-*Tert* treatment results in increased proliferation of ATII cells

To further understand the molecular mechanisms by which *Tert* gene therapy results in significant remission and healing of pulmonary fibrosis owing to short telomeres, we next studied telomere length specifically in the ATII cells of mice treated with either AAV9-*Tert* or the empty vector. To this end, we performed an immuno-FISH experiment with an antibody (anti-Sfptc) to detect ATII cells followed by telomere Q-FISH analysis. First, we found that ATII cells from mice treated with the empty vector showed significantly shorter telomeres and an increased percentage of short telomeres compared to the surrounding non-ATII cells (see relative average telomere length and percentage of short telomeres of ATII cells compared to non-ATII cells in Fig. 16A,B). The fact that ATII cells have shorter telomeres than non-ATII cells in telomerase-deficient mice is in agreement with our previous findings indicating that they are important for the regeneration of lung damage induced by dysfunctional telomeres, thus undergone more cell divisions (Povedano et al., 2015). Interestingly, ATII cells in mice treated with AAV9-*Tert* showed the same telomere length and percentage of short telomeres than the surrounding non-ATII, suggesting that telomerase treatment is preserving telomeres in ATII cells in the context of lung fibrosis (**Fig. 20A-C**). In summary, these results indicate that specific targeting of ATII cells with AAV9-*Tert*

results in improved telomere length homeostasis of ATII cells compared to these cells from mice treated with empty vectors.

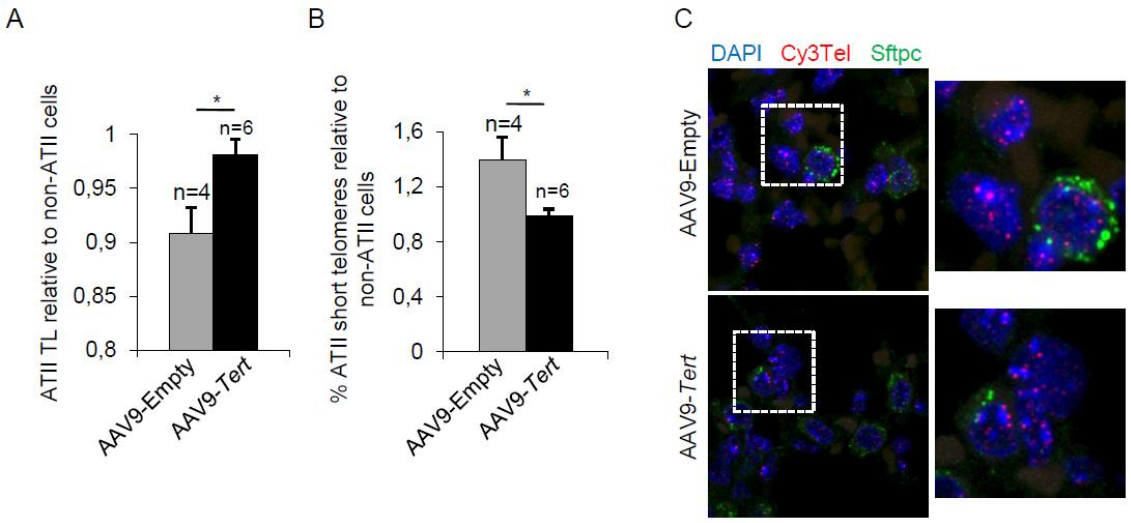

Figure 20. AAV9-*Tert* results in telomere length maintenance after tissue regeneration. (A-B) Fold change in telomere length in ATII cells telomere length (A) and percentage of short telomeres (B) relative to non-ATII cells. **(C)** Representative images of immuno-QFISH with Cy3Telomere probe (in red), Sftpc (in green) and DAPI (in blue).

We addressed the effects of *Tert* treatment on the ability of ATII cells to proliferate and regenerate the damaged lung tissue upon fibrosis diagnose. To this end, double immunofluorescence against the ATII cells specific marker, Sftpc, and the proliferation marker, Ki67, was performed (Materials and Methods). We found that *Tert*-treated mice showed a 2-fold increase in Ki67 positive cells in whole lung tissue sections compared to controls (**Fig. 21D-E**). When specifically looking at ATII cells, we observed 2-fold increase in the total number of Sftpc positive cells and 2.5-fold increase in Ki67 positive ATII cells in AAV9-*Tert* treated lungs compared to empty vector controls (**Fig. 21D,F-G**). These results show that increased *Tert* expression in ATII cells provokes an increased proliferation of ATII cells, suggesting a higher potential for lung regeneration and the remission of lung fibrosis.

Figure 21. AAV9-*Tert* results in increased proliferation of total lung cells and specifically ATII cells. (A) Representative images of double immunofluorescence against Sftpc (in red) and Ki67 (in red). **(B-D)** Quantification of percentage of Ki67 positive cells (B), Sftpc positive cells (C) and Ki67 positive cells relative to Sftpc positive cells (D).

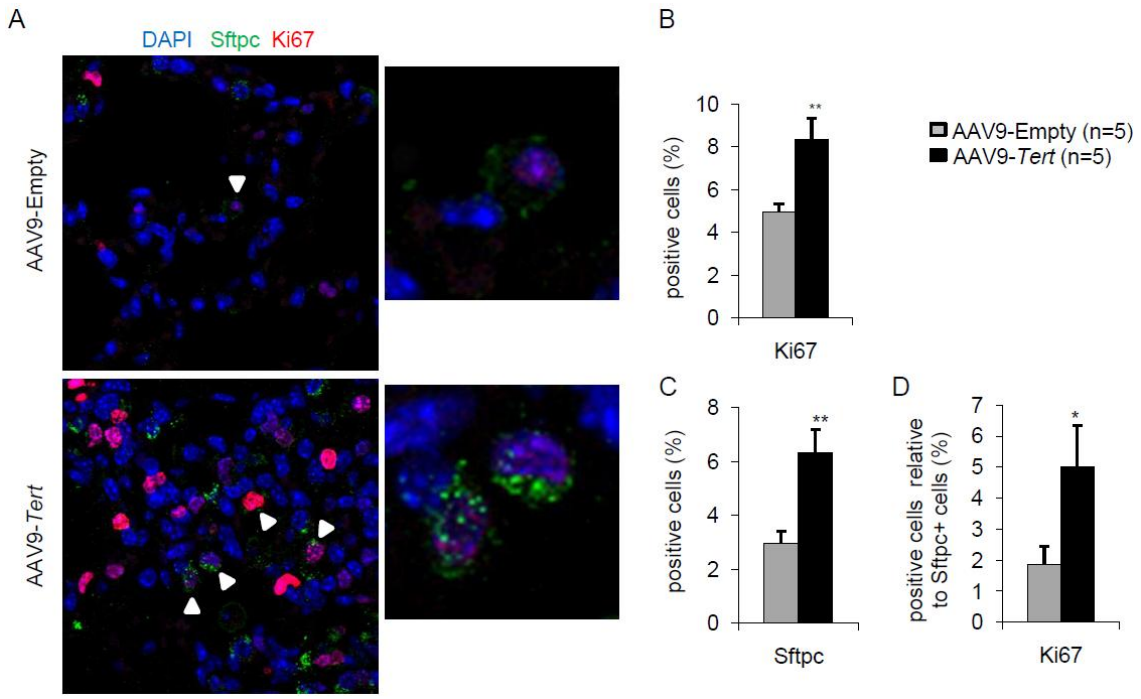

AAV9-*Tert* treatment leads to gene expression changes indicative of higher regeneration potential

We studied gene expression changes induced by *Tert* expression in the context of lung fibrosis. To this aim, we first performed DNA microarray analysis from the post-caval lung lobe from mice diagnosed with pulmonary fibrosis which were treated either with AAV9-*Tert* or with the empty vector and sacrificed at 8 weeks post-treatment (5 mice were included per group). We found that 53 genes were significantly upregulated (FDR<0.05) in AAV9-*Tert* treated mice compared to mice treated with empty-vector (**Table 3**). We performed Gene Set Enrichment Analysis (GSEA) to address those pathways affected by *Tert* gene therapy in fibrotic lungs. The results showed significant differences of signatures related with DNA replication and mitosis, apoptosis, DNA repair, the Wnt pathway, the leukocyte transendothelial migration pathway, and extension of telomeres (**Fig. 22A,B**). Using RT-PCR, we validated a random selection of the more differentially expressed genes within these pathways: *Apc*, *Ctnnb1*, *Fzd5*, *Lrp6*, *Lrp5*, *Bim, Flir, Bid*, *Mcl1*, *Mmp-9* and *Cenpq* (**Fig. 22C**). Upregulation of the "extension of telomeres pathway" is in line with improved telomere maintenance in ATII cells treated with *Tert* (**Fig. 22B**). Similarly, upregulation of DNA replication and mitosis pathways (**Fig. 22A**) is in accordance with increased proliferation of ATII cells (**Fig. 21A,D**). Of note, downregulation of the Wnt pathway in AAV9-*Tert* treated adult lungs is in contrast with the notion that *Tert* can activate Wnt/β-catenin pathway during development (Park et al., 2009). Instead, our results go in line with recent findings

showing that high levels of the Wnt pathway genes, *Lrp5* and *Lrp6*, are linked to bad prognosis of IPF patients (Lam et al., 2014). Interestingly, we found *Mmp-9* upregulation in *Tert*-treated lungs, in agreement with previous work showing that *Mmp-9* overexpression attenuates fibrosis in bleomycin-induced IPF (Cabrera et al., 2007).

Gene symbol	GeneName	adj.P.Val
Apol9a	apolipoprotein L 9a	0.0015
Oas2	2'-5' oligoadenylate synthetase 2	0.0015
Apol9a	apolipoprotein L 9a	0.0015
Apol9b	apolipoprotein L 9b	0.0015
Gm4955	predicted gene 4955	0.0015
Irf7	interferon regulatory factor 7	0.0015
Ifi27l2a	interferon, alpha-inducible protein 27 like 2A	0.0017
EG545385	predicted gene, EG545385	0.0024
Oas1a	2'-5' oligoadenylate synthetase 1A	0.0030
Isg15	ISG15 ubiquitin-like modifier	0.0032
Oas1a	2'-5' oligoadenylate synthetase 1A	0.0032
Ifi44	interferon-induced protein 44	0.0032
Ifit1	interferon-induced protein with tetratricopeptide repeats 1	0.0045
Mx1	myxovirus (influenza virus) resistance 1	0.0053
Zbp1	Z-DNA binding protein 1	0.0056
Oas1f	2'-5' oligoadenylate synthetase 1F	0.0057
Zbp1	Z-DNA binding protein 1	0.0083
Isg15	ISG15 ubiquitin-like modifier	0.0083
Mx2	myxovirus (influenza virus) resistance 2	0.0083
LOC100048309	similar to interferon activated gene 204	0.0083
Oasl1	2'-5' oligoadenylate synthetase-like 1	0.0093
Phf11	PHD finger protein 11	0.0099
Oasl2	2'-5' oligoadenylate synthetase-like 2	0.0102
Ccl4	chemokine (C-C motif) ligand 4	0.0117
Plac8	placenta-specific 8	0.0117
Oas3	2'-5' oligoadenylate synthetase 3	0.0123
Ifi204	interferon activated gene 204	0.0132
Nkg7	natural killer cell group 7 sequence	0.0183
Plac8	placenta-specific 8	0.0191
Csprs	component of Sp100-rs	0.0217
Klra23	killer cell lectin-like receptor subfamily A, member 23	0.0219
Slfn2	schlafen 2	0.0303
Klra23	killer cell lectin-like receptor subfamily A, member 23	0.0312
Lgals3bp	lectin, galactoside-binding, soluble, 3 binding protein	0.0315
Ifng	interferon gamma	0.0354
Klra16	killer cell lectin-like receptor, subfamily A, member 16	0.0364

Gene symbol	GeneName	adj.P.Val
Klra7	killer cell lectin-like receptor, subfamily A, member 7	0.0364
Mefv	Mediterranean fever	0.0364
LOC635676	hypothetical protein LOC635676	0.0364
Slfn4	schlafen 4	0.0364
Cmpk2	cytidine monophosphate (UMP-CMP) kinase 2, mitochondrial	0.0371
LOC100041903	similar to putative G-protein coupled receptor	0.0375
Klra22	killer cell lectin-like receptor subfamily A, member 22	0.0396
C79246	expressed sequence C79246	0.0396
Ccl5	chemokine (C-C motif) ligand 5	0.0396
LOC631406	similar to schlafen 8	0.0414
Fasl	Fas ligand (TNF superfamily, member 6)	0.0435
Pyhin1	pyrin and HIN domain family, member 1	0.0438
Ms4a6c	membrane-spanning 4-domains, subfamily A, member 6C	0.0456
Ms4a4c	membrane-spanning 4-domains, subfamily A, member 4C	0.0482
D14Ertd668e	DNA segment, Chr 14, ERATO Doi 668, expressed	0.0482
Klra23	killer cell lectin-like receptor subfamily A, member 23	0.0493
Gm4902	predicted gene 4902	0.0493

Table 3. Differentially expressed genes compared between AAV9-*Tert* and empty vector treated fibrotic lungs (FDR<0.05). The FDR is calculated by Benjamini and Hochberg FDR correction.

Figure 22 (next page). Upregulation of GSEAs and DEGs of gene expression profile upon *Tert* overexpression in lungs. (A) Summary table indicating various differentially regulated gene sets overregulated in *Tert* treated mice compared with empty vector. Gene set overregulated in the empty vector group is specified between brackets. **(B)** GSEA plots for the indicated pathways in lung tissue. A heatmap of indicated core-enriched genes is displayed on the right of each enrichment plot. Microarray genes were ranked based on the two-tailed t-statistic tests obtained from the AAV9-*Tert* versus AAV9-empty by pair-wise comparisons. The red to blue horizontal bar represents the ranked list. Those genes showing higher expression levels for each cohort are located at the edges of the bar (AAV9-empty; AAV9-Tert). The genes located at the central area of the bar show small differences in gene expression fold changes between both groups. **(C)** Fold change mRNA expression levels of candidate genes related with canonical Wnt pathway, apoptosis, mitosis and transendothelial migration in AAV9-*Tert* relative to empty vector.

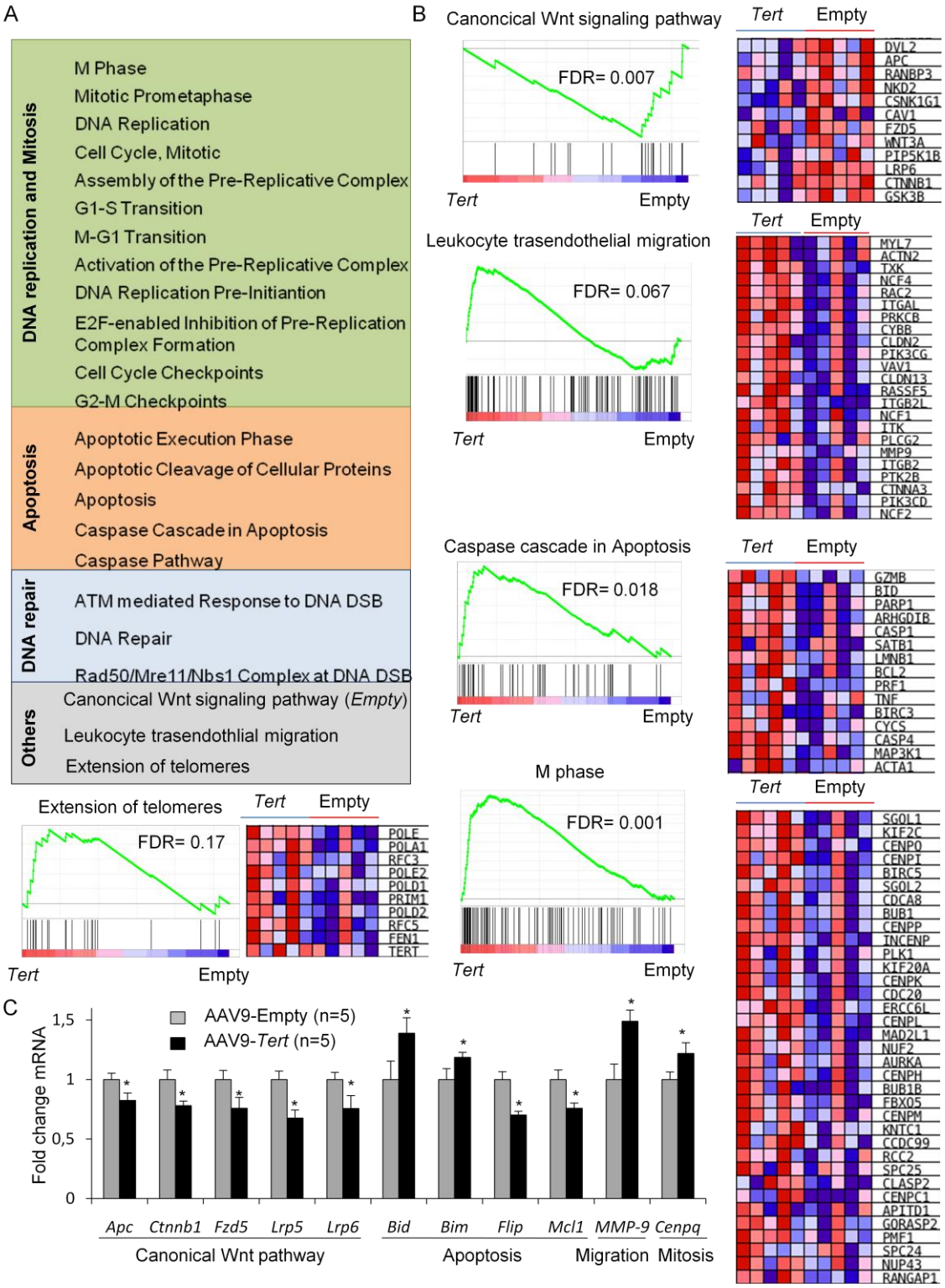

Interestingly, out of the nine pathways downregulated by *Tert* (**Fig. 23A**), four are related with fibroblast growth factor receptors; i.e., the FGFR2C, FGFR4, FGFR and the FGFR1 ligand binding and activation cascades (**Fig. 23A-C**). As FGF1-FGFRc

over-expression has been shown to contribute to pathogenesis in IPF patients (MacKenzie et al., 2015), these findings suggest that *Tert* treatment impairs fibroblast activation, thus facilitating fibrosis regression. In line with this, we found a trend towards downregulation of the TGF-β pathway (FDR=0.2507) in the AAV9-*Tert* treated lungs (**Fig. 23D**). This is in agreement with our previous findings that *Tert* overexpression in mouse embryonic fibroblasts (MEFs) induces downregulation of TGF-β (Geserick et al., 2006). TGF-β pathway has been linked to fibroblast activation and differentiation to myofibroblast (Pedroza et al., 2015). Indeed, perfinidone has been proven to significantly slow down pulmonary fibrosis progression by blocking TGF-β (Hunninghake, 2014; Karimi-Shah and Chowdhury, 2015; King et al., 2014).

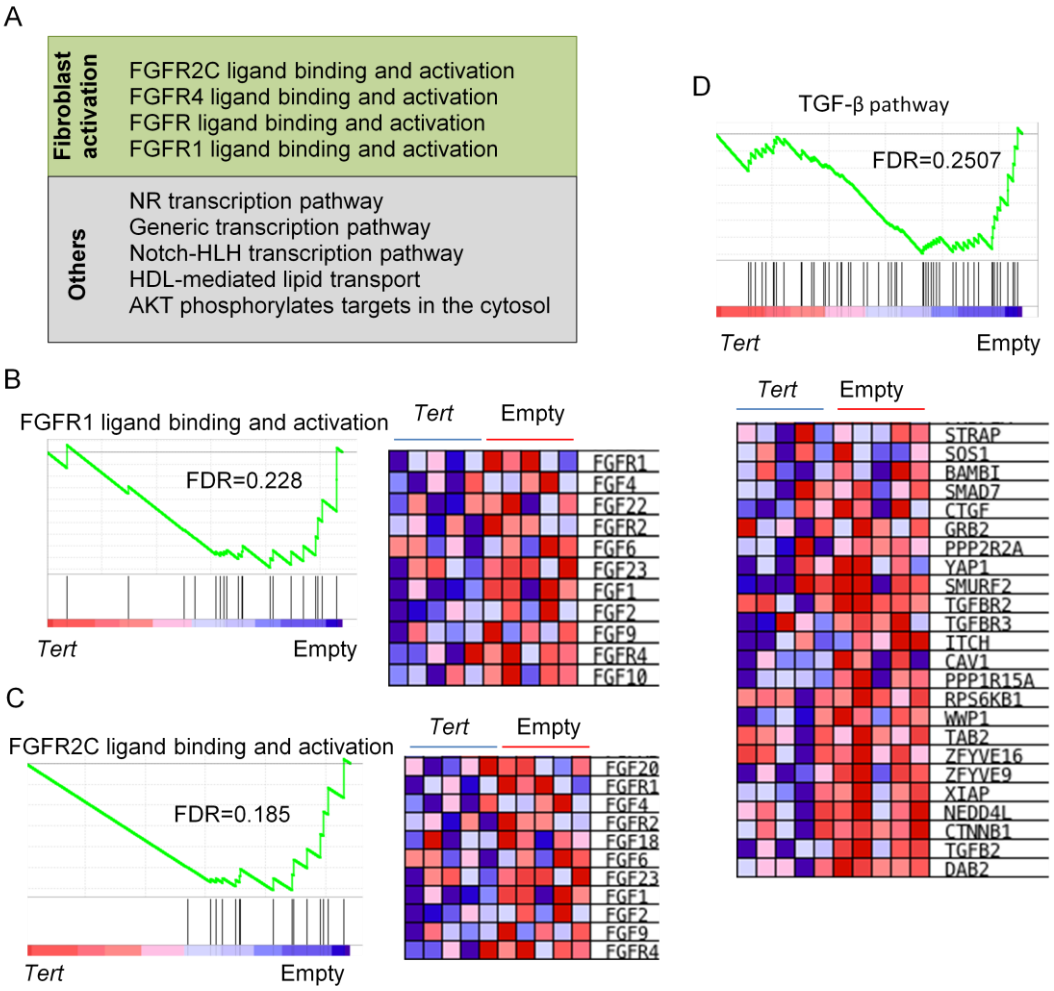

Figure 23. Downregulation of fibroblast activation-related pathways in *Tert*-treated lungs. (A) Summary table indicating various differentially regulated gene sets downregulated in *Tert* treated mice compared with empty vector. **(B-C)** GSEA plots for the indicated pathways in lung tissue. **(D)** GSEA plot for TGF-β pathway in lung tissue. A heatmap of indicated core-enriched genes is displayed on the right of each enrichment plot. A heatmap of indicated core-enriched genes is displayed on the right of each enrichment plot. Microarray genes were ranked based on the two-tailed t-statistic tests obtained from the

AAV9-*Tert* versus AAV9-empty by pair-wise comparisons. The red to blue horizontal bar represents the ranked list. Those genes showing higher expression levels for each cohort are located at the edges of the bar (AAV9-empty; AAV9-Tert). The genes located at the central area of the bar show small differences in gene expression fold changes between both groups.

We set to analyze to what cell type the observed gene expression changes corresponded. To this end, we compared the AAV9-*Tert* lung signature with the genes normally expressed in different cell populations (*The Gene Expression Barcode 3.0*). Most upregulated genes (0<Fc<1) corresponded to genes specifically expressed by ATII cells (**Fig. 24A**), with a minority of the genes being normally expressed in leukocytes or embryonic fibroblasts. Similar findings were found for the downregulated genes (-1<Fc<0) (**Fig. 24B**).

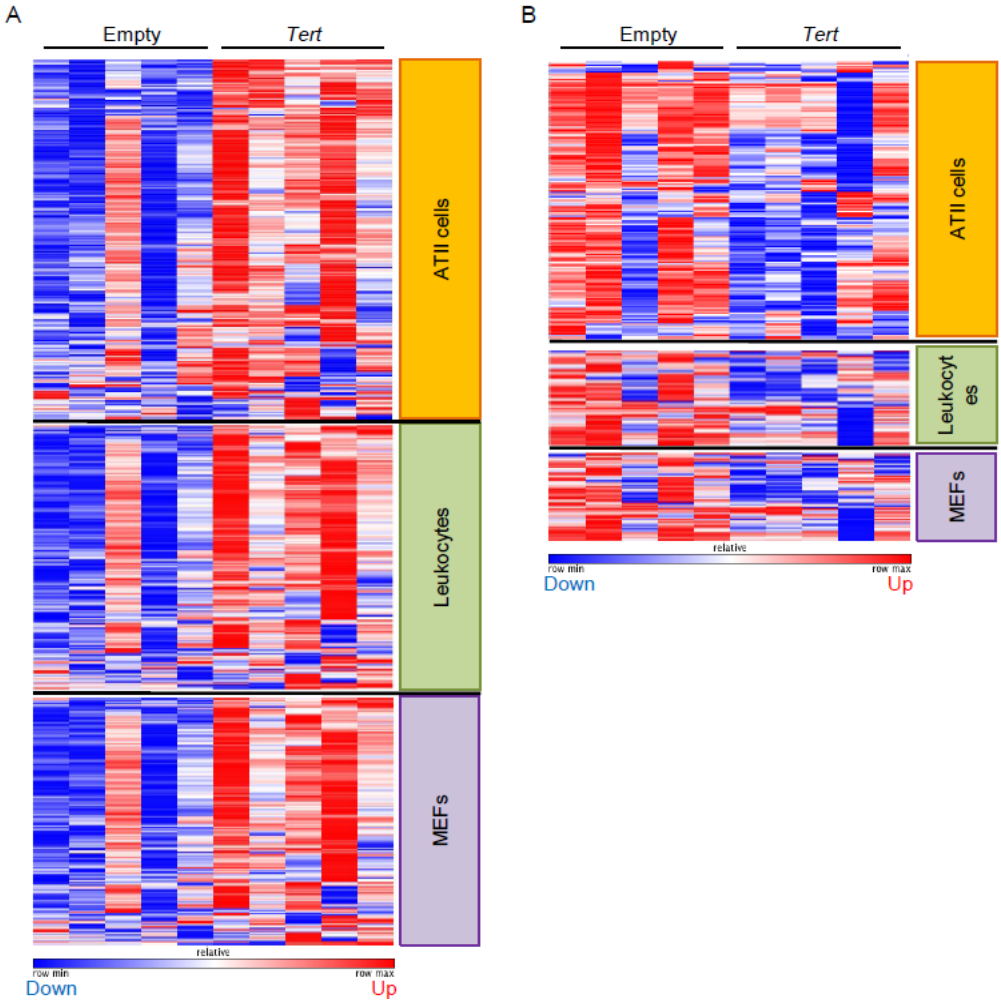

Figure 24. Differentially expressed genes from AAV9-*Tert* treated mice correlate with ATII cell gene expression signature. Heat maps representing the upregulated genes (**A**) and downregulated genes (**B**) in AAV9-*Tert* compared to empty vector treated mice that corresponded to ATII cells, lung leukocytes and mouse embryonic fibroblast (MEFs). The red/blue bars represent an over/down-expression of the gene in this sample compared with the other cohort.

To further confirm that gene expression changes stemmed from *Tert* upregulation in ATII cells, we performed gene expression profiling in isolated ATII cells at one week after treatment of fibrotic lungs with AAV9-*Tert* and empty vectors. ATII cells were identified as EpCAM^{+} LysoTracker^{+} cells, and non-ATII cells as EpCAM^{+} LysoTracker^{-} (**Fig. 25A**). Expression of the ATII-specific marker *Sftpc* by RT-PCR was used to validate the FACS sorting (**Fig. 25B**). FACS-sorted ATII cells from AAV9-*Tert* treated mice showed *Tert* mRNA expression while it was undetectable in FACS-sorted ATII cells from empty vector-treated controls (**Fig. 25C**). We also validated decreased p53 and p21 mRNA expression by RT-PCR in ATII cells from *Tert*-treated mice compared with empty vector-treated mice (**Fig. 25D,E**).

Importantly, GSEA analysis showed downregulation of p53 signaling pathway and the base excision repair pathway, in line with lower DNA damage in lungs from *Tert*-treated mice compared to those from empty vector-treated mice (**Fig. 25D,G**). ATII cells showed downregulation of apoptosis and TGF-β signaling pathways, in agreement with lower apoptosis and fibrosis in the lungs from *Tert*-treated mice (**Fig. 25H,I**). Together, these results further validate that ATII cells are transduced by AAV9-*Tert*, leading to increased telomerase expression, and to downregulation of DNA damage and fibrotic pathways.

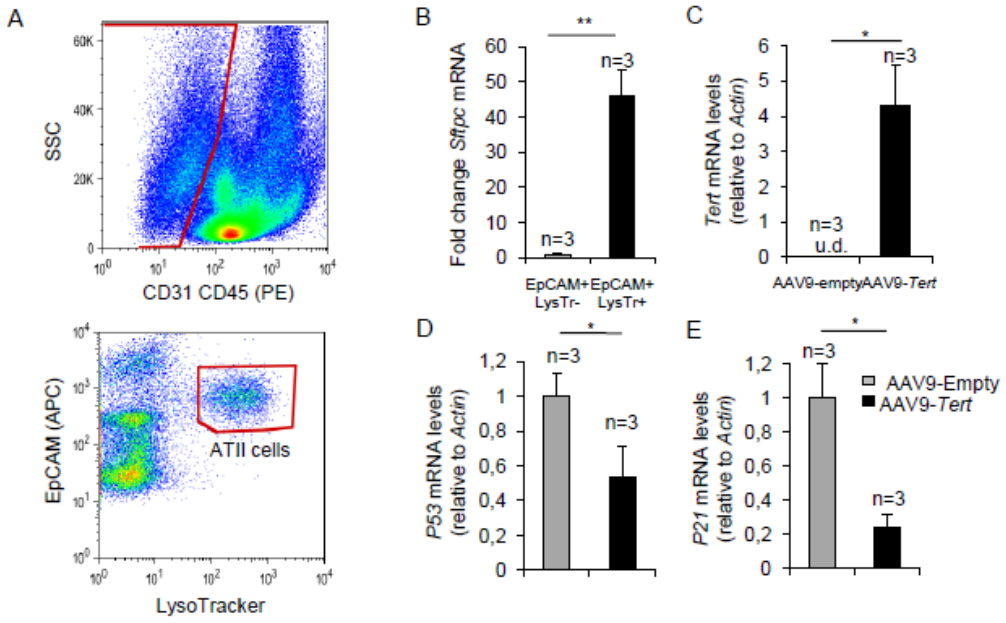

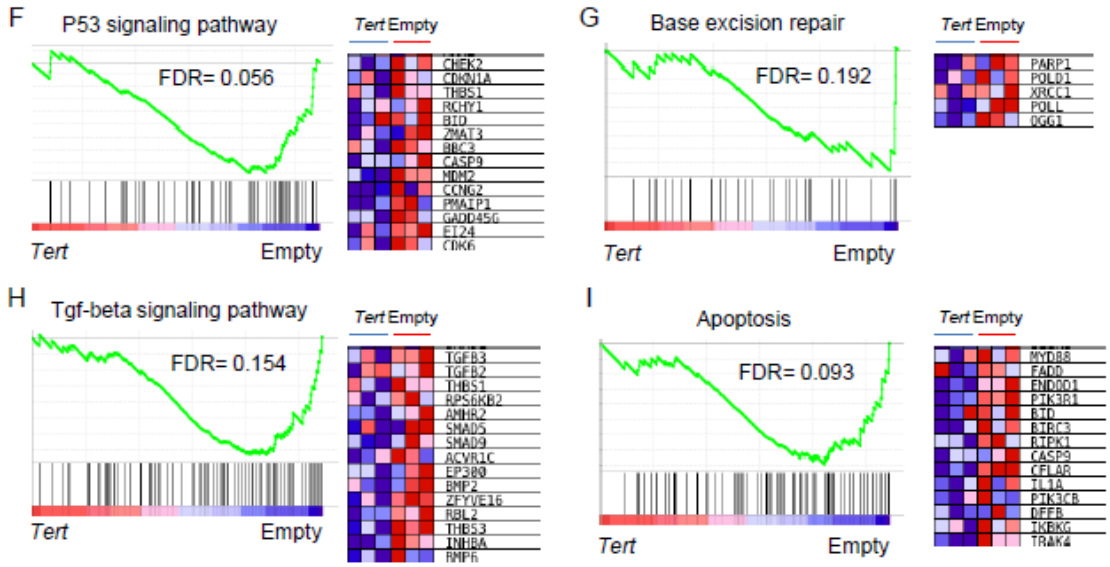

Figure 25. Isolated ATII cells overexpress *Tert* and show p53 and p21 downregulation. (A) Representative dot plots. The epithelial cell population was identified as CD31CD45 double negative and from those we looked at the expression of LysoTracker and EpCAM to identify the ATII cells as double positive cells. Those cells were isolated by cell sorting. **(B)** Validation of specific ATII cells marker *Sfpc* by RT-qPCR. **(C)** Transcriptional levels of *Tert* in ATII cells from fibrotic lungs upon IV tail injection after 1 week. **(D-E)** mRNA expression levels of *p53* (C) and *p21* (D) genes in ATII cells 1 week post-IV tail injection of AAV9 treatment. **(F-I)** GSEA plots for the indicated pathways in ATII cells. A heatmap of indicated core-enriched of the top 14 genes is displayed on the right of each enrichment plot.

Finally, we find of interest the fact that similar findings were found by us on the amelioration of heart function after infarct in mice treated with AAV9-*Tert*(Bar et al., 2014). In particular, *Tert* treatment leads to lower fibrotic scarring of the heart and increased cardiac myocyte proliferation concomitant with transcriptional changes suggestive of a regenerative signature (Bar et al., 2014). Interestingly, the gene expression changes in AAV9-*Tert* treated lungs at 8 weeks post-treatment correlate with the regenerative heart signature described by Haubner *et al* for neonatal mice (Haubner et al., 2012) (**Fig. 27**) as well as those described in previous works from the laboratory in the context of improved cardiac regeneration upon infarct by AAV9-*Tert* treatment (Bar et al., 2014).

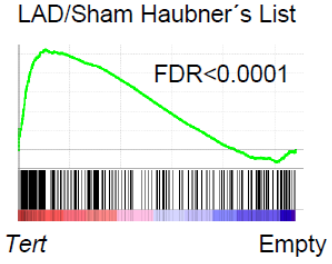

Figure 26. *Tert* overexpression in fibrotic lungs mimic neonatal regenerative heart tissue after infarctation. GSEA plot for LAD/Sham List from Haubner *et al.* study.

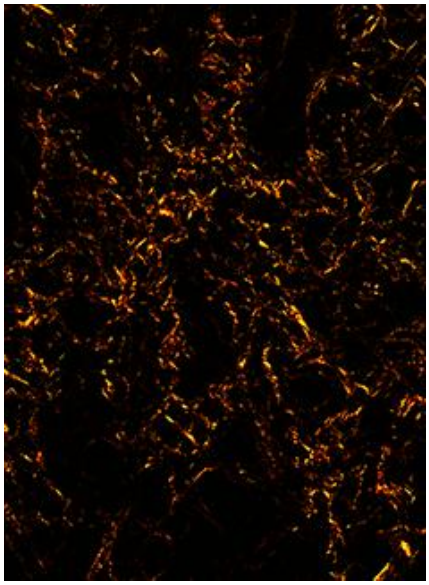

Discussion

Trf1 deletion in ATII cells provokes pulmonary fibrosis

Telomeres represent a small percentage of the whole genome DNA. However, telomeres and shelterins have been demonstrated to be very important for chromosomal integrity, cell viability and proliferation (Blasco, 2007; Blasco et al., 1997; Lee et al., 1998; Martinez et al., 2009). Thus, constitutive deletion of the shelterin components results in embryonic lethality, with the only exception of *Rap1* deletion (Celli and de Lange, 2005; Chiang et al., 2004; Hockemeyer et al., 2006; Karlseder et al., 2003; Kibe et al., 2010; Lazzerini Denchi et al., 2006; Martinez and Blasco, 2011; Martinez et al., 2010; Wu et al., 2006). The shelterin complex prevents the telomeres from degradation and fusion with other chromosomes (de Lange, 2005). In this Thesis we decided to conditionally deplete *Trf1* in ATII cells based on previous studies showing that *Trf1* deletion triggers a strong DNA damage response (DDR), what leads to activation of p53 and p21, cell cycle arrest, senescence or apoptosis (Beier et al., 2012; Martinez et al., 2009; Povedano et al., 2015). In this thesis we tested whether telomere dysfunction induced by *Trf1* deletion in ATII cells provoked IPF in mice without any additional insult.

Our results showed that telomere dysfunction associated to *Trf1* deletion in ATII cells induces a high burden of telomere-induced DNA damage (up to 10% of all lung cells; and >90% of ATII cells), activating the p53/p21 and p19ARF pathways what leads to massive cell senescence and apoptosis in this cell type (**Fig. 27**). This, combined with the fact that TRF1 deficiency provokes decreased ability of stem cells to regenerate tissues (Flores et al., 2005; Schneider et al., 2013) leads to development of pulmonary fibrosis.

Our findings are consistent with a model where the lost of ATII cells hampers lung regeneration capacity (Barkauskas et al., 2013; Serrano-Mollar et al., 2007). ATII cell loss and decreased regenerative capacity associated to severe telomere dysfunction trigger aberrant lung healing by fibroblasts eventually leading to scar formation and pulmonary fibrosis. However, our results are in contrast to a recent work showing that telomere dysfunction due to *Trf2* deletion impairs lung stem function leading to an inflammatory response and susceptibility to lung injury, although this did not induce the development of pulmonary fibrosis (Alder et al., 2015). In this work, the authors challenged the TRF2-depleted lungs with bleomycin (>1mg/kg body weight) leading to a high mortality in the first 2 weeks after bleomycin inoculation, thus not having sufficient time for IPF to develop (Alder et al., 2015). Moreover, the authors did not address the effect of *Trf2* deletion in adulthood without any additional challenge with

bleomycin (Alder et al., 2015). In conclusion, our results clearly demonstrate that induction of telomere dysfunction upon *Trf1* deletion in type II alveolar cells is sufficient to induce pulmonary fibrosis.

Short telomeres synergize with damaging agents to cause pulmonary fibrosis

Short telomeres are considered to be causal factor for aging and age-related diseases (Armanios, 2013; Armanios and Blackburn, 2012; Blasco, 2007; Lopez-Otin et al., 2013). Furthermore, short telomeres are found in familial and sporadic IPF cases (Alder et al., 2008; Alder et al., 2011; Armanios et al., 2007). However, mice with short telomeres do not develop pulmonary fibrosis (Blasco et al., 1997; Lee et al., 1998). The different outcome in humans and in mice can be due to the fact that mouse telomeres are longer than human telomeres as well as to absence of environmental insults in hosting facility (Alder et al., 2011; Blasco, 2007). It has previously been reported that short telomeres synergize with genetic, chemical and surgical damage to develop fibrosis in a low proliferative organ such as liver (Rudolph et al., 2000). In this Thesis we sought to address whether short telomeres contributed to the development of pulmonary fibrosis in mice after bleomycin insult.

Bleomycin was initially used as a chemotherapeutic for cancer treatment for human patients, resulting in some cases in lung toxicity as a side effect (Umezawa, 1974; Umezawa et al., 1967). Due to its lung toxicity, bleomycin has been widely used to induce pulmonary fibrosis in wild-type mice (Cabrera et al., 2007; Inomata et al., 2014; Moore and Hogaboam, 2008; Mouratis and Aidinis, 2011; Oku et al., 2008; Serrano-Mollar et al., 2007). Inoculation with a high bleomycin dose (> 1 mg/kg) induces DNA damage above the tolerated threshold by the lungs in wild-type and *Tert*-deficient mice (Degryse et al., 2012). Interestingly, we demonstrated here that a low bleomycin dose, which is well tolerated by wild-type mice, causes full-blown pulmonary fibrosis in telomerase-deficient mice due to the additional damage stemming from the short telomeres, thus mimicking the human situation (**Fig. 27**). These mice show activation of the p53/p21 and p19ARF pathways, leading to cell senescence and apoptosis. In addition, mice with short telomeres show an impaired regeneration capacity what hampers lung regeneration leading to fibrosis. In line with this, the fibrotic process is common to several degenerative diseases such as heart infarct, kidney fibrosis, liver cirrhosis, as well as spinal cord injury (Rudolph et al., 2000; Ruschel et al., 2015). Although the origin of the damage in each case can be different, all of them have in common the lack of regenerative capacity of the tissue upon injury (Flores et al., 2005).

Lately, improving the regenerative capacity of the damage tissues by different approaches is being implemented in the clinics (Ruschel et al., 2015).

We found that female mice were more resistant than male mice to develop pulmonary fibrosis associated to telomere dysfunction, further recapitulating the human situation. The reasons why women are less prone to suffer pulmonary fibrosis are still unknown. Some studies suggested that the history of smoking and occupational exposure are risk factors for IPF giving a possible explanation for the differences in gender incidence (Ekstrom et al., 2014). Another likely explanation for this could be that *Tert* is transcriptionally activated by estrogens due to the presence of estrogens receptor recognition sequence in its promoter. In agreement with this, women have longer telomeres than men (Calado et al., 2009; Gardner et al., 2014; Kyo et al., 1999).

Telomere dysfunction as trigger of IPF

All these findings together support a model for the pathobiology of human disease. Thus, persistent DNA damage stemming from dysfunctional telomeres associated to mutations in telomere maintenance genes or telomere shortening as the consequence of aging can synergize with additional cellular damages to trigger pulmonary fibrosis. We have demonstrated that a high burden of telomeric DNA damage induced by severe telomere dysfunction, even in the absence of telomere shortening, is sufficient to trigger pulmonary fibrosis in the absence of any additional DNA damage in the genome (**Fig. 27**). In addition, we showed that short telomeres synergize with a lung insult, i.e. bleomycin, to induce pulmonary fibrosis. The mouse models generated during this Thesis constitute valuable tools for the preclinical testing of potential therapeutic strategies.

Figure 27 (next page). Model for pulmonary fibrosis associated to telomeric DNA damage. Depletion of TRF1 protein (red circle) from telomeres (orange rectangle) in lung ATII cells leads to a persistent and severe DNA damage response at telomeres characterized by increased γH2AX (purple star) in 10% of total lung cells and up to 90% of alveolar type II cells, and activation of the p53/p21 pathway. Application of a low dose of bleomycin (0.5 mg/kg BW dose) to wild-type lungs does not lead to a significant increase in the number of damaged cells (less than 1% of total lung cells). The same bleomycin dose in telomerase deficient mice with short telomeres enhances significantly the DNA damage burden in lung cells reaching 6% of total lung cells showing DNA damage, and to activation of the p53/p21 pathway. In both models cell loss mediated by senescence and apoptosis leads and impairs regeneration what may lead to aberrant lung healing and formation of fibrotic scars.

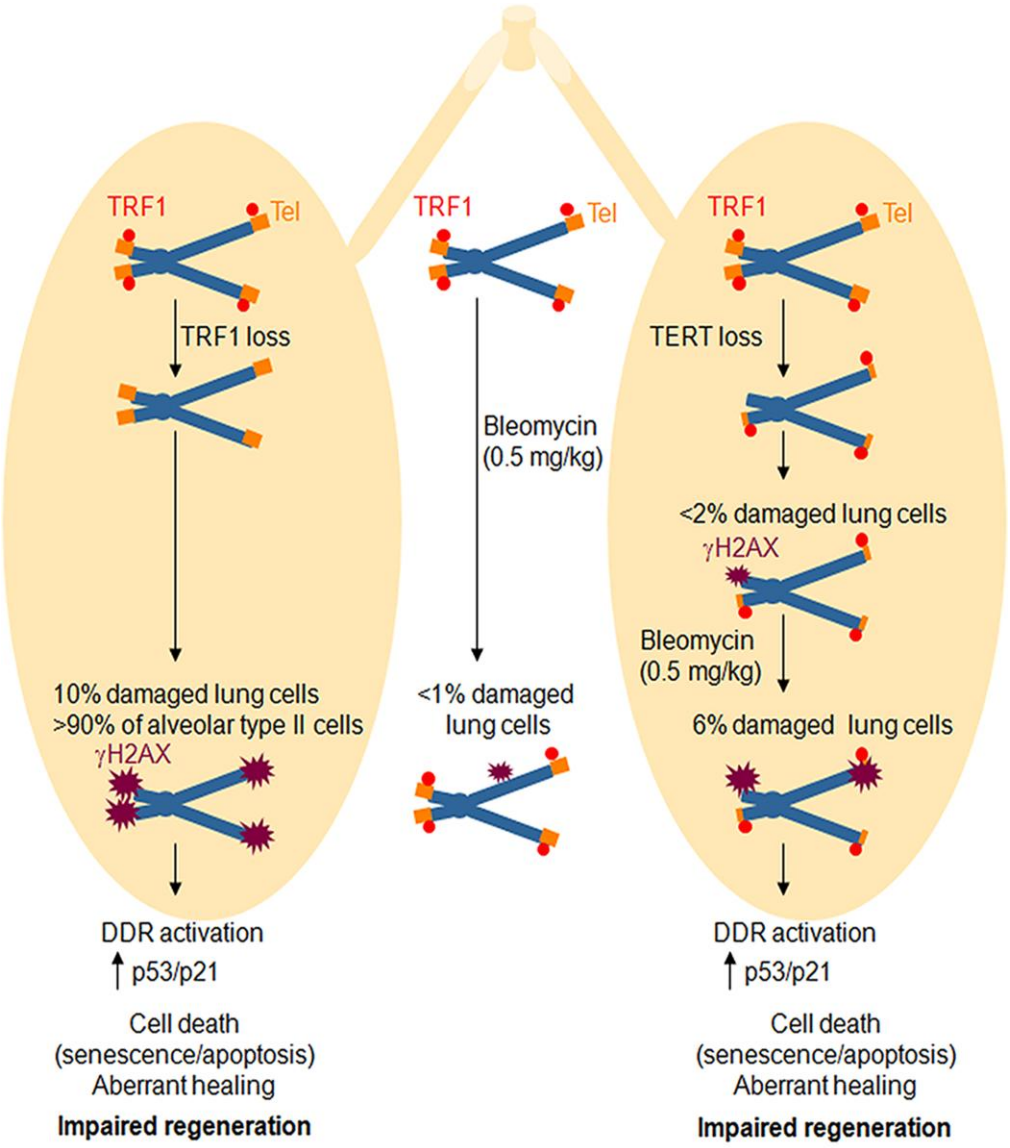

Telomerase as a potential therapy for IPF

No effective treatments for human IPF have been developed yet, although the role of different cell types in the disease and molecular pathways have been studied for a long time. In spite of recent therapeutic advances for the treatment of pulmonary fibrosis, most of the patients still face a fatal outcome, where the only curative treatment is lung transplantation. The recently FDA approved drugs nintedanib and pirfenidone can significantly ameliorate pulmonary fibrosis in patients although no full-remissions have been observed (Hunninghake, 2014; Karimi-Shah and Chowdhury, 2015; King et al., 2014). Thus, new therapeutic strategies aimed to cure the disease are still needed.

We have addressed the potential of telomerase gene therapy in the treatment of idiopathic pulmonary fibrosis (IPF) in *Tert*$^{-/-}$ mice inoculated with a low dose of

bleomycin. AAV9-*Tert* therapy was previously shown to improve both mice fitness and longevity (Bernardes de Jesus et al., 2012). In addition, previous work from our laboratory showed that AAV9-*Tert* therapy protects from scarring following myocardial infarction as well as increasing survival of mice with aplastic anaemia owing to short telomeres without increasing cancer incidence (Bar et al., 2014; Bar et al., 2016).

We observed that increased *Tert* expression in ATII cells results in improved telomere maintenance and proliferation of these cells, which is concomitant with decreased fibrosis, inflammation, DNA damage as well as decreased presence of apoptotic and senescence cells. These results are in line with the notion that short telomeres can impair the ability of stem cells to regenerate tissues (Blasco, 2007; Flores et al., 2008), and with recent findings suggesting that IPF is the result of defective regeneration upon repetitive epithelial cell injury (Cao et al., 2016; Hinz et al., 2007; Ryu et al., 2014). In this work, we demonstrated that *Tert* gene therapy (AAV9-*Tert*) of mice diagnosed with pulmonary fibrosis leads to significant regression and in some cases to full remission of pulmonary fibrosis at 8 weeks post-treatment.

Bleomycin-induced pulmonary fibrosis model has been extensively used to explore new therapeutic strategies for the last decades. In this model, the therapeutic window to address the efficacy of new treatments is short due to the regenerative capacity of the lung in wild-type mice. Therefore, the pharmacological treatment under study has usually been administrated in a prophylactic manner impeding to reproduce patients situation (Inomata et al., 2014; Oku et al., 2008; Tanaka et al., 2012). However, our mouse model allowed us to mimic the clinical situation; i.e. first disease diagnosis and then treating those affected mice with full-blown pulmonary fibrosis.

Changes in gene expression profile upon telomerase gene therapy

We found that *Tert* treatment leads to changes in gene expression, which are in line with increased proliferation of epithelial cells and with a decreased fibrotic response. Interestingly, similar findings were found by us on the amelioration of heart function after infarct in mice treated with AAV9-*Tert* (Bar et al., 2014). In particular, *Tert* treatment leads to lower fibrotic scarring of the heart and increased cardiac myocyte proliferation concomitant with transcriptional changes suggestive of a regenerative signature (Bar et al., 2014).

Of relevance for this Thesis, we show that AAV9-*Tert* expression in fibrotic lungs leads to downregulation of pathways involved in fibroblast activation and, in particular, of the

tumor growth factor β (TGF-β) pathway as early as 1 week after *Tert* treatment of fibrotic lungs. In addition, downregulation of several FGFR pathways were observed at 8 weeks post-treatment, what indicates that upon *Tert* gene therapy an antifibrotic process is activated. These pathways are known to be important players in IPF both in mice and in humans. Indeed, pirfenidone and nintedanib, both recently approved treatments for IPF target different fibrotic pathways such us TGF-β or FGFR pathways (Inomata et al., 2014; Oku et al., 2008).

Telomerase as bona fide efficient treatment for IPF

The available IPF treatments, pirfenidone and nintedanib, do not induce disease remission either in patients or in preclinical mouse models (Inomata et al., 2014; Oku et al., 2008; Tanaka et al., 2012). The mechanisms of action of either pirfenidone, which is an inhibitor of the TGF-β pathway (Inomata et al., 2014; Oku et al., 2008; Tanaka et al., 2012), or nintedanib, which is an antagonist of the fibroblast growth factor receptor (FGFR), the platelet-derived growth factor receptor (PDGFR), and vascular endothelial growth factor receptor (VEGFR), target fibroblast differentiation, survival, and proliferation pathways as well as blood vessel activation pathways affecting fiber deposition in lung (Wollin et al., 2015).

We show in this Thesis that AAV9-*Tert* therapy effectively reverts fibrosis in mice diagnosed with pulmonary fibrosis. This is likely due to the fact that AAV9-*Tert* therapy targets one of the molecular causes of the disease, namely short telomeres (Alder et al., 2008; Armanios et al., 2007; Povedano et al., 2015). AAV9-*Tert* treatment results in decreased DNA damage and improved proliferative potential of the ATII cells, and subsequently in decreased fibrosis and inflammation (**Fig. 28**). In contrast, pirfenidone and nintedanib act on downstream events, particularly on reducing fibrosis, while the molecular cause of the disease (i.e. damaged telomeres and loss of the regenerative potential of epithelial cells), persists (Alder et al., 2008; Armanios et al., 2007; Povedano et al., 2015).

In summary, the findings described in this Thesis demonstrate the therapeutic potential of *Tert* gene therapy to efficiently revert and cure pulmonary fibrosis.

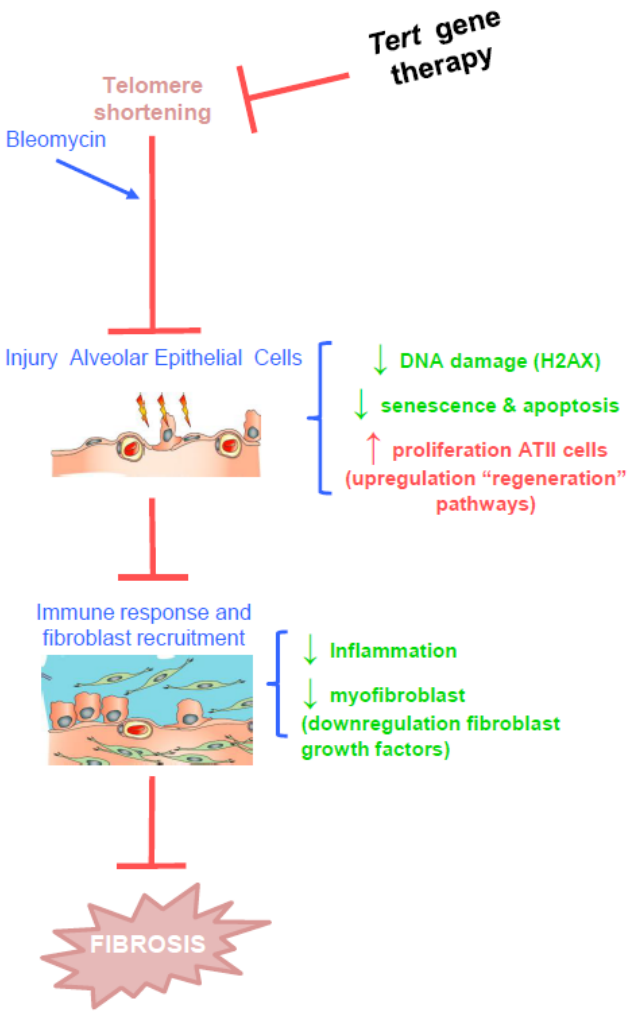

Figure 28. *Tert* gene therapy targets the basis of pulmonary fibrosis. Representation of the working model in this work presented, highlighting the way of action and main molecular changes provoked by *Tert* gene therapy.

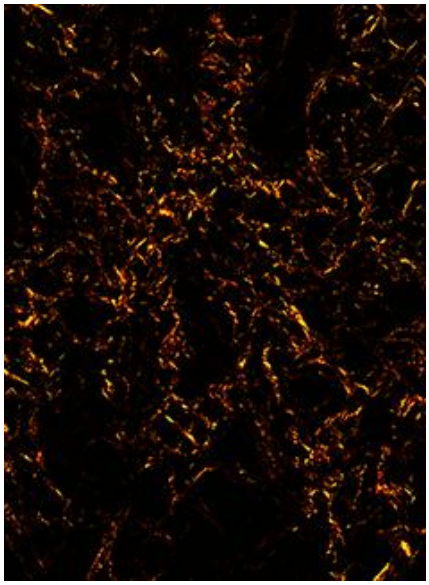

Conclusions

Modeling Human Idiopathic Pulmonary Fibrosis

1. Telomere dysfunction due to *Trf1* deletion in alveolar type II cells leads to lethal pulmonary fibrosis.

2. Low dose of bleomycin synergizes with short telomeres to develop pulmonary fibrosis.

Telomerase Gene Therapy

1. AAV9-*Tert* gene therapy targets alveolar type II cells maintaining their telomere length, reduces DNA damage, senescence and apoptosis, and stimulates their proliferation, leading to tissue regeneration.

2. *Tert* gene therapy constitutes a novel efficient therapeutic strategy for the treatment of IPF associated to short telomeres.

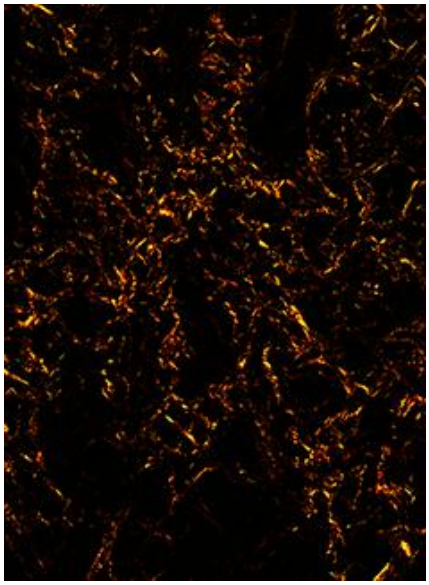

References

Ahluwalia, N., Shea, B.S., and Tager, A.M. (2014). New therapeutic targets in idiopathic pulmonary fibrosis. Aiming to rein in runaway wound-healing responses. American journal of respiratory and critical care medicine *190*, 867-878.

Alder, J.K., Barkauskas, C.E., Limjunyawong, N., Stanley, S.E., Kembou, F., Tuder, R.M., Hogan, B.L., Mitzner, W., and Armanios, M. (2015). Telomere dysfunction causes alveolar stem cell failure. Proc Natl Acad Sci U S A.

Alder, J.K., Chen, J.J., Lancaster, L., Danoff, S., Su, S.C., Cogan, J.D., Vulto, I., Xie, M., Qi, X., Tuder, R.M*., et al.* (2008). Short telomeres are a risk factor for idiopathic pulmonary fibrosis. Proceedings of the National Academy of Sciences of the United States of America *105*, 13051-13056.

Alder, J.K., Guo, N., Kembou, F., Parry, E.M., Anderson, C.J., Gorgy, A.I., Walsh, M.F., Sussan, T., Biswal, S., Mitzner, W*., et al.* (2011). Telomere length is a determinant of emphysema susceptibility. American journal of respiratory and critical care medicine *184*, 904-912.

Armanios, M. (2012). Telomerase and idiopathic pulmonary fibrosis. Mutation research *730*, 52-58.

Armanios, M. (2013). Telomeres and age-related disease: how telomere biology informs clinical paradigms. The Journal of clinical investigation *123*, 996-1002.

Armanios, M., and Blackburn, E.H. (2012). The telomere syndromes. Nature reviews. Genetics *13*, 693-704.

Armanios, M.Y., Chen, J.J., Cogan, J.D., Alder, J.K., Ingersoll, R.G., Markin, C., Lawson, W.E., Xie, M., Vulto, I., Phillips, J.A., 3rd*, et al.* (2007). Telomerase mutations in families with idiopathic pulmonary fibrosis. The New England journal of medicine *356*, 1317-1326.

Ayuso, E., Blouin, V., Lock, M., McGorray, S., Leon, X., Alvira, M.R., Auricchio, A., Bucher, S., Chtarto, A., Clark, K.R*., et al.* (2014). Manufacturing and characterization of a recombinant adeno-associated virus type 8 reference standard material. Human gene therapy *25*, 977-987.

Bandaria, J.N., Qin, P., Berk, V., Chu, S., and Yildiz, A. (2016). Shelterin Protects Chromosome Ends by Compacting Telomeric Chromatin. Cell *164*, 735-746.

Bar, C., Bernardes de Jesus, B., Serrano, R., Tejera, A., Ayuso, E., Jimenez, V., Formentini, I., Bobadilla, M., Mizrahi, J., de Martino, A.*, et al.* (2014). Telomerase expression confers cardioprotection in the adult mouse heart after acute myocardial infarction. Nature communications *5*, 5863.

Bar, C., Povedano, J.M., Serrano, R., Benitez-Buelga, C., Popkes, M., Formentini, I., Bobadilla, M., Bosch, F., and Blasco, M.A. (2016). Telomerase gene therapy rescues telomere length, bone marrow aplasia and survival in mice with aplastic anemia. Blood.

Barkauskas, C.E., Cronce, M.J., Rackley, C.R., Bowie, E.J., Keene, D.R., Stripp, B.R., Randell, S.H., Noble, P.W., and Hogan, B.L. (2013). Type 2 alveolar cells are stem cells in adult lung. The Journal of clinical investigation *123*, 3025-3036.

Beier, F., Foronda, M., Martinez, P., and Blasco, M.A. (2012). Conditional TRF1 knockout in the hematopoietic compartment leads to bone marrow failure and recapitulates clinical features of dyskeratosis congenita. Blood *120*, 2990-3000.

Bernardes de Jesus, B., and Blasco, M.A. (2012). Potential of telomerase activation in extending health span and longevity. Current opinion in cell biology *24*, 739-743.

Bernardes de Jesus, B., Vera, E., Schneeberger, K., Tejera, A.M., Ayuso, E., Bosch, F., and Blasco, M.A. (2012). Telomerase gene therapy in adult and old mice delays aging and increases longevity without increasing cancer. EMBO molecular medicine *4*, 691-704.

Blackburn, E.H. (2001). Switching and signaling at the telomere. Cell *106*, 661-673.

Blasco, M.A. (2005). Telomeres and human disease: ageing, cancer and beyond. Nat Rev Genet *6*, 611-622.

Blasco, M.A. (2007). Telomere length, stem cells and aging. Nature chemical biology *3*, 640-649.

Blasco, M.A., Lee, H.W., Hande, M.P., Samper, E., Lansdorp, P.M., DePinho, R.A., and Greider, C.W. (1997). Telomere shortening and tumor formation by mouse cells lacking telomerase RNA. Cell *91*, 25-34.

Broytman, O., Braun, R.K., Morgan, B.J., Pegelow, D.F., Hsu, P.N., Mei, L.S., Koya, A.K., Eldridge, M., and Teodorescu, M. (2015). Effects of chronic intermittent hypoxia on allergen-induced airway inflammation in rats. American journal of respiratory cell and molecular biology *52*, 162-170.

Cabrera, S., Gaxiola, M., Arreola, J.L., Ramirez, R., Jara, P., D'Armiento, J., Richards, T., Selman, M., and Pardo, A. (2007). Overexpression of MMP9 in macrophages attenuates pulmonary fibrosis induced by bleomycin. The international journal of biochemistry & cell biology *39*, 2324-2338.

Calado, R.T., Yewdell, W.T., Wilkerson, K.L., Regal, J.A., Kajigaya, S., Stratakis, C.A., and Young, N.S. (2009). Sex hormones, acting on the TERT gene, increase telomerase activity in human primary hematopoietic cells. Blood *114*, 2236-2243.

Canela, A., Vera, E., Klatt, P., and Blasco, M.A. (2007). High-throughput telomere length quantification by FISH and its application to human population studies. Proceedings of the National Academy of Sciences of the United States of America *104*, 5300-5305.

Cao, Z., Lis, R., Ginsberg, M., Chavez, D., Shido, K., Rabbany, S.Y., Fong, G.H., Sakmar, T.P., Rafii, S., and Ding, B.S. (2016). Targeting of the pulmonary capillary vascular niche promotes lung alveolar repair and ameliorates fibrosis. Nature medicine *22*, 154-162.

Celli, G.B., and de Lange, T. (2005). DNA processing is not required for ATM-mediated telomere damage response after TRF2 deletion. Nature cell biology *7*, 712-718.

Codd, V., Nelson, C.P., Albrecht, E., Mangino, M., Deelen, J., Buxton, J.L., Hottenga, J.J., Fischer, K., Esko, T., Surakka, I.*, et al.* (2013). Identification of seven loci affecting mean telomere length and their association with disease. Nature genetics *45*, 422-427, 427e421-422.

Collado, M., Blasco, M.A., and Serrano, M. (2007). Cellular senescence in cancer and aging. Cell *130*, 223-233.

Chiang, Y.J., Kim, S.H., Tessarollo, L., Campisi, J., and Hodes, R.J. (2004). Telomere-associated protein TIN2 is essential for early embryonic development through a telomerase-independent pathway. Molecular and cellular biology *24*, 6631-6634.

Chong, L., van Steensel, B., Broccoli, D., Erdjument-Bromage, H., Hanish, J., Tempst, P., and de Lange, T. (1995). A human telomeric protein. Science *270*, 1663-1667.

Davis, G.S., Leslie, K.O., and Hemenway, D.R. (1998). Silicosis in mice: effects of dose, time, and genetic strain. Journal of environmental pathology, toxicology and oncology : official organ of the International Society for Environmental Toxicology and Cancer *17*, 81-97.

de Lange, T. (2005). Shelterin: the protein complex that shapes and safeguards human telomeres. Genes & development *19*, 2100-2110.

Degryse, A.L., Xu, X.C., Newman, J.L., Mitchell, D.B., Tanjore, H., Polosukhin, V.V., Jones, B.R., McMahon, F.B., Gleaves, L.A., Phillips, J.A., 3rd*, et al.* (2012). Telomerase deficiency does not alter bleomycin-induced fibrosis in mice. Exp Lung Res *38*, 124-134.

Dieguez-Hurtado, R., Martin, J., Martinez-Corral, I., Martinez, M.D., Megias, D., Olmeda, D., and Ortega, S. (2011). A Cre-reporter transgenic mouse expressing the far-red fluorescent protein Katushka. Genesis *49*, 36-45.

Dobbs, L.G. (1990). Isolation and culture of alveolar type II cells. The American journal of physiology *258*, L134-147.

Eferl, R., Hasselblatt, P., Rath, M., Popper, H., Zenz, R., Komnenovic, V., Idarraga, M.H., Kenner, L., and Wagner, E.F. (2008). Development of pulmonary fibrosis through a pathway involving the transcription factor Fra-2/AP-1. Proceedings of the National Academy of Sciences of the United States of America *105*, 10525-10530.

Ekstrom, M., Gustafson, T., Boman, K., Nilsson, K., Tornling, G., Murgia, N., and Toren, K. (2014). Effects of smoking, gender and occupational exposure on the risk of severe pulmonary fibrosis: a population-based case-control study. BMJ open *4*, e004018.

Ferron, S., Mira, H., Franco, S., Cano-Jaimez, M., Bellmunt, E., Ramirez, C., Farinas, I., and Blasco, M.A. (2004). Telomere shortening and chromosomal instability abrogates proliferation of adult but not embryonic neural stem cells. Development *131*, 4059-4070.

Flores, I., Canela, A., Vera, E., Tejera, A., Cotsarelis, G., and Blasco, M.A. (2008). The longest telomeres: a general signature of adult stem cell compartments. Genes & development *22*, 654-667.

Flores, I., Cayuela, M.L., and Blasco, M.A. (2005). Effects of telomerase and telomere length on epidermal stem cell behavior. Science *309*, 1253-1256.

Garcia-Cao, I., Garcia-Cao, M., Martin-Caballero, J., Criado, L.M., Klatt, P., Flores, J.M., Weill, J.C., Blasco, M.A., and Serrano, M. (2002). "Super p53" mice exhibit enhanced DNA damage response, are tumor resistant and age normally. The EMBO journal *21*, 6225-6235.

Gardner, M., Bann, D., Wiley, L., Cooper, R., Hardy, R., Nitsch, D., Martin-Ruiz, C., Shiels, P., Sayer, A.A., Barbieri, M.*, et al.* (2014). Gender and telomere length: systematic review and meta-analysis. Experimental gerontology *51*, 15-27.

Geserick, C., Tejera, A., Gonzalez-Suarez, E., Klatt, P., and Blasco, M.A. (2006). Expression of mTert in primary murine cells links the growth-promoting effects of telomerase to transforming growth factor-beta signaling. Oncogene *25*, 4310-4319.

Gonzalez-Suarez, E., Samper, E., Flores, J.M., and Blasco, M.A. (2000). Telomerase-deficient mice with short telomeres are resistant to skin tumorigenesis. Nat Genet *26*, 114-117.

Greider, C.W., and Blackburn, E.H. (1985). Identification of a specific telomere terminal transferase activity in Tetrahymena extracts. Cell *43*, 405-413.

Harley, C.B., Futcher, A.B., and Greider, C.W. (1990). Telomeres shorten during ageing of human fibroblasts. Nature *345*, 458-460.

Haubner, B.J., Adamowicz-Brice, M., Khadayate, S., Tiefenthaler, V., Metzler, B., Aitman, T., and Penninger, J.M. (2012). Complete cardiac regeneration in a mouse model of myocardial infarction. Aging *4*, 966-977.

Hemann, M.T., Hackett, J., A, I.J., and Greider, C.W. (2000). Telomere length, telomere-binding proteins, and DNA damage signaling. Cold Spring Harbor symposia on quantitative biology *65*, 275-279.

Herrera, E., Samper, E., Martin-Caballero, J., Flores, J.M., Lee, H.W., and Blasco, M.A. (1999). Disease states associated with telomerase deficiency appear earlier in mice with short telomeres. The EMBO journal *18*, 2950-2960.

Hinz, B., Phan, S.H., Thannickal, V.J., Galli, A., Bochaton-Piallat, M.L., and Gabbiani, G. (2007). The myofibroblast: one function, multiple origins. The American journal of pathology *170*, 1807-1816.

Hockemeyer, D., Daniels, J.P., Takai, H., and de Lange, T. (2006). Recent expansion of the telomeric complex in rodents: Two distinct POT1 proteins protect mouse telomeres. Cell *126*, 63-77.

Hunninghake, G.M. (2014). A new hope for idiopathic pulmonary fibrosis. The New England journal of medicine *370*, 2142-2143.

Idiopathic Pulmonary Fibrosis Clinical Research, N., Martinez, F.J., de Andrade, J.A., Anstrom, K.J., King, T.E., Jr., and Raghu, G. (2014). Randomized trial of acetylcysteine in idiopathic pulmonary fibrosis. The New England journal of medicine *370*, 2093-2101.

Inomata, M., Kamio, K., Azuma, A., Matsuda, K., Kokuho, N., Miura, Y., Hayashi, H., Nei, T., Fujita, K., Saito, Y.*, et al.* (2014). Pirfenidone inhibits fibrocyte accumulation in the lungs in bleomycin-induced murine pulmonary fibrosis. Respiratory research *15*, 16.

Karimi-Shah, B.A., and Chowdhury, B.A. (2015). Forced vital capacity in idiopathic pulmonary fibrosis--FDA review of pirfenidone and nintedanib. The New England journal of medicine *372*, 1189-1191.

Karlseder, J., Kachatrian, L., Takai, H., Mercer, K., Hingorani, S., Jacks, T., and de Lange, T. (2003). Targeted deletion reveals an essential function for the telomere length regulator Trf1. Molecular and cellular biology *23*, 6533-6541.

Kibe, T., Osawa, G.A., Keegan, C.E., and de Lange, T. (2010). Telomere protection by TPP1 is mediated by POT1a and POT1b. Molecular and cellular biology *30*, 1059-1066.

King, T.E., Jr., Bradford, W.Z., Castro-Bernardini, S., Fagan, E.A., Glaspole, I., Glassberg, M.K., Gorina, E., Hopkins, P.M., Kardatzke, D., Lancaster, L.*, et al.* (2014). A phase 3 trial of pirfenidone in patients with idiopathic pulmonary fibrosis. The New England journal of medicine *370*, 2083-2092.

King, T.E., Jr., Pardo, A., and Selman, M. (2011). Idiopathic pulmonary fibrosis. Lancet *378*, 1949-1961.

Kolb, M., Margetts, P.J., Anthony, D.C., Pitossi, F., and Gauldie, J. (2001). Transient expression of IL-1beta induces acute lung injury and chronic repair leading to pulmonary fibrosis. The Journal of clinical investigation *107*, 1529-1536.

Korfhagen, T.R., Swantz, R.J., Wert, S.E., McCarty, J.M., Kerlakian, C.B., Glasser, S.W., and Whitsett, J.A. (1994). Respiratory epithelial cell expression of human transforming growth factor-alpha induces lung fibrosis in transgenic mice. The Journal of clinical investigation *93*, 1691-1699.

Kyo, S., Takakura, M., Kanaya, T., Zhuo, W., Fujimoto, K., Nishio, Y., Orimo, A., and Inoue, M. (1999). Estrogen activates telomerase. Cancer research *59*, 5917-5921.

Lam, A.P., Herazo-Maya, J.D., Sennello, J.A., Flozak, A.S., Russell, S., Mutlu, G.M., Budinger, G.R., DasGupta, R., Varga, J., Kaminski, N.*, et al.* (2014). Wnt coreceptor Lrp5 is a driver of idiopathic pulmonary fibrosis. American journal of respiratory and critical care medicine *190*, 185-195.

Lama, V.N. (2009). Update in lung transplantation 2008. American journal of respiratory and critical care medicine *179*, 759-764.

Lazzerini Denchi, E., Celli, G., and de Lange, T. (2006). Hepatocytes with extensive telomere deprotection and fusion remain viable and regenerate liver mass through endoreduplication. Genes & development *20*, 2648-2653.

Lee, H.W., Blasco, M.A., Gottlieb, G.J., Horner, J.W., 2nd, Greider, C.W., and DePinho, R.A. (1998). Essential role of mouse telomerase in highly proliferative organs. Nature *392*, 569-574.

Leri, A., Franco, S., Zacheo, A., Barlucchi, L., Chimenti, S., Limana, F., Nadal-Ginard, B., Kajstura, J., Anversa, P., and Blasco, M.A. (2003). Ablation of telomerase and telomere loss leads to cardiac dilatation and heart failure associated with p53 upregulation. The EMBO journal *22*, 131-139.

Liu, Y., Snow, B.E., Hande, M.P., Yeung, D., Erdmann, N.J., Wakeham, A., Itie, A., Siderovski, D.P., Lansdorp, P.M., Robinson, M.O.*, et al.* (2000). The telomerase reverse transcriptase is limiting and necessary for telomerase function in vivo. Curr Biol *10*, 1459-1462.

Lopez-Otin, C., Blasco, M.A., Partridge, L., Serrano, M., and Kroemer, G. (2013). The hallmarks of aging. Cell *153*, 1194-1217.

MacKenzie, B., Korfei, M., Henneke, I., Sibinska, Z., Tian, X., Hezel, S., Dilai, S., Wasnick, R., Schneider, B., Wilhelm, J.*, et al.* (2015). Increased FGF1-FGFRc expression in idiopathic pulmonary fibrosis. Respiratory research *16*, 83.

Martinez, P., and Blasco, M.A. (2011). Telomeric and extra-telomeric roles for telomerase and the telomere-binding proteins. Nature reviews. Cancer *11*, 161-176.

Martinez, P., Thanasoula, M., Carlos, A.R., Gomez-Lopez, G., Tejera, A.M., Schoeftner, S., Dominguez, O., Pisano, D.G., Tarsounas, M., and Blasco, M.A. (2010). Mammalian Rap1 controls telomere function and gene expression through binding to telomeric and extratelomeric sites. Nature cell biology *12*, 768-780.

Martinez, P., Thanasoula, M., Munoz, P., Liao, C., Tejera, A., McNees, C., Flores, J.M., Fernandez-Capetillo, O., Tarsounas, M., and Blasco, M.A. (2009). Increased telomere fragility and fusions resulting from TRF1 deficiency lead to degenerative pathologies and increased cancer in mice. Genes & development *23*, 2060-2075.

McDonald, S., Rubin, P., Chang, A.Y., Penney, D.P., Finkelstein, J.N., Grossberg, S., Feins, R., and Gregory, P.K. (1993). Pulmonary changes induced by combined mouse beta-interferon (rMuIFN-beta) and irradiation in normal mice--toxic versus protective effects. Radiotherapy and oncology : journal of the European Society for Therapeutic Radiology and Oncology *26*, 212-218.

Meier, A., Fiegler, H., Munoz, P., Ellis, P., Rigler, D., Langford, C., Blasco, M.A., Carter, N., and Jackson, S.P. (2007). Spreading of mammalian DNA-damage response factors studied by ChIP-chip at damaged telomeres. The EMBO journal *26*, 2707-2718.

Moore, B.B., and Hogaboam, C.M. (2008). Murine models of pulmonary fibrosis. American journal of physiology. Lung cellular and molecular physiology *294*, L152-160.

Mouratis, M.A., and Aidinis, V. (2011). Modeling pulmonary fibrosis with bleomycin. Current opinion in pulmonary medicine *17*, 355-361.

Noth, I., Anstrom, K.J., Calvert, S.B., de Andrade, J., Flaherty, K.R., Glazer, C., Kaner, R.J., Olman, M.A., and Idiopathic Pulmonary Fibrosis Clinical Research, N. (2012). A placebo-controlled randomized trial of warfarin in idiopathic pulmonary fibrosis. American journal of respiratory and critical care medicine *186*, 88-95.

Oku, H., Shimizu, T., Kawabata, T., Nagira, M., Hikita, I., Ueyama, A., Matsushima, S., Torii, M., and Arimura, A. (2008). Antifibrotic action of pirfenidone and prednisolone: different effects on pulmonary cytokines and growth factors in bleomycin-induced murine pulmonary fibrosis. European journal of pharmacology *590*, 400-408.

Park, J.I., Venteicher, A.S., Hong, J.Y., Choi, J., Jun, S., Shkreli, M., Chang, W., Meng, Z., Cheung, P., Ji, H.*, et al.* (2009). Telomerase modulates Wnt signalling by association with target gene chromatin. Nature *460*, 66-72.

Pedroza, M., Le, T.T., Lewis, K., Karmouty-Quintana, H., To, S., George, A.T., Blackburn, M.R., Tweardy, D.J., and Agarwal, S.K. (2015). STAT-3 contributes to pulmonary fibrosis through epithelial injury and fibroblast-myofibroblast differentiation. FASEB journal : official publication of the Federation of American Societies for Experimental Biology.

Povedano, J.M., Martinez, P., Flores, J.M., Mulero, F., and Blasco, M.A. (2015). Mice with Pulmonary Fibrosis Driven by Telomere Dysfunction. Cell reports *12*, 286-299.

Raghu, G. (2006). Idiopathic pulmonary fibrosis: treatment options in pursuit of evidence-based approaches. The European respiratory journal *28*, 463-465.

Raghu, G., Collard, H.R., Egan, J.J., Martinez, F.J., Behr, J., Brown, K.K., Colby, T.V., Cordier, J.F., Flaherty, K.R., Lasky, J.A.*, et al.* (2011). An official ATS/ERS/JRS/ALAT statement: idiopathic pulmonary fibrosis: evidence-based guidelines for diagnosis and management. American journal of respiratory and critical care medicine *183*, 788-824.

Rock, J.R., Barkauskas, C.E., Cronce, M.J., Xue, Y., Harris, J.R., Liang, J., Noble, P.W., and Hogan, B.L. (2011). Multiple stromal populations contribute to pulmonary fibrosis without evidence for epithelial to mesenchymal transition. Proceedings of the National Academy of Sciences of the United States of America *108*, E1475-1483.

Rudolph, K.L., Chang, S., Millard, M., Schreiber-Agus, N., and DePinho, R.A. (2000). Inhibition of experimental liver cirrhosis in mice by telomerase gene delivery. Science *287*, 1253-1258.

Ruschel, J., Hellal, F., Flynn, K.C., Dupraz, S., Elliott, D.A., Tedeschi, A., Bates, M., Sliwinski, C., Brook, G., Dobrindt, K.*, et al.* (2015). Axonal regeneration. Systemic administration of epothilone B promotes axon regeneration after spinal cord injury. Science *348*, 347-352.

Ryu, J.H., Moua, T., Daniels, C.E., Hartman, T.E., Yi, E.S., Utz, J.P., and Limper, A.H. (2014). Idiopathic pulmonary fibrosis: evolving concepts. Mayo Clinic proceedings *89*, 1130-1142.

Schneider, R.P., Garrobo, I., Foronda, M., Palacios, J.A., Marion, R.M., Flores, I., Ortega, S., and Blasco, M.A. (2013). TRF1 is a stem cell marker and is essential for the generation of induced pluripotent stem cells. Nat Commun *4*, 1946.

Selman, M., King, T.E., Pardo, A., American Thoracic, S., European Respiratory, S., and American College of Chest, P. (2001). Idiopathic pulmonary fibrosis: prevailing and evolving hypotheses about its pathogenesis and implications for therapy. Annals of internal medicine *134*, 136-151.

Serrano-Mollar, A., Nacher, M., Gay-Jordi, G., Closa, D., Xaubet, A., and Bulbena, O. (2007). Intratracheal transplantation of alveolar type II cells reverses bleomycin-

induced lung fibrosis. American journal of respiratory and critical care medicine *176*, 1261-1268.

Snetselaar, R., van Moorsel, C.H., Kazemier, K.M., van der Vis, J.J., Zanen, P., van Oosterhout, M.F., and Grutters, J.C. (2015). Telomere length in interstitial lung diseases. Chest *148*, 1011-1018.

Stanley, S.E., Chen, J.J., Podlevsky, J.D., Alder, J.K., Hansel, N.N., Mathias, R.A., Qi, X., Rafaels, N.M., Wise, R.A., Silverman, E.K.*, et al.* (2015). Telomerase mutations in smokers with severe emphysema. The Journal of clinical investigation *125*, 563-570.

Subramanian, A., Tamayo, P., Mootha, V.K., Mukherjee, S., Ebert, B.L., Gillette, M.A., Paulovich, A., Pomeroy, S.L., Golub, T.R., Lander, E.S.*, et al.* (2005). Gene set enrichment analysis: a knowledge-based approach for interpreting genome-wide expression profiles. Proceedings of the National Academy of Sciences of the United States of America *102*, 15545-15550.

Sun, L., Louie, M.C., Vannella, K.M., Wilke, C.A., LeVine, A.M., Moore, B.B., and Shanley, T.P. (2011). New concepts of IL-10-induced lung fibrosis: fibrocyte recruitment and M2 activation in a CCL2/CCR2 axis. American journal of physiology. Lung cellular and molecular physiology *300*, L341-353.

Tanaka, K., Azuma, A., Miyazaki, Y., Sato, K., and Mizushima, T. (2012). Effects of lecithinized superoxide dismutase and/or pirfenidone against bleomycin-induced pulmonary fibrosis. Chest *142*, 1011-1019.

Tang, W., Geba, G.P., Zheng, T., Ray, P., Homer, R.J., Kuhn, C., 3rd, Flavell, R.A., and Elias, J.A. (1996). Targeted expression of IL-11 in the murine airway causes lymphocytic inflammation, bronchial remodeling, and airways obstruction. The Journal of clinical investigation *98*, 2845-2853.

Tomas-Loba, A., Flores, I., Fernandez-Marcos, P.J., Cayuela, M.L., Maraver, A., Tejera, A., Borras, C., Matheu, A., Klatt, P., Flores, J.M.*, et al.* (2008). Telomerase reverse transcriptase delays aging in cancer-resistant mice. Cell *135*, 609-622.

Umezawa, H. (1974). Chemistry and mechanism of action of bleomycin. Federation proceedings *33*, 2296-2302.

Umezawa, H., Ishizuka, M., Maeda, K., and Takeuchi, T. (1967). Studies on bleomycin. Cancer *20*, 891-895.

Van der Velden, J.L., Bertoncello, I., and McQualter, J.L. (2013). LysoTracker is a marker of differentiated alveolar type II cells. Respiratory research *14*, 123.

Vera, E., Bernardes de Jesus, B., Foronda, M., Flores, J.M., and Blasco, M.A. (2012). The rate of increase of short telomeres predicts longevity in mammals. Cell reports *2*, 732-737.

Wells, A.U., Behr, J., Costabel, U., Cottin, V., and Poletti, V. (2012). Triple therapy in idiopathic pulmonary fibrosis: an alarming press release. The European respiratory journal *39*, 805-806.

Wollin, L., Wex, E., Pautsch, A., Schnapp, G., Hostettler, K.E., Stowasser, S., and Kolb, M. (2015). Mode of action of nintedanib in the treatment of idiopathic pulmonary fibrosis. The European respiratory journal *45*, 1434-1445.

Wu, L., Multani, A.S., He, H., Cosme-Blanco, W., Deng, Y., Deng, J.M., Bachilo, O., Pathak, S., Tahara, H., Bailey, S.M.*, et al.* (2006). Pot1 deficiency initiates DNA damage checkpoint activation and aberrant homologous recombination at telomeres. Cell *126*, 49-62.

Zhang, H.Y., Gharaee-Kermani, M., Zhang, K., Karmiol, S., and Phan, S.H. (1996). Lung fibroblast alpha-smooth muscle actin expression and contractile phenotype in bleomycin-induced pulmonary fibrosis. Am J Pathol *148*, 527-537.

Zhu, Z., Homer, R.J., Wang, Z., Chen, Q., Geba, G.P., Wang, J., Zhang, Y., and Elias, J.A. (1999). Pulmonary expression of interleukin-13 causes inflammation, mucus hypersecretion, subepithelial fibrosis, physiologic abnormalities, and eotaxin production. The Journal of clinical investigation *103*, 779-788.

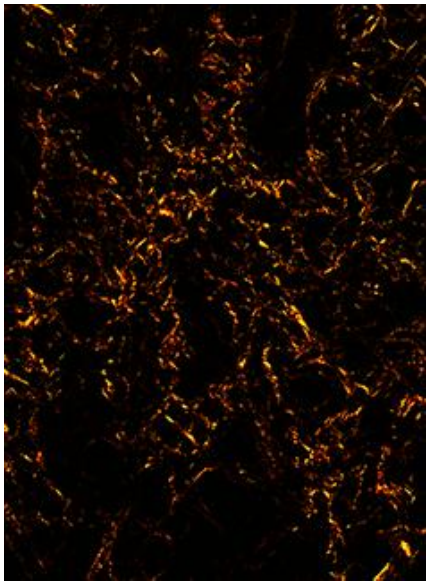

Annexes

Articles published and under revision related to this Thesis:

- Povedano J. M., Martinez P., Flores J. M., Mulero F. and Blasco M. A. Telomere dysfunction in lung alveolar type II cells is sufficient to trigger progressive pulmonary fibrosis in mice. (2015) ***Cell Rep.*** 12, 1-14.
- Povedano J. M., Martinez P., Gómez G., Bobadilla M., Flores J. M. and Blasco M. A. Telomerase gene therapy of mice with pulmonary fibrosis owing to short telomeres induces disease reversal by increasing survival and proliferation of alveolar type II cells. ***Under revision*.**

Other articles:

- Bär C., Povedano J. M., Serrano R., Popkes M., Benitez-Buelga C., Formentinin I., Bobadilla M., Bosch F. and Blasco M. A. Telomerase gene therapy rescues telomere length, bone marrow aplasia and survival in a mouse model of aplastic anaemia. (2016) ***Blood.*** pii: blood-2015-08-667485.